International Journal of Innovation Engineering and Science Research

Editorial Board

International Journal of Innovation Engineering and Science Research

Volume 4 ISSUE 5 September-October 2020

International Journal of Innovation Engineering and Science Research
(ISSN: 2581-4591)

www.ijiesr.com

Modeling and Simulation of Robot Fish

Mustafa TINKIR
NecmettinErbakan University, Department of Mechanical Engineering, Konya, Turkey
mtinkir@erbakan.edu.tr

Celil TOPAKCI
NecmettinErbakan University, Department of Mechanical Engineering, Konya, Turkey
celil_topakci07@outlook.com

ABSTRACT

Fish are the best swimmers of the sea. The use of flexible tail movements is for good swimmers, for fast swimming and sudden swapping movements. This resulted in fish inspirations in the design of underwater vehicles.In this study, it is aimed to imitate four degrees of freedom (DOF) of the structure of the carangiform fish that is based on the results of previous studies. The equations of the motion of the carangiform type carp fish robot are obtained to simulate angle values required for the robot fish swimming using Matlab/Simulink/SimMechanics software. While determining the backbone structure of the robot fish, four joints are designed considering the dimensions of real carp fish and, also the joints are placed in positions where the robot fish can best mimic the movement of the tail. Moreover three actuators are located to body for advancement, rotation and sinking movements. Modeling and simulations results of the proposed research are given in figures and important findings are realized for future control studies in terms of the modeling approaches.

Keywords—*Carangiform type, carp fish robot, 4 degrees of freedom, modeling, simulation.*

I. INTRODUCTION

Living creatures in nature have adapted very well to their environment. Designers noticed this and started to design by examining the living things in the places where their designs would be used. This design method is called biomimetic design. Biomimetic design is used today in robot technology, aircraft technology and many fields. In this study, a robot fish is designed according to the body size of a fish by using biomimetic design. The reason for choosing fish in this design is that the fish can swim fast in the water and have sudden maneuverability. The forward and rotational movement of the fish is provided by the tail movements of the fish. It provides the sinking and rising movement with air sacs. In this study, the sinking and rising movement was achieved with the help of fins placed next to the fish.

Robot fish studies first started in the 1990s. These studies were initially carried out on a large scale. In the studies, new designs were created by examining the hydrodynamic structure of fish. One of these designs is the eight-joint RoboTuna, developed by MIT in 1994 [1]. In this research, by examining the hydrodynamic structure of the fish, a design has been made in accordance with the dimensions of the real tuna with eight joints in a way that its movement resembles the movement of the fish. Designs that work with a hydraulic drive system have also been made. One of these designs has produced a robot fish called VCUUV, which looks like a Thunniform fish, designed by the Drapper Laboratory [2].This design is a world first as a hydraulic driven design and, itsdimensions are 2.4m long and weigh 173kg. A robot lampreywhich aimed to provide mine countermeasures,was produced by applying shape memory alloy (SMA) by Northwestern University[3]. In Japan, Nagoya University developed a micro robotic fish using ICPF Actuators[4], while Tokai University produced a robot Blackbass[5] in order to research the propulsion characteristics of pectoral fins. The National Maritime Research Institute in Japan developed many kinds of robotic fish prototypes ranging from PF300 to PPF-09[6] to exploit up-down and effective swimming characteristics of fish. Mitsubishi Heavy Industries built a robot fish named coelacanth robot[7]. In China, Beihang University (BUAA) developed three kinds of robot fish[8] and the Institute of Automation Chinese Academy of Sciences (CASIA) made progress in developing four-joint robot fish[9]. Liu and Hu [10],presented a 3D simulator used for studying the motion control and autonomous navigation of roboticfish. The simulator's system structure and computation flow are presented and simplified kinematics and hydrodynamicsmodels for a virtual robotic fish are obtained.Their experimental results showed that the simulator provides a realistic and convenient way to develop autonomous navigation algorithms for robotic fish.

Korkmaz[11], developed a carangiform type biomimetic robotic fish prototype with two-link flexible tail mechanism, which has three dimensional autonomous swimming ability and, intelligent control of three-dimensional motion of the robotic fish wasrealized with the proposed biomimetic control structure. In this PhD thesis, in order to carry out simulation studies and design control algorithms, three-dimensional 6 Degrees of Freedom (DoF) nonlinear mathematical model of the robotic fish was obtained. Also lagrange method was used to obtain this model and hydrodynamic forces acting on the tail were calculated to derive the realistic effects of water for the design procedure of the robotic fish prototype, morphological characteristics of a real Carangiform carp fish was adapted. Moreover Central Pattern Generator (CPG) model inspired by the spinal cord neurons of Lamprey was applied to perform locomotion control of the robotic fish. The neural Lamprey CPG model was composed of unidirectional and chain linked oscillator series. Rhythmic, oscillatory and sinusoidal output signals were obtained with this model to drive servo motors of the tail. A sensory feedback mechanism based on Lamprey neuron and two different fuzzy controllers were established to achieve the closed loop control structure of the robotic fish and Central Nervous System (CNS) was developed. In order to validate the proposed methods, open and closed loop analyzes of robotic fish prototype were performed both in the simulation environment and experimental pool. In the open loop experiments, forward and turning motions of the prototype were analyzed and characteristic features of the robotic fish were determined. In the closed loop experiments, controls of the yaw angle, autonomous swimming avoiding the obstacles and yaw angle avoiding the obstacles were performed. Thus, sensory feedback closed loop forward and turning motion controls were achieved depending on the characteristic features of the robotic fish. In addition, pitch angle was controlled to provide up/down motions with center of gravity control mechanism of the robotic fish. The effectiveness and performance of the three dimensional motions of the designed robotic fish prototype were shown with the simulation and experimental studies and very successful results have been achieved.

In scope of this work, a robot fish with four joints is designed, inspired by the carangiform fish. The size of the robot fish is decided by determining the carp fish, a type of carangiform fish. Three actuators are used for the swinging motion of the robot fish tail. Robot fish model is created using both Lagrange formulation and rigid body dynamics approach of Matlab/Sim Mechanics software. Also these models are combined to simulate robot fish movements. The content of the article is constituted in that: Section II includes dynamic modeling. Section III describes results and discussion. Finally, conclusion part of the paper is presented in Section IV.

II. DYNAMIC MODELING

Previous studies are examined while determining the backbone structure of the fish. As a result of these studies, it is concluded that the movement of carangiform fish in the water would be better for the design. Therefore, carp fish, which is one of the carangiform type fish, is chosen as the model fish. Since such fish can reach 80 cm in length, so the length of the robot fish is determined as 80 cm.Spine structure of the proposed robot fish is given in Figure 1.

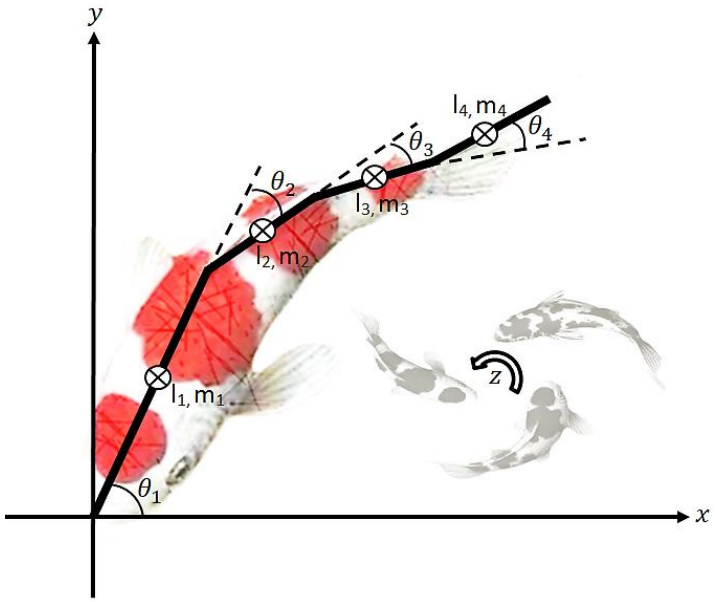

Fig. 1.Spine structure of the robot fish.

In this study, the equationsof the motion of the robot fish whose backbone structure isdetermined, are obtained using the Lagrange formulation with kinetic and potential energies given in Equation (1)

$$\frac{d}{dt}\left(\frac{\partial E_k}{\partial \dot{q}_i}-\frac{\partial E_p}{\partial \dot{q}_i}\right)-\frac{\partial E_k}{\partial q_i}+\frac{\partial E_p}{\partial q_i}=Q_i \quad (1)$$

Where$q_i$is generalizedcoordinatesandQ_i is generalizedforces. Positionsaredeterminedaccordingtothenose of thefish. Thevelocities of thepositionsarefoundbytakingthefirstderivativeswithrespectto time.

Positions and velocities of the first limb in the x and y axes are given as follows:

$$X_1 = a_1 * \cos\theta_1 \text{and} \dot{X}_1 = -a_1 * \dot{\theta}_1 * \sin\theta_1 \quad (2)$$

$$\dot{Y}_1 = -a_1 * \dot{\theta}_1 * \sin\theta_1 \text{and} \dot{Y}_1 = -a_1 * \dot{\theta}_1 * \sin\theta_1 \quad (3)$$

Positions and velocities of the second limb in the x and y axes are given as follows:

$$X_2 = L_1 * \cos\theta_1 + a_2 * \cos(\theta_1+\theta_2) \text{and} \dot{X}_2 = -L_1 * \dot{\theta}_1 * \sin\theta_1 - a_2 * (\dot{\theta}_1+\dot{\theta}_2) * \sin(\theta_1+\theta_2) \quad (4)$$

$$Y_2 = L_1 * \sin\theta_1 + a_2 * \sin(\theta_1+\theta_2) \text{and} \dot{Y}_2 = L_1 * \dot{\theta}_1 * \cos\theta_1 + a_2 * (\dot{\theta}_1+\dot{\theta}_2) * \cos(\theta_1+\theta_2) \quad (5)$$

Positions and velocities of the third limb in the x and y axes are given as follows:

$$X_3 = L_1 * \cos\theta_1 + L_2 * \cos(\theta_1+\theta_2) + a_3\cos(\theta_1+\theta_2+\theta_3) \text{and,} \quad (6)$$

$$\dot{X}_3 = -L_1 * \dot{\theta}_1 * \sin\theta_1 - L_2 * (\dot{\theta}_1+\dot{\theta}_2) * \sin(\theta_1+\theta_2) - a_3(\dot{\theta}_1+\dot{\theta}_2+\dot{\theta}_3) * \sin(\dot{\theta}_1+\dot{\theta}_2+\dot{\theta}_3) \quad (7)$$

$$Y_3 = L_1 * \sin\theta_1 + L_2 * \sin(\theta_1+\theta_2) + a_3 + \sin(\theta_1+\theta_2+\theta_3) \text{and,} \quad (8)$$

$$\dot{Y}_3 = L_1 * \dot{\theta}_1 * \cos\theta_1 + L_2 * (\dot{\theta}_1+\dot{\theta}_2) * \cos(\theta_1+\theta_2) + a_3 * (\dot{\theta}_1+\dot{\theta}_2+\dot{\theta}_3) * \cos(\theta_1+\theta_2+\theta_3) \quad (9)$$

Positions and velocities of the fourth limb in the x and y axes are given as follows:

$$X_4 = L_1 * \cos\theta_1 + L_2 * \cos(\theta_1+\theta_2) + L_3\cos(\theta_1+\theta_2+\theta_3) + a_4 * \cos(\theta_1+\theta_2+\theta_3+\theta_4) \text{and,} \quad (10)$$

$$\dot{X}_4 = -L_1 * \dot{\theta}_1 * \sin\theta_1 - L_2 * (\dot{\theta}_1+\dot{\theta}_2) * \sin(\theta_1+\theta_2) - L_3(\dot{\theta}_1+\dot{\theta}_2+\dot{\theta}_3) * \sin(\theta_1+\theta_2+\theta_3) - a_4 * (\dot{\theta}_1+\dot{\theta}_2+\dot{\theta}_3+\dot{\theta}_4) * \sin(\theta_1+\theta_2+\theta_3+\theta_4) \quad (11)$$

$$Y_4 = L_1 * \sin\theta_1 + L_2 * \sin(\theta_1+\theta_2) + L_3 * \sin(\theta_1+\theta_2+\theta_3) + a_4 * (\theta_1+\theta_2+\theta_3+\theta_4) \quad (12)$$

$$\dot{Y}_4 = L_1 * \dot{\theta}_1 * \cos\theta_1 + L_2 * (\dot{\theta}_1+\dot{\theta}_2) * \cos(\theta_1+\theta_2) + L_3 * (\dot{\theta}_1+\dot{\theta}_2+\dot{\theta}_3) * \cos(\theta_1+\theta_2+\theta_3) + a_4 + (\dot{\theta}_1+\dot{\theta}_2+\dot{\theta}_3+\dot{\theta}_4) * \cos(\theta_1+\theta_2+\theta_3+\theta_4) \quad (13)$$

As a result of the examination of previous studies [11], hydrodynamic forces acting on the tail finare given in Figure 2.

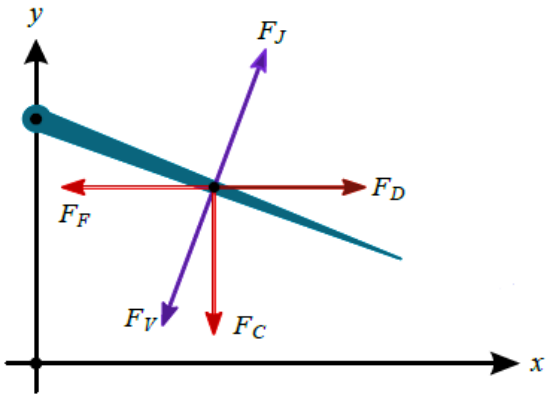

Fig. 2.Forcesacting on a limb of a fish.

Where $F_D$representsthedragforce, F_V is theaccelerationforce, F_J is thebuoyancyforce, F_F is theresultantforce on the x-axisand, F_C is theresultantforce on the y axis.

$$F_V = (\pi * \rho * L * C^2 * \dot{U} * \sin\alpha) + (\pi * \rho * L * C^2 * U * \dot{\alpha} * \cos\alpha) \quad (13)$$

Wherep is thedensity of thefluidand α is theangle of attack of thelimb, U is therelativeflow rate, L and C aretheverticallength of thetailfinandhalfthelaterallength,respectively.

$$F_J = (2 * \pi * \rho * L * C^2 * U * \sin\alpha * \cos\alpha) \quad (14)$$

$$F_F = (F_V - F_J) * \sin(360 - \textstyle\sum_{i=1}^{N} \theta_1) \quad (15)$$

$$F_C = (F_V - F_J) * \cos(360 - \textstyle\sum_{i=1}^{N} \theta_i) \quad (16)$$

Theequationforthetailmovements of therobot fish is obtainedandtheequations of themotionforeachlimbaregiven as follows, respectively.

$$\ddot{\theta}_1 = \Big[F_C l - F_F l\theta_1 - \frac{\theta_1 \dot{\theta_1}^2 c}{2} - \frac{c}{2}\ddot{\theta}_2\left(4\theta_1\theta_2 + {\theta_1}^2 + 3{\theta_2}^2 + 3\right) - \frac{c}{2}\dot{\theta}_2\left(4\theta_1\dot{\theta}_2 + 2\theta_2\dot{\theta}_2 + 4\dot{\theta}_1\theta_2 + 6\theta_1\dot{\theta}_1\right) - \frac{c}{2}\dot{\theta}_1\left(6\theta_1\dot{\theta}_2 + 2\theta_2\dot{\theta}_2 + 6\dot{\theta}_1\theta_2 + 18\theta_1\dot{\theta}_1\right) - \frac{50c}{4}\ddot{\theta}_2 - \frac{26c}{4}\ddot{\theta}_3 - \frac{7c}{4}\ddot{\theta}_4 + c\left(\frac{5}{2}\theta_1 + \frac{3}{2}\theta_2 + \frac{1}{2}\theta_3\right)\left(-\frac{1}{2}(\theta_1 + \theta_2 + \theta_3)(\ddot{\theta}_2 + \ddot{\theta}_3) - (\theta_1 + \theta_2)\ddot{\theta}_2 - \frac{1}{2}\left(\dot{\theta}_1 + \dot{\theta}_2 + \dot{\theta}_3\right)^2 - \left(\dot{\theta}_1 + \dot{\theta}_2\right)^2 - \left(\dot{\theta}_1\right)^2\right) + c\left(\frac{7}{2}\theta_1 + \frac{5}{2}\theta_2 + \frac{3}{2}\theta_3 + \frac{1}{2}\theta_3\right)\left(-\frac{1}{2}(\theta_1 + \theta_2 + \theta_3 + \theta_4)(\ddot{\theta}_2 + \ddot{\theta}_3 + \ddot{\theta}_4) - (\theta_1 + \theta_2 + \theta_3)(\ddot{\theta}_2 + \ddot{\theta}_3) - (\theta_1 + \theta_2)\ddot{\theta}_2 - \frac{1}{2}\left(\dot{\theta}_1 + \dot{\theta}_2 + \dot{\theta}_3 + \dot{\theta}_4\right)^2 - \left(\dot{\theta}_1 + \dot{\theta}_2 + \dot{\theta}_3\right)^2 - \left(\dot{\theta}_1 + \dot{\theta}_2\right)^2 - \left(\dot{\theta}_1\right)^2\right) - I_2\ddot{\theta}_2 - I_3(\ddot{\theta}_2 + \ddot{\theta}_3) - I_4(\ddot{\theta}_2 + \ddot{\theta}_3 + \ddot{\theta}_4) + \frac{c}{4}\theta_1{\dot{\theta}_1}^2 + \frac{c}{4}\left(\dot{\theta}_2 + 3\dot{\theta}_1\right)\left(\theta_2(\dot{\theta}_1 + \dot{\theta}_2) + \theta_1(3\dot{\theta}_1 + \dot{\theta}_2)\right)\Big] / \Big[\frac{c}{4}\left({\theta_1}^2 + 1\right) + \frac{c}{2}\left(6\theta_1\theta_2 + {\theta_2}^2 + 9{\theta_1}^2 + 9\right) + \frac{74c}{4} + c\left(\frac{5}{2}\theta_1 + \frac{3}{2}\theta_2 + \frac{1}{2}\theta_3\right)^2 + c\left(\frac{7}{2}\theta_1 + \frac{5}{2}\theta_2 + \frac{3}{2}\theta_3 + \frac{1}{2}\theta_3\right)^2 + I_1 + I_2 + I_3 + I_4\Big] \quad (17)$$

$$\ddot{\theta}_2 = \Big[F_C l - F_F l(\theta_1+\theta_2) + T_1 - \tfrac{c}{4}\dot{\theta}_2\big(2\theta_1\dot{\theta}_2 + 2\theta_2\dot{\theta}_2 + 2\dot{\theta}_1\theta_2 + 2\theta_1\dot{\theta}_1\big) - \tfrac{c}{4}\dot{\theta}_1\big(4\theta_1\dot{\theta}_2 + 2\theta_2\dot{\theta}_2 + 4\dot{\theta}_1\theta_2 + 6\theta_1\dot{\theta}_1\big) - \tfrac{50c}{4}\ddot{\theta}_1 - \tfrac{18c}{4}\ddot{\theta}_3 - \tfrac{5c}{4}\ddot{\theta}_4 + c\left(\tfrac{3}{2}\theta_1 + \tfrac{3}{2}\theta_2 + \tfrac{1}{2}\theta_3\right)\Big(-\tfrac{1}{2}(\theta_1+\theta_2+\theta_3)(\ddot{\theta}_1+\ddot{\theta}_3) - (\theta_1+\theta_2)\ddot{\theta}_1 - \tfrac{1}{2}\big(\dot{\theta}_1+\dot{\theta}_2+\dot{\theta}_3\big)^2 - \big(\dot{\theta}_1+\dot{\theta}_2\big)^2 - \big(\dot{\theta}_1\big)^2\Big) + c\left(\tfrac{5}{2}\theta_1 + \tfrac{5}{2}\theta_2 + \tfrac{3}{2}\theta_3 + \tfrac{1}{2}\theta_3\right)\Big(-\tfrac{1}{2}(\theta_1+\theta_2+\theta_3+\theta_4)(\ddot{\theta}_1+\ddot{\theta}_3+\ddot{\theta}_4) - (\theta_1+\theta_2+\theta_3)(\ddot{\theta}_1+\ddot{\theta}_3) - (\theta_1+\theta_2)\ddot{\theta}_1 - \tfrac{1}{2}\big(\dot{\theta}_1+\dot{\theta}_2+\dot{\theta}_3+\dot{\theta}_4\big)^2 - \big(\dot{\theta}_1+\dot{\theta}_2+\dot{\theta}_3\big)^2 - \big(\dot{\theta}_1+\dot{\theta}_2\big)^2 - \big(\dot{\theta}_1\big)^2\Big) - I_2\ddot{\theta}_1 - I_3(\ddot{\theta}_1+\ddot{\theta}_3) - I_4(\ddot{\theta}_1+\ddot{\theta}_3+\ddot{\theta}_4) - c/2(\dot{\theta}_1+\dot{\theta}_2)((\theta_1+\theta_2)(\dot{\theta}_1+\dot{\theta}_2) + \theta_1\dot{\theta}_1))\Big] / \Big[\tfrac{c}{4}\big(2\theta_1\theta_2 + {\theta_2}^2 + {\theta_1}^2 + 1\big) + \tfrac{34c}{4} + c\left(\tfrac{3}{2}\theta_1 + \tfrac{3}{2}\theta_2 + \tfrac{1}{2}\theta_3\right)^2 + c\left(\tfrac{5}{2}\theta_1 + \tfrac{5}{2}\theta_2 + \tfrac{3}{2}\theta_3 + \tfrac{1}{2}\theta_3\right)^2 + I_2 + I_3 + I_4\Big] \quad (18)$$

$$\ddot{\theta}_3 = \Big[F_C l - F_F l(\theta_1+\theta_2+\theta_3) + T_2 - \tfrac{26c}{4}\ddot{\theta}_1 - \tfrac{18c}{4}\ddot{\theta}_2 - \tfrac{3c}{4}\ddot{\theta}_4 + c/2(\theta_1+\theta_2+\theta_3)\Big(-\tfrac{1}{2}(\theta_1+\theta_2+\theta_3)(\ddot{\theta}_1+\ddot{\theta}_2) - (\theta_1+\theta_2)(\ddot{\theta}_1+\ddot{\theta}_2) - \tfrac{1}{2}\big(\dot{\theta}_1+\dot{\theta}_2+\dot{\theta}_3\big)^2 - \big(\dot{\theta}_1+\dot{\theta}_2\big)^2 - \big(\dot{\theta}_1\big)^2\Big) + c\left(\tfrac{3}{2}\theta_1 + \tfrac{3}{2}\theta_2 + \tfrac{3}{2}\theta_3 + \tfrac{1}{2}\theta_4\right)\Big(-\tfrac{1}{2}(\theta_1+\theta_2+\theta_3+\theta_4)(\ddot{\theta}_1+\ddot{\theta}_2+\ddot{\theta}_4) - (\theta_1+\theta_2+\theta_3)(\ddot{\theta}_1+\ddot{\theta}_2) - (\theta_1+\theta_2)(\ddot{\theta}_1+\ddot{\theta}_2) - \tfrac{1}{2}\big(\dot{\theta}_1+\dot{\theta}_2+\dot{\theta}_3+\dot{\theta}_4\big)^2 - \big(\dot{\theta}_1+\dot{\theta}_2+\dot{\theta}_3\big)^2 - \big(\dot{\theta}_1+\dot{\theta}_2\big)^2 - \big(\dot{\theta}_1\big)^2\Big) - I_3(\ddot{\theta}_1+\ddot{\theta}_2) - I_4(\ddot{\theta}_1+\ddot{\theta}_2+\ddot{\theta}_4)\Big] / \Big[\tfrac{10c}{4} + \tfrac{c}{4}(\theta_1+\theta_2+\theta_3)^2 + c\left(\tfrac{3}{2}\theta_1 + \tfrac{3}{2}\theta_2 + \tfrac{3}{2}\theta_3 + \tfrac{1}{2}\theta_4\right)^2 + I_3 + I_4\Big] \quad (19)$$

$$\ddot{\theta}_4 = \Big[\tfrac{F_C l}{2} - F_F l(\theta_1+\theta_2+\theta_3+\theta_4) + T_3 - \tfrac{7c}{4}\ddot{\theta}_1 - \tfrac{5c}{4}\ddot{\theta}_2 - \tfrac{3c}{4}\ddot{\theta}_3 + c/2(\theta_1+\theta_2+\theta_3+\theta_4)\Big(-\tfrac{1}{2}(\theta_1+\theta_2+\theta_3+\theta_4)(\ddot{\theta}_1+\ddot{\theta}_2+\ddot{\theta}_3) - (\theta_1+\theta_2+\theta_3)(\ddot{\theta}_1+\ddot{\theta}_2) - (\theta_1+\theta_2)(\ddot{\theta}_1+\ddot{\theta}_2) - \theta_1\ddot{\theta}_1 - \tfrac{1}{2}\big(\dot{\theta}_1+\dot{\theta}_2+\dot{\theta}_3+\dot{\theta}_4\big)^2 - \big(\dot{\theta}_1+\dot{\theta}_2+\dot{\theta}_3\big)^2 - \big(\dot{\theta}_1+\dot{\theta}_2\big)^2 - \big(\dot{\theta}_1\big)^2\Big) - I_4(\ddot{\theta}_1+\ddot{\theta}_2+\ddot{\theta}_4)\Big] / \Big[\tfrac{c}{4} + \tfrac{c}{4}(\theta_1+\theta_2+\theta_3+\theta_3)^2 + I_3 + I_4\Big] \quad (20)$$

Whilefindingtheequation of motion in the Z axis, it is assumedthattheweight of thefishandthebuoyantforceexertedbythewaterare in balance. Inotherwords, the robot fishstays in balancewhenplaced in thewater. Itsupanddownmovement is providedbytheliftingforcecreatedbythefins on theside. Bymakingthisforcedownward, the robot fish is allowedtosink. Thefin is placed in thecenter of gravity of the robot fish in such a waythat it creates a liftingforce. Solution is realizedusing Newton formulation.

$$F_L = m\ddot{z} \quad (21)$$

Where $F_L$is buoyancycreatedbythefinanddefined as:

$$F_L = C_L\alpha\tfrac{1}{2}\rho c V^2 \quad (22)$$

Where C_L is thecoefficient of buoyancy, α is theangle of attack,ρindicatesthedensity of water,V referstothespeed of thefish, and c representsthewingwidth.

Therequiredforcesaremodeledtosolvetheequations of themotionusingMatlab/Simulinksoftwaregiven in Figure 3.Alsoapart of theequations of themotion is shown in Figure 4.

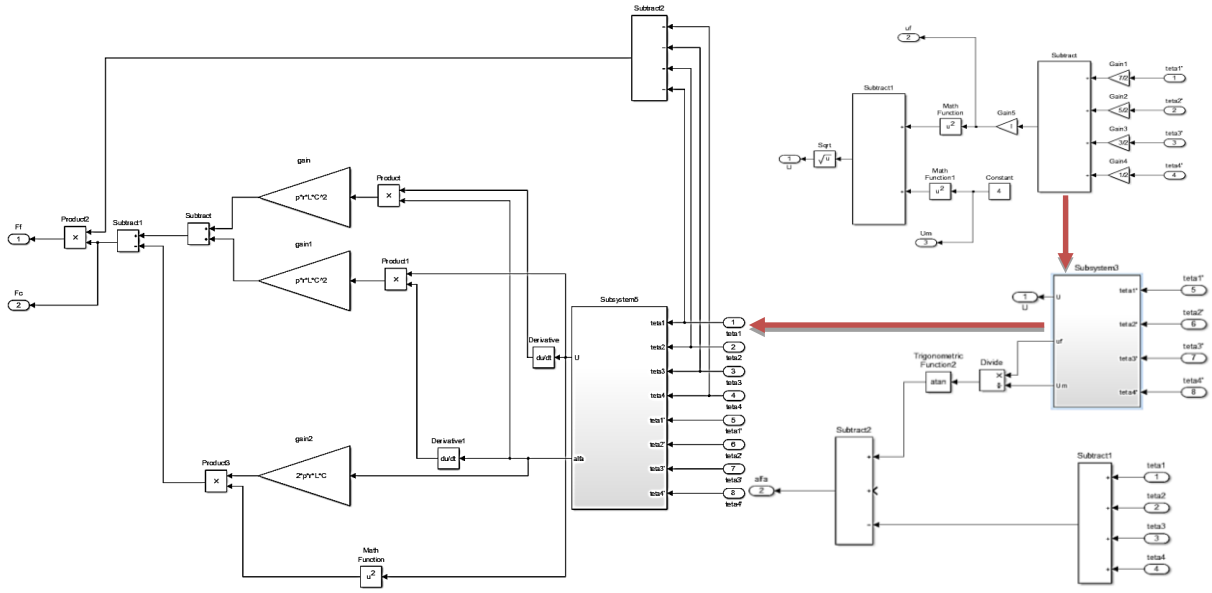

Fig. 3.Themodeling of theforces.

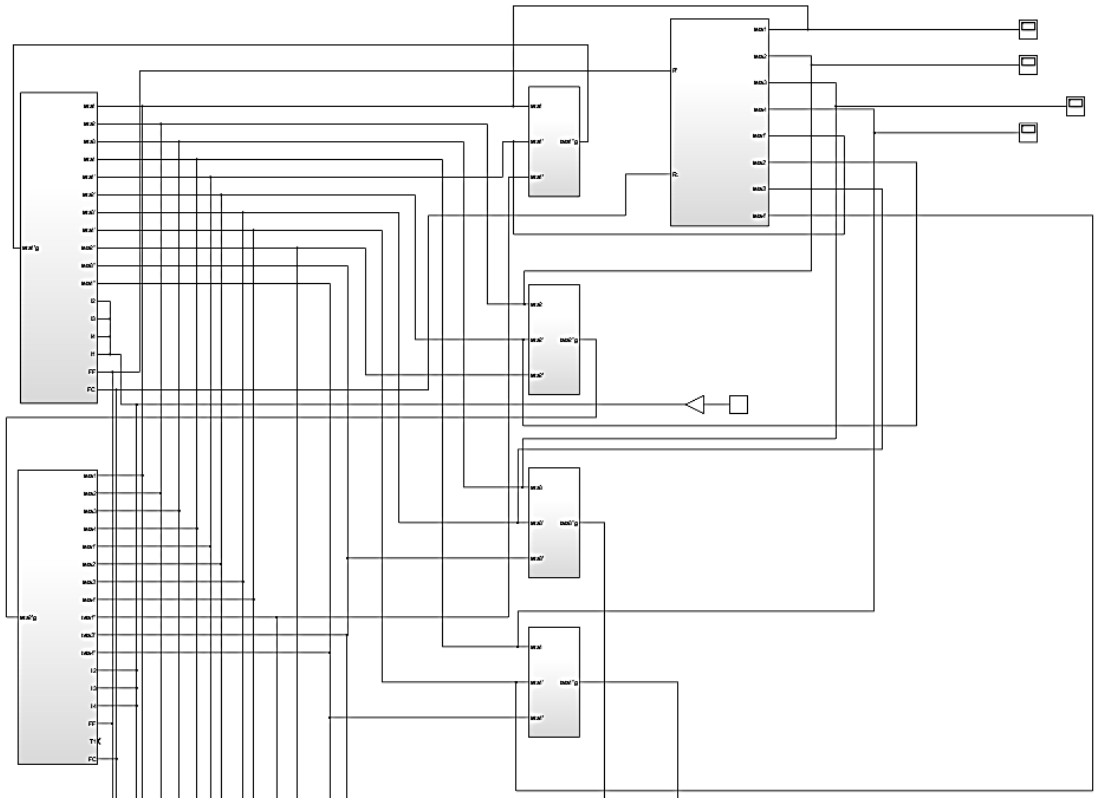

Fig. 4.Themodeling of theequations of themotion.

Indynamicmodeling of theproposed robot fish, theequations of themotion of the robot fish is usedwithMatlab/SimMechanics model torealizedisplacementmotions in x and y axes, rotationmotion in z axis. Thismodelingapproach is given in Figure 5.

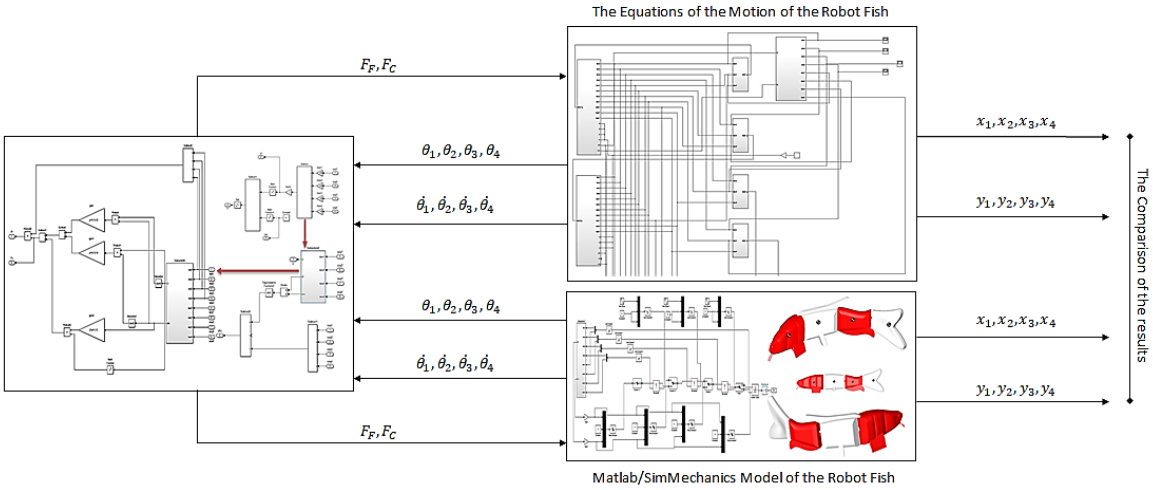

Fig. 5.The dynamicmodelingmethodology of theproposed robot fish model.

III.Results and Disccussion

The proposed carangiform type carp fish robot is simulated using Matlab/SimMechanics software shown in Figure 6and, the parameters of the system is explained in Table 1.

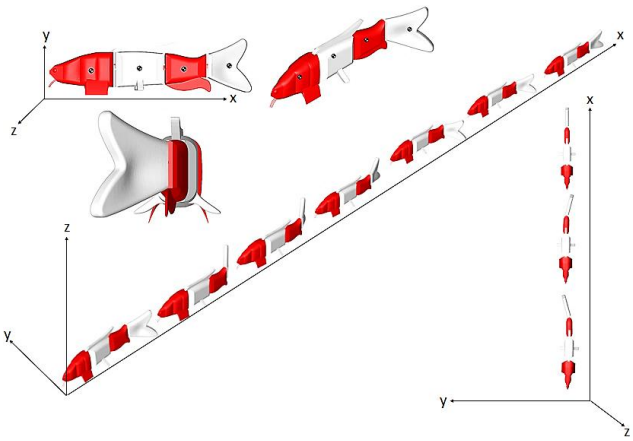

Fig.6.Animations of thesimulations.

TABLE I.Thesystemparameters

Weight	10 kg
Length	0.8 m
Max. Height of the Body	0.23
Max. Width of the Body	0.12

Angleandangularvelocity of the robot fishheadaregivenFigure 7and, Figure 8 showstaildisplacement in y axis. Simulationmeasurementsaretakenfromcenter of thegravity (CG) in allgivengraphicsbetweenFigure 7 andFigure 16. Thedisplacements, velocitiesandaccelerations of the robot head in simulationsaregivenFigures 9-14.

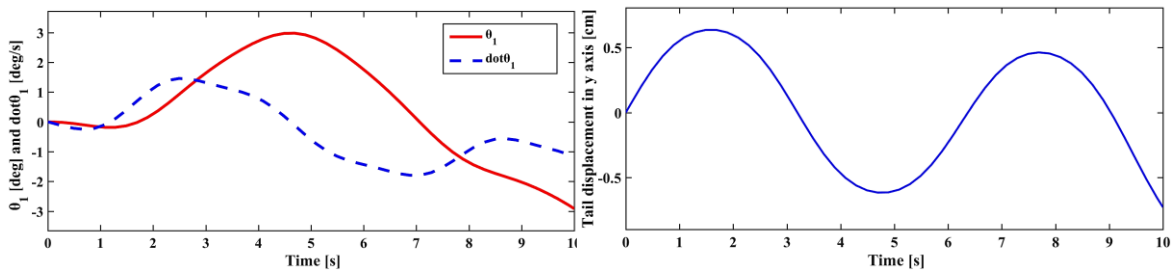

Fig.7.Angleandangularvelocity of the robot fishhead. Fig.8.Taildisplacement in y axis.

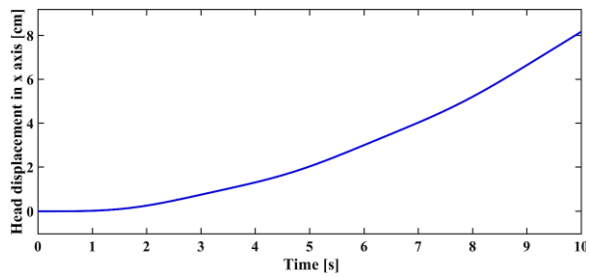

Fig.9.Headdisplacement in x axis.

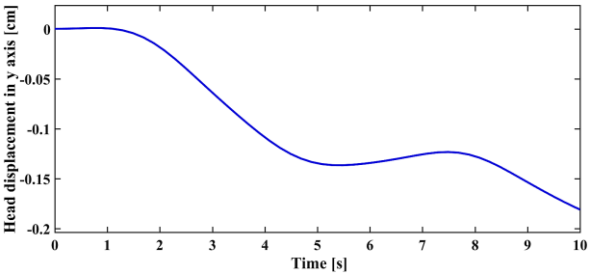

Fig.10.Headdisplacement in y axis.

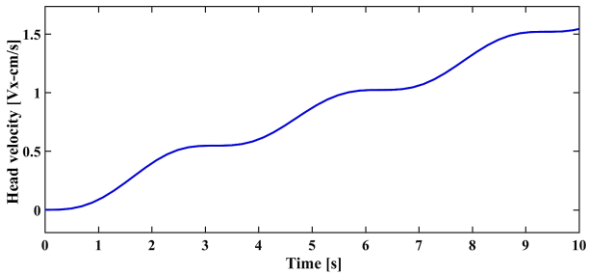

Fig.11.Headvelocity in x axis.

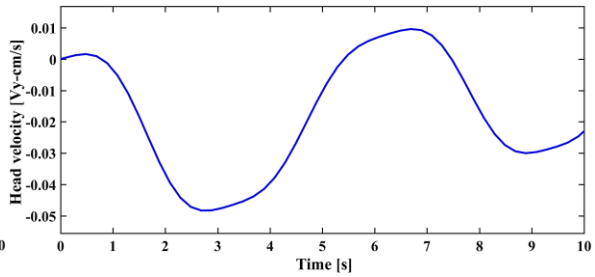

Fig.12.Headveclocity in y axis.

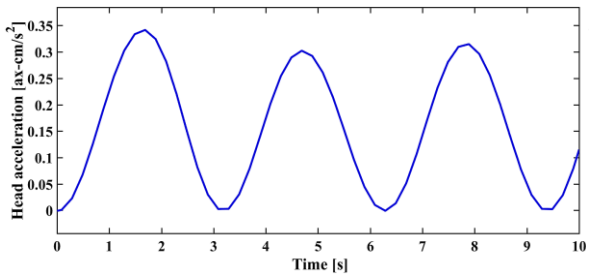

Fig.13.Headacceleartion in x axis.

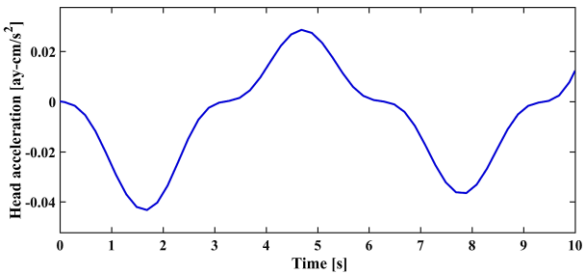

Fig.14.Headacceleration in y axis.

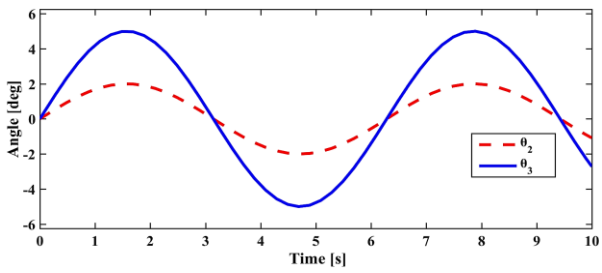

Fig.15.Angles of the rest of the body.

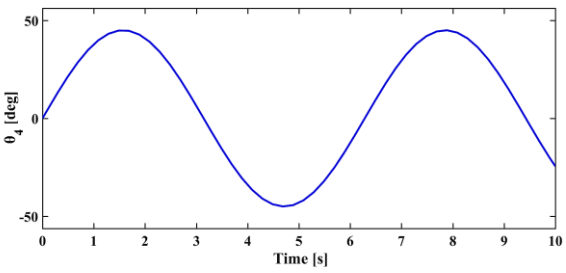

Fig.16.Tailangle of the body.

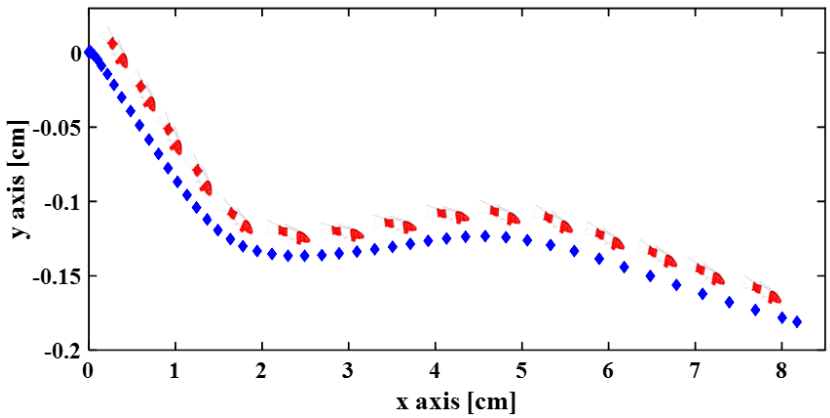

Fig.17.Movement of therobot fish in x and y axes.

Theobtainedangles of the rest of the body in simulationsaregiven in Figures 15-16. Accordingtogivenfigures, theproposed robot fish can movealongthe x and y axiswiththeforcesderivedfromrotatinalmotionaround z axis. Inthesesimulations time is restricted as 10 seconds, otherwisethe robot fishcontinuestoimitatetheswimmingmovement. MoreoverFigure 17 is giventoshowthemovementof the robot fish in the x andy axesmoreclearly. As a result of thesimulations, it can be saidthattheproposed robot fish model acts in both x and y axestoreachthetargetlike a carpfishswimmingmovements.

IV. CONCLUSIONS

In this paper, it is aimed to imitate four degrees of freedom (DOF) of the carangiform type robot fish that is based on the results of previous studies. While determining the spine structure of the robot fish, four joints are designed considering the dimensions of real carp fish and, also the joints are placed in positions where the robot fish can best mimic the movement of the tail. The dynamic equations of the robot fish model are obtained using Lagrange formulation and simulated using Matlab/Simulink/SimMechanics software. According to modeling and simulations results of the proposed study, it is possible to say that the created robot fish model can be developed and used in future control studies.

References

[1] K. Streitlien, G. S. Triantafyllou, M. S. Triantafyllou, Efficient foil propulsion through vortex control, AIAA Journal, vol. 34, pp. 2315−2319, 1996.

[2] J. M. Anderson, Vorticity Control for Efficient Propulsion, Ph.D. dissertation, Massachusetts Inst. Technol, Woods HoleOceanographic Inst. Joint Program, Woods Hole, MA, 1996.

[3] http://www.dac.neu.edu/msc/burp.html, 2004.

[4] S. Guo, T. Fukuda, Norihiko Kato, Keisuke Oguro, Development of underwater microrobot using ICPF actuator, Proceedings of the 1998 IEEE International Conference on Robotics & Automation, pp. 1829−1834, 1998.

[5] N. Kato, Control performance in the horizontal plane of a fish robot with mechanical pectoral fins, IEEE Journal of Oceanic Engineering, vol. 25, no. 1, pp. 121−129, 2000.

[6] http://www.nmri.go.jp/eng/khirata/fish, 2004.

[7] http://www.mhi.co.jp/enews/e 0898.html, 2004.

[8] J. Liang, etc, Researchful development of underwater robofish II–development of a small experimental robofish, Robot, vol. 24, no. 3, 2002.

[9] J. Z. Yu, E.K. Chen, S. Wang, M. TAN, Research evolution and analysis of biomimetic robot fish, Control Theory and Application, accepted in Chinese, 2002.

[10] J. Liu, H.Hu, "A 3D Simulator for Autonomous Robotic Fish", International Journal of Automation and Computing, 1, 2004, 42-50.

[11] D. Korkmaz, "Intelligent Control of Three-Dimensional Motion of the Robotic Fish with CentralPattern Generator",FıratUniversity, PhD Thesis of Electrical and Electronics Engineering Technologies Program, 186 pages.

[12] C. Topakcı, "Robot Fish Design and Control", NecmettinErbakan University, Department of Mechanical Engineering, Graduation project thesis, 2020, 40 pages.

International Journal of Innovation Engineering and Science Research
(ISSN: 2581-4591)
www.ijiesr.com

MatrixRotation Range of Rotary Regenerators for Good Heat Transfer and Acceptable Fluid CarryoverLeakage

Paulo Cesar Mioralli, Guilherme Lanzi Ernandes, Elson Avallone, Paulo Henrique Palota,Claiton Eduardo Luizete, Pablo Sampaio Gomes Natividade
Department of Industry
Federal Institute of São Paulo – IFSP
Catanduva-SP, Brazil

ABSTRACT

Three typical rotary regenerators with both streams under the laminar flow regime are computationally analyzed from changes in matrix rotation. The mass flow rate, the inlet temperatures of gas streams and the geometric dimensions of the regenerators were fixed in the analysis. The ratio of residence time t_{res} of flow on each side of the equipment to the time t_0 required for a complete matrix rotation is calculated for the regenerators, representing the fluid carryover leakage. The convective heat transfer coefficient is obtained from correlation. The heat transfer rate is determined using the Effectiveness-NTU method specific to rotary regenerators. Ranges of the matrix rotation values and the ratio (t_{res}/t_0) that provide good heat transfer rate and acceptable fluid carryover are chosen for each investigated equipment. Additionally, an analysis of the regenerator effectiveness as function of the time required for a complete matrix rotation is presented. The results reveal that the chosen matrix rotation ranges shorten as the size of the rotary regenerator increases and the limit levels of the chosen matrix rotation decrease as the dimensions and typical operating conditions of the rotary regenerators increase.

Keywords—*rotary regenerator; matrix rotation; carryover leakage; computational analysis.*

NOMENCLATURE

A free flow cross-sectional area, m^2
A_m matrix cross-sectional area, m^2
A_T total cross-sectional frontal area $(A+A_m)$, m^2
A_{tr} heat exchange area, m^2
C heat capacity rate of fluids, W/K
C_r matrix heat capacity rate, W/K
C_r^* matrix heat capacity rate ratio on the cold or hot side
c_p specific heat of gas under constant pressure, $J/kg\ K$
c_m specific heat of matrix, $J/kg\ K$
D_h hydraulic diameter, m
e thickness of the plates that constitute the matrix channels, m
h convective heat transfer coefficient, W/m^2K
k thermal conductivity, W/mK
L length of matrix, m
$\dot{m}$ gas mass flow rate, kg/s
m_m mass of matrix, kg
n rotational speed, rpm
NTU number of heat transfer units on the cold or hot side
Nu Nusselt number
P periphery of the channel, m
Pr Prandtl number
Q heat transfer rate, W
Re Reynolds number
r_h hydraulic radius $(D_h/4)$, m
T temperature, K
t_0 time required for a complete matrix rotation, s
t_{res} residence time, s
u fluid velocity in the channel, m/s

Greek Symbols

μ dynamic viscosity, Ns/m^2
ε_0 effectiveness of counterflow heat exchanger
ε_r regenerator effectiveness
φ_r correction factor
ρ fluid density, kg/m^3
σ porosity

Subscripts

i inlet
o outlet
c cold
h hot
min minimum
max maximum

I. INTRODUCTION

The rotary regenerator is a device that receives thermal energy from a hot flow, stores it temporarily in a porous matrix, and releases it to a cold flow. The matrix continuously rotates between the two hot and cold streams that flow in opposite directions. A peculiarity in the operation of rotary regenerators is appointed as fluid carryover leakage. It is an unavoidable carryover of a small fraction of the fluid trapped in the passage to the other fluid stream just after switching of the fluids [1]. This characteristic makes the rotary regenerator suitable for gas-to-gas heat transfer operations with focus in waste heat recovery, often in ventilation and air conditioning systems (HVAC) and thermal power plants. These two areas of application involve different sizes and operating conditions of the equipment. HVAC systems generally require smaller rotary regenerators with faster rotational speeds and thermal power plants demand larger equipment at slower rotational speeds. The matrix rotational speed affects the amount of the heat transferred and the contamination from fluid carryover leakage. Higher rotational speeds lead to larger carryover leakage and lower rotational speeds reduce the heat exchange. Both aspects influence negatively the performance of the equipment.

Analysis of rotary regenerators with attention to the matrix rotation have been conducted by researchers. Some authors investigated the influence of matrix rotational speed on the rotary regenerator effectiveness or heat transfer rate. Ghodsipour and Sadrameli [2] simulated a rotary regenerator by solving a mathematical model and analyzed the effect of dimensionless parameters on the effectiveness of equipment. The maximum effectiveness was estimated as a function of matrix rotational speed and air velocities of streams. Sanaye et al. [3] investigated the optimal operational conditions of an air-to-air rotary regenerator using genetic algorithm. The objective function in the optimization technique was the thermal effectiveness. The matrix rotational speed was used as one of the decision variables. Eljšan et al. [4] presented a mathematical model of a rotary air preheater that allows rotational speed to vary and quantify its influence upon heat transfer in the equipment. The results showed that there is the rotational speed at which the maximum heat transfer is achieved. Rao and Patel [5] and Raja et al. [6] used different algorithms to maximize regenerator effectiveness and minimize regenerator pressure drop. The first authors used the artificial bee colony algorithm for optimization of rotary regenerator and the second researchers investigated a tutorial training and self-learning inspired teaching-learning-based optimization (TS-TLBO) algorithm. In these works, seven and six variables, respectively,were considered for optimization, including the matrix rotational speed. O'Connor et al. [7] studied the effect of the matrix rotation of thermal wheel into a wind tower system on the ventilation rate and heat recovery for a range of rotation speeds between 0-500 rpm. Using computational fluid dynamics analysis, the results showed that the optimum operating range of the rotary thermal wheel could be determined between 5 rpm and 20 rpm. Chen et al. [8] investigated how performance parameters of a rotary heat exchanger such as effectiveness, fluid and metal temperature fields, and ammonium bisulfate deposition area vary with matrix rotational speed using the effectiveness–modified number of transfer units (ε-NTU) method and a finite difference method. They verified that the results calculated by ε-NTU method are greater than those obtained by the finite difference method notably at low matrix rotation. In a few works [9-11], empirical correlations that take into account the effects of rotational speed and matrix heat capacity rate on the regenerator effectiveness were developed.

Other studies that take into account the matrix rotation of rotary regenerators focuses on the analysis of different aspects of the equipment. Zheng at al. [12] showed that the matrix rotational speed is a key control parameter to achieve optimal dehumidifier performance in a desiccant wheel. They also presented results of the effect of isotherm shape, maximum desiccant matrix moisture uptake and number of transfer units (NTU) on the dehumidification performance of the equipment. Buyukalaca and Dogruyol [13] investigated experimentally a rotary regenerator constructed with aluminium plates. The experiments were performed at a range of matrix rotational speed in order to verify the influence of some parameters of the heat exchanger. The results showed that the studied parameters were little affected in the experiments. Wu et al. [14] proposed a numerical algorithm to analyze the influence of variations in rotating speed and other characteristics on dynamic responses of the regenerator. Numerical results were compared with experimental measurements and with theoretical predications of energy efficiencies. Bennhold and Wilson [15] presented a numerical analysis of the thermal behavior of rotary regenerator with the matrix rotating in an indexed fashion. The results indicated significant differences in the patterns of thermal gradient development between the indexing regenerator and the continuously rotating regenerator. Grzebielec et al. [16] showed results from modeling a regenerator that normally does not operate under optimal conditions due to climate changes throughout the year. The authors presented dependence regenerator efficiency as a function of the rotational speed. Ruivo et al. [17] used experimental data measured in an air-handling unit and data provided by the manufacturer software to predict the influence of the matrix rotation speed on the performance of a desiccant wheel. The results revealed that the matrix rotation plays a significant role in affecting the effectiveness parameters of rotary wheel. Duan et al. [18] analyzed

theoretically and experimentally the influence of the operational parameters on contact heat transfer between granular materials and heating plates inside a rotary regenerator. It was verified that the time-average contact heat transfer coefficient increases with the increase of rotational speed and that this time-average follows a positive power law with matrix rotation. Abroshan and Goodarzi [19] modeled a rotary regenerator by combining mathematical modelling and CFD simulations. The equipment was optimized using a genetic algorithm and, among other parameters, optimal matrix rotational speed was obtained to maximize the heat transfer rate and minimize the pressure drop in the regenerator from the introduction of a fuel saving parameter. Rotary regenerators impregnated with a hygroscopic material are often used in air dehumidification and enthalpy recovery applications. Systems with these applications were studied focusing on the matrix rotational speed of desiccant wheels. Researchers [20-27] verified the existence of an optimal rotation speed that implies in better performance for dehumidification. Niu and Zhang [28] calculated the optimum rotary speeds for sensible heat recovery, latent heat recovery and air dehumidification in a desiccant wheel. The results showed that the optimum rotary speed for air dehumidification is much lower than those for enthalpy recovery and that the optimum rotary speed is a function of matrix wall thickness.Nóbrega and Brum [29] developed a simple mathematical model to describe the heat and mass transfers in rotary regenerators and introduced dimensionless parameters in the analysis. They concluded that the enthalpy recovery reaches a maximum point and exhibits a great dependence on the nondimensional period of revolution. A group of researchers has studied the influence of matrix rotation of rotary regenerators operating under frosting conditions. Jedlikowski et al. [30-31] evaluated the effect of rotor speed on the formation of frost area accumulation in the rotary regenerators. Among the analyzed cases, they verified that the increase in rotor speed results in an increase in regenerator effectiveness with simultaneous decrease in the size of the frost area accumulation. Smith and Svendsen [32] developed a short plastic rotary regenerator for single-room ventilation. Even though significant leakage, the experimental results showed that the lower rotational speeds decrease heat recovery, which is required to prevent frost accumulation.

Although many researchers have investigated the effects of matrix rotation on different performance parameters of rotary regenerators, studies assessing the fluid carryover leakage as a function of matrix rotational speed are less available in the literature. Some authors have proposed or used methods to investigate the rotary regenerator performance. The methods considered the matrix rotation and incorporated the effects of carryover leakage [33-34] and the effects of carryover leakage combined with pressure leakage or fluid bypass [35-42]. The aforementioned works covering carryover leakage do not present results that indicates the matrix rotation and fluid contamination levels that are suitable for the rotary regenerator to operate close to the optimum conditions. Regarding studies that present results with greater emphasis on the relationship between carryover leakage and matrix rotational speed, Kay and London [9] warned that the design of rotary regenerators requires the provision of matrix rotation level with minimum carryover leakage. De Antonellis et al. [43] informed that the optimal matrix rotational speed exists because the contamination from the fluid carryover leakage becomes relevant when the matrix rotates too fast. The authors just reported that the typical rotational speed is around 10-20 rpm, depending on airflow rates and geometric characteristics of rotary regenerator. Mioralli [44] numerically analyzed a rotary thermal regenerator using finite volume method. Alhusseny and Turan [45] numerically analyzed the equipment using a porous media approach. Both works showed graphically that the contamination from fluid carryover leakage tends to increase with increasing matrix rotation. The results also confirmed that there are no significant changes in rotary heat exchanger effectiveness after a certain rotational speed level. Chung et al. [46] optimized the design parameters of a plastic rotary regenerator considering leakage and adsorption. The results showed that the effect of carryover leakage on the heat transfer effectiveness of rotary regenerator is small from changes in matrix rotational speed.Despite appreciable efforts has been dedicated to rotary regenerators analysis, a recommendation of minimum and maximum limits for rotational speed and carryover leakage as suitable for good performance of equipment apparently is absent. This work computationally analyzes typical rotary regenerators focusing on three aspects simultaneously: matrix rotational speed, carryover leakage and heat transfer rate. The mainly purpose is to choose minimum and maximum limits for matrix rotation that imply good heat transfer rate and acceptable contamination from fluid carryover leakage. Furthermore, ranges of a parameter that describes the propagation of carryover leakage also are chosen and an analysis of the regenerator effectiveness as a function of the time required for a complete matrix rotation changes is presented.

II. Problem Setting

A. Rotary Regenerator Features

The schematic of the rotary regenerator is show in Fig. 1. Two gas streams are introducedcounterflow-wise through the parallel ducts of the air preheater. Cold gas is injected inside one duct and hot gas inside the other. The porous matrix, that stores energy, continuously rotates through these parallel ducts. The matrix receives heat from the hot gas on one side and transfers this energy to the cold gas on the other side. The matrix channels were assumed smooth. The fluid velocity was considered constant inside each channel.

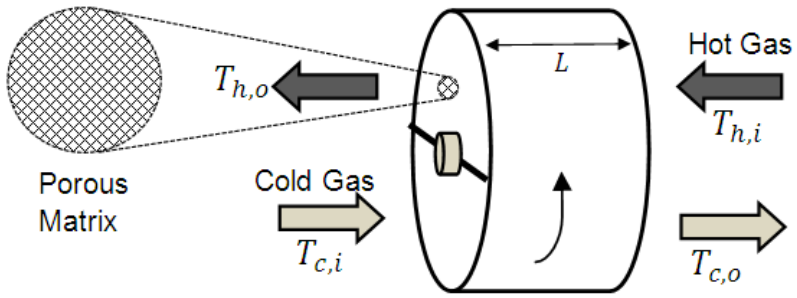

Fig. 1. Schematic of the rotary regenerator.

The actual time that cold gas takes to flow through a hot regenerator matrix is called the cold period and the time that hot gas flows through the cold regenerator matrix is called the hot period. The cold and hot periods are dependent on the matrix rotation. Fig. 2 illustrates a fixed point in the matrix of the regenerator, represented by a channel, which runs through the sides of the cold and hot gas streams during one revolution of the matrix. The parameters t_c e t_h represent the cold and hot periods, respectively.

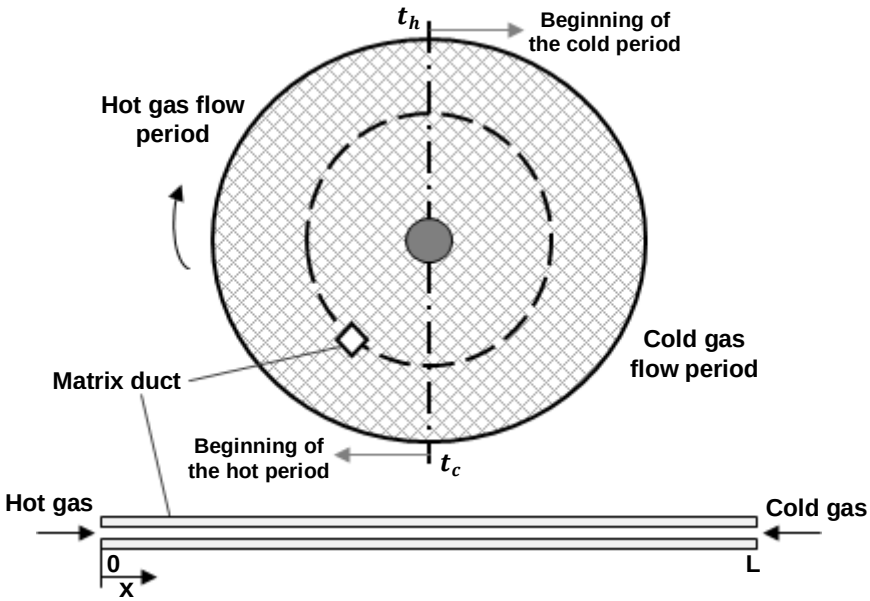

Fig. 2. Cold and hot periods of the rotary regenerator.

Contamination between the fluids streams occurs when an amount of one of the fluids in the matrix passages is lugged from one fluid stream to the other by the rotation of the matrix [37]. For negligible contamination, the time it takes the gas particles to travel through the matrix passages must be sufficiently less than the rotation time of the matrix. Fig. 3 illustrates the contamination from the fluid carryover leakage.

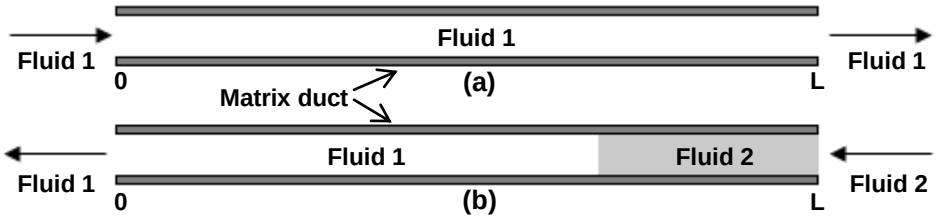

Figure 3. Contamination from the fluid carryover leakage: (a) The end of period 1, (b) The beginning of period 2.

The time of fluid particle passing through the matrix ducts is called the residence time t_{res} defined as the ratio of the length L of the matrix ducts to the bulk stream velocity u in ducts

$$t_{res} = L/u \tag{1}$$

To describe the propagation of carryover leakage, Banks [34] introduced a parameter defined as the ratio of residence time t_{res} of flow on each side to the time t_0 required for a complete matrix rotation.Analysis of typical rotary regenerators operating close to optimal conditions showed that this ratio must be up to 1.5% for negligible contamination between fluids [44], that is

$$\left(t_{res}/t_0\right) \leq 0.015 \tag{2}$$

Geometric parameters of the rotary regenerator can be expressed based on Figs. 1 and 2. The total frontal cross-sectional area A_T is determined by the sum of the free flow cross-sectional area A and the matrix cross-sectional area A_m of the air preheater

$$A_T = A + A_m \tag{3}$$

The matrix porosity σ is defined by the ratio between A and A_T

$$\sigma = \frac{A}{A_T} \tag{4}$$

The hydraulic radius r_h is defined by the ratio between A and the perimeter P of the plates that compose the matrix. The matrix perimeter can be written as function of the matrix cross-sectional area A_m

$$r_h = \frac{D_h}{4} = \frac{A}{P} \tag{5}$$

$$P = \frac{A_m}{(e/2)} \tag{6}$$

where D_h and e are the matrix duct hydraulic diameter and the matrix duct wall thickness, respectively.

The porosity and the hydraulic radius are dependent on each other and influence the thermal exchange in the rotary regenerator. The hydraulic radius can be written as function of the porosity and the matrix duct wall thickness from the definitions above and algebraic manipulations

$$r_h = \frac{\sigma}{1-\sigma}\left(\frac{e}{2}\right) \tag{7}$$

The hydraulic radius is an important parameter and its use is justified in the correlation for Nusselt number. Since the geometric characteristics of the regenerator are known, the heat transfer in the equipment can be calculated using the Effectiveness-NTU method for rotary regenerators.

B. Effectiveness-NTU Method for Rotary Regenerators

The Effectiveness-NTU method for rotary regenerators [9] consists of calculating the effectiveness ε_0 of a conventional counterflow heat exchanger and correcting this effectiveness by a correction

factor φ_r that takes into account the rotational speed and the matrix heat capacity rate of the exchanger. Thus, the effectiveness of the regenerator ε_r is given by

$$\varepsilon_r = \varepsilon_0 \, \varphi_r \tag{8}$$

The effectiveness ε_0 of a conventional counterflow heat exchanger is defined by

$$\varepsilon_0 = \begin{cases} \dfrac{1-exp\left[-NTU\left(1-C^*\right)\right]}{1-C^* exp\left[-NTU\left(1-C^*\right)\right]}; & C^* < 1 \\ \dfrac{NTU}{1+NTU}; & C^* = 1 \end{cases} \tag{9}$$

where C^* is the ratio between the fluids heat capacity rates and NTU is the number of heat transfer units defined as follows

$$C^* = \frac{C_{mim}}{C_{max}} \tag{10}$$

$$NTU = \frac{1}{C_{min}} \left[\frac{1}{\left(1/hA_{tr}\right)_c + \left(1/hA_{tr}\right)_h} \right] \tag{11}$$

where h is the convective heat transfer coefficient and A_{tr} is the matrix thermal exchange area on the side of the hot or cold stream. The parameters C_{mim} and C_{max} correspond to the minimum and maximum values of the fluids heat capacity rates.

The correction factor φ_r in Eq. (8) is given by Buyukalaca and Yilmaz, [11] that provides good results even for very low rotational speeds

$$\varphi_r = \frac{1}{\left[1+3\left(\varepsilon_0 / C_r^*\right)^2 + \left(\varepsilon_0 / C_r^*\right)^4\right]^{1/4}} \tag{12}$$

$$C_r^* = \frac{C_r}{C_{min}} \tag{13}$$

$$C_r = \frac{n}{60} m_m \, c_m \tag{14}$$

where C_r is the matrix heat capacity rate, n is the matrix rotational speed, m_m is the matrix mass and c_m is the specific heat of matrix.

Finally, the total heat transfer Q in the rotary regenerator is obtained in the same way as the Effectiveness-NTU method for conventional heat exchangers

$$Q = \varepsilon_r \, Q_{max} \tag{15}$$

$$Q_{max} = C_{min} \left(T_{h,i} - T_{c,i}\right) \tag{16}$$

where Q_{max} is the maximum possible heat transfer and the term between parenthesis corresponds to the difference between the inlet temperature of the hot stream and the inlet temperature of the cold stream.

C. Hydrodynamic and Thermal Analysis

The hydrodynamic and thermal analysis are performed for each gas stream. The mass flow rate and the inlet temperatures of each gas stream are established in the rotary regenerator. The convective heat transfer coefficient is obtained from correlation for Nusseltnumber Nu. Correlation for smooth ducts with circular cross-sectional area was used based on the hydraulic diameter of matrix ducts considering laminar flow regime. The correlation take into account hydrodynamically fully developed flow with thermal entrance length and constant wall temperature boundary condition.

$$Nu = 3.66 + \frac{0.0668\left(\frac{D_h}{L}\right)Re_{D_h}Pr}{1+0.04\left[\left(\frac{D_h}{L}\right)Re_{D_h}Pr\right]^{\frac{2}{3}}} \tag{17}$$

where Re_{D_h} is the Reynolds number and Pr is the Prandtl number.

The convective heat transfer coefficient h is expressed in terms of Nusselt number

$$h = \frac{Nu\,k}{D_h} \tag{18}$$

where k is the fluid thermal conductivity.

D. Fluid and Matrix Properties

The fluid properties were obtained at the average temperature of each gas stream. The fluid density for gases with moderate values of pressure and temperature is well represented by the equation of state of an ideal gas

$$\rho = \frac{p}{RT} \tag{19}$$

where p is the pressure of fluid, T is the average temperature of gas stream and R is the ideal gas constant. The values of air atmospheric pressure $p = 10^5\,Pa$ and ideal gas constant for air $R = 287\,Nm/kgK$ were assumed.

The dynamic viscosity μ and the thermal conductivity k of fluids can be approximated by the Sutherland equations [47] as follows

$$\frac{\mu}{\mu_0} \approx \left(\frac{T}{T_0}\right)^{3/2}\frac{T_0+S}{T+S} \tag{20}$$

$$\frac{k}{k_0} \approx \left(\frac{T}{T_0}\right)^{3/2}\frac{T_0+S}{T+S} \tag{21}$$

where S is the Sutherland constant temperature, which is characteristic of each gas. Considering air $S = 111\,K$ for dynamic viscosity and $S = 194\,K$ for thermal conductivity. The parameters T_0, μ_0 and k_0 are reference constants whose values are $T_0 = 273\,K$, $\mu_0 = 1.716\cdot 10^{-5}\,Pa\cdot s$ and $k_0 = 0.0241\,W/mK$ for air.

The specific heat of gas under constant pressure c_p is obtained by a polynomial equation [48] for several gases in the temperature range between 300 and 1,000 K

$$\frac{c_p}{R} = \alpha_0 + \beta_0 T + \gamma_0 T^2 + \delta_0 T^3 + \lambda_0 T^4 \tag{22}$$

where $\alpha_0 = 3.653$, $\beta_0 = -1.337\cdot 10^{-3}$, $\gamma_0 = 3.294\cdot 10^{-6}$, $\delta_0 = -1.913\cdot 10^{-9}$ and $\lambda_0 = 0.2763\cdot 10^{-12}$ are the air constants.

The Prandtl number Pr is obtained from the ratio between some fluid properties, as follow

$$Pr = \frac{\mu\,c_p}{k} \tag{23}$$

The matrix properties of the regenerative air preheater were assumed constant. The AISI 1010 low alloy carbon steel and the 2024-T6 aluminum alloy materials were considered for the matrix. Table 1 shows the matrix properties used in this study, where ρ_m is the density of matrix.

Table 1. Matrix properties of the regenerative air preheater.

Material	$c_m\ (J/kg\ K)$	$\rho_m\ (kg/m^3)$
2024-T6 aluminum	875	2,770
AISI 1010 alloy carbon steel	434	7,832

E. Computer Program

A computer program written in *C* programming language was developed for the simulation of rotary regenerator. The *Dev-C++* software was used for compilation and recording results. Three typical sizes of equipment were simulated: small, medium-sized and large. The material AISI 1010 low alloy carbon steel was used for the medium-sized and the large heat exchangers in the simulations. The 2024-T6 aluminum alloy was used for the small regenerator. The total heat transfer in the rotary regenerator and the outlet temperatures of gas streams were calculated for different matrix rotation from the prescribed mass flow rate and inlet temperatures of each gas stream. The other geometric parameters of the equipment were fixed.

An iterative process was used to obtain the fluid flow and the heat transfer. An outlet temperature values of each stream was assumed at the beginning of this process. Then, the fluid properties were evaluated at the average temperature of each gas stream. Based on these properties, the fluid flow and the heat transfer were obtained from correlations and the Effectiveness-NTU method for rotary regenerators. The iterative process continued until convergence of the outlet temperatures for both streams. The whole process was repeated for each assumed rotation value of matrix. The subrelaxation factor 0.5 was used to the convergence of the outlet temperature values. The tolerance for convergence iterative procedure was adjusted as 10^{-3} for the outlet temperatures. The calculations were performed considering the steady-periodic condition of the regenerator, indicating that the temperatures no longer changed in any angular or axial position of the matrix. The schematic diagram of the calculation process is shown in Fig. 4.

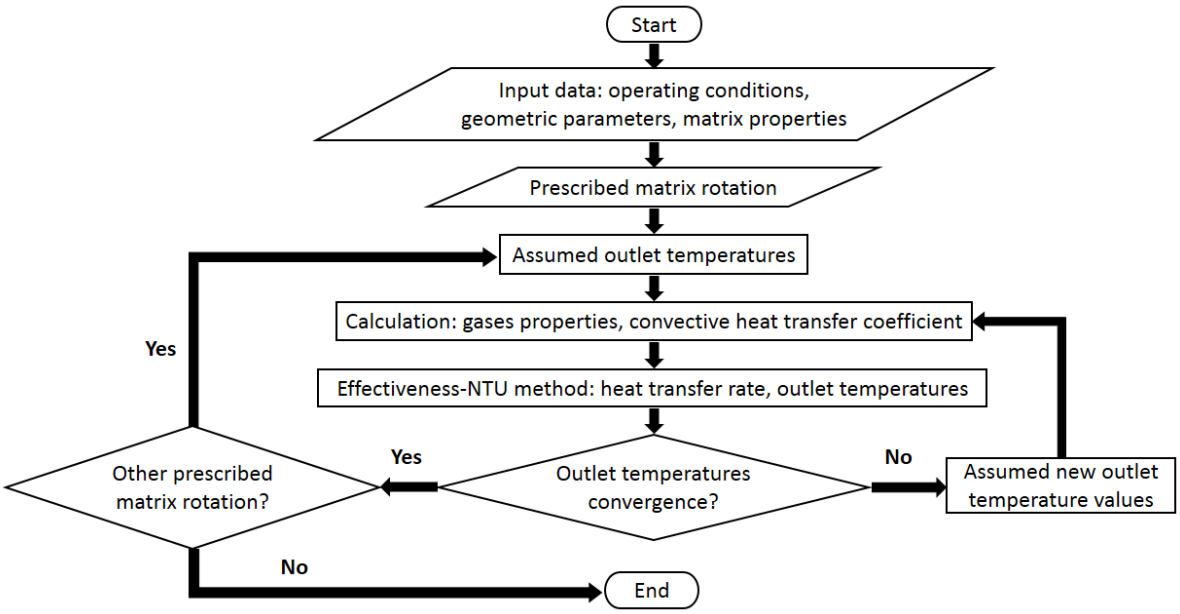

Fig. 4. Schematic diagram of the calculation process.

In order to check the reliability of the developed computer program, the outlet temperatures of gas streams were calculated at a medium-sized rotary regenerator with corrugated ducts. Correlations for corrugated ducts [49] were used for the hydrodynamic and thermal analysis in this case. The results were compared with field data from a rotary regenerator operating in a petroleum refinery. Table 2 shows the comparison between the results of the present study and the field data. It is observed that the results are in reasonable agreement with a greater difference for the hot outlet temperature values. Since the pressure leakage and fluid bypass of rotary regenerator are not considered in this study, this difference could be minimized by including these parameters.

Table 2. Comparison of the present data with field data.

Outlet temperature (°C)	Present work	Field data	Difference
$T_{c,o}$	433.31	405.65	0.068
$T_{h,o}$	164.95	194.27	0.151

III. Results and Discussion

The input data of the developed computer program are listed in Table 3. The operating conditions of the rotary regenerators are based on information from literature and industry. The simulations were carried out from different matrix rotation values and considering the gas streams under the laminar flow regime.

Table 3. Input data for computer program of typical rotary regenerators.

Rotary regenerator	L (m)	e (m)	D (m)	σ	Inlet Temp. (°C)		Flow Rate (kg/s)	
					$T_{h,i}$	$T_{c,i}$	$\dot{m}_h$	$\dot{m}_c$
Small	0.2	0.00035	0.7	0.83	50	20	0.68	0.76
Medium-sized	1.5	0.00050	6.0	0.90	450	80	39.00	49.00
Large	3.5	0.00060	15.0	0.90	600	150	260.00	292.00

Fig. 5 shows the total heat transfer as a function of the matrix rotation for the small rotary regenerator. The total heat transfer changes significantly up to matrix rotation values close to $n = 6.0\,rpm$. As a comparison, the heat transfer rate is $Q \cong 1.5\,kW$ for the matrix rotation $n = 0.1\,rpm$ while $Q \cong 9.6\,kW$ for $n = 6.0\,rpm$. The increase in the heat transfer rate in this case is close to 540%. The heat transfer rate does not change significantly to matrix rotation values greater than $n = 6.0\,rpm$ .Thus, based on Fig. 5, the matrix rotation values $n \geq 6.0\,rpm$ provide high heat transfer rate in the small rotary regenerator. However, this result does not take into account the contamination from the fluid carryover leakage. Fig. 6 shows the ratio (t_{res}/t_0) of both gas streams as a function of the matrix rotation for the small rotary regenerator.Based on the ratio $(t_{res}/t_0) \leq 0.015$, (2), Fig. 6 demonstrates that the matrix rotation values must be less than $n = 17.5\,rpm$ for negligible contamination between fluids in the small rotary regenerator. Finally, the simultaneous analysis of the results observed in Figs. 5 and 6 indicates that the range $6.0 \leq n \leq 17.5\,rpm$ of matrix rotation values can be chosen as suitable for good heat transfer rate and acceptable fluid carryover leakage in the small rotary regenerator.

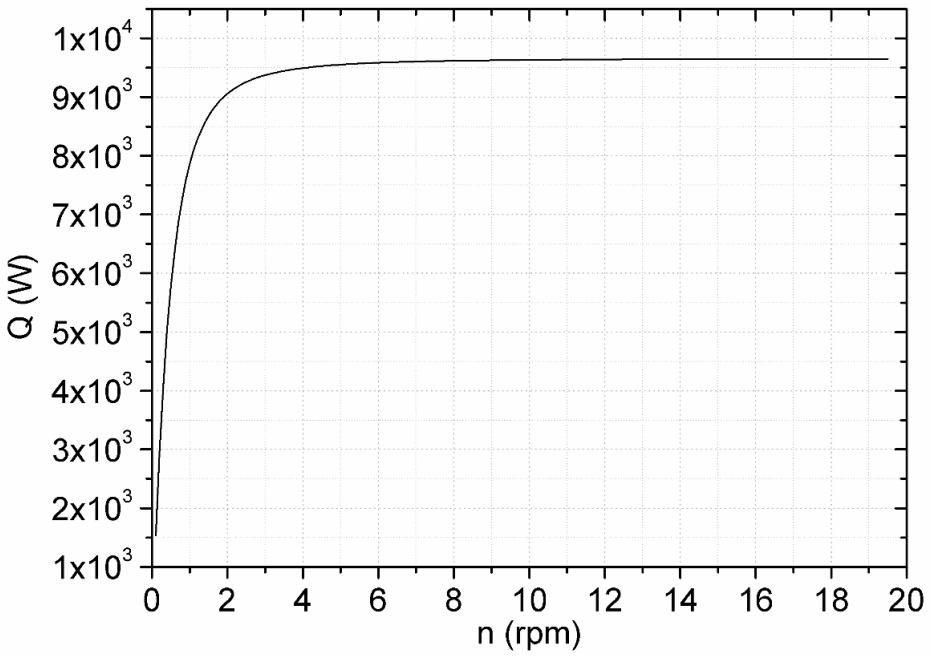

Fig. 5. Heat transfer versus matrix rotation for small rotary regenerator.

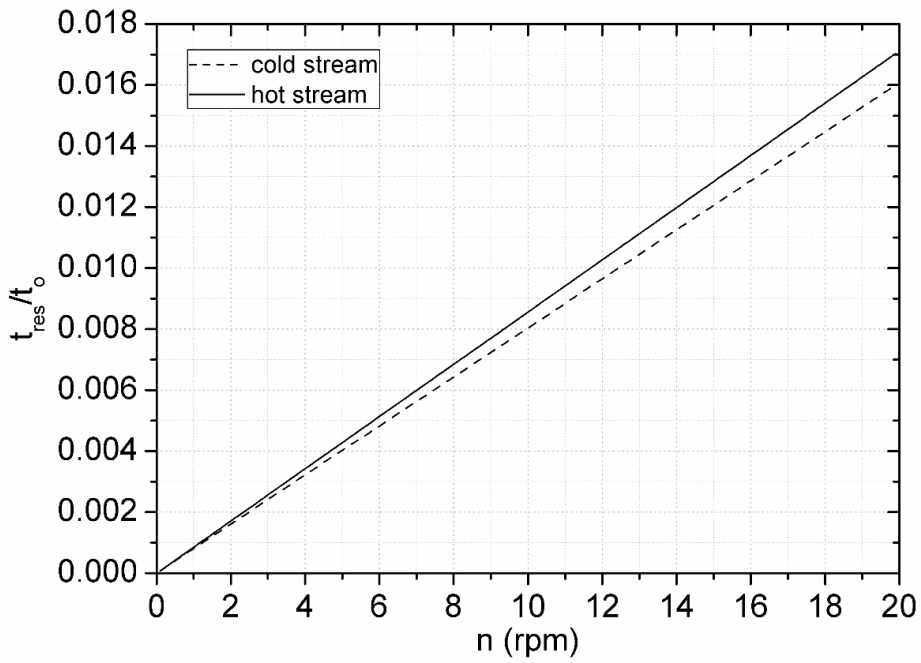

Fig. 6. Contamination from fluid carryover leakage versus matrix rotation for small rotary regenerator.

Fig. 7 shows the total heat transfer as a function of the matrix rotation for the medium-sized rotary regenerator. The total heat transfer changes significantly upto matrix rotation values close to $n = 2.0\,rpm$. It is observed that the heat transfer rate is $Q \cong 5.8\,MW$ for the matrix rotation $n = 0.1\,rpm$ while $Q \cong 9.04\,MW$ for $n = 2.0\,rpm$. In this case, the increase in the heat transfer rate is close to 56%. The heat transfer rate does not change significantly to matrix rotation values greater than $n = 2.0\,rpm$ .Hence, based on Fig. 7, the matrix rotation values $n \geq 2.0\,rpm$ provide high heat transfer rate in the medium-sized rotary regenerator. Taking into account the contamination from the fluid carryover leakage in the medium-sized rotary regenerator, Fig. 8 shows the ratio (t_{res}/t_0) of both gas streams as a function of the matrix rotation. Note that the matrix rotation values must be less than $n = 3.1\,rpm$ for negligible contamination between fluids in Fig. 8, according to (2). Thus, the simultaneous analysis of the results observed in Figs. 7 and 8 shows that the range $2.0 \leq n \leq 3.1\,rpm$ of matrix rotation values can be chosen as suitable for good heat transfer rate and acceptable fluid carryover leakage in the medium-sized rotary regenerator.

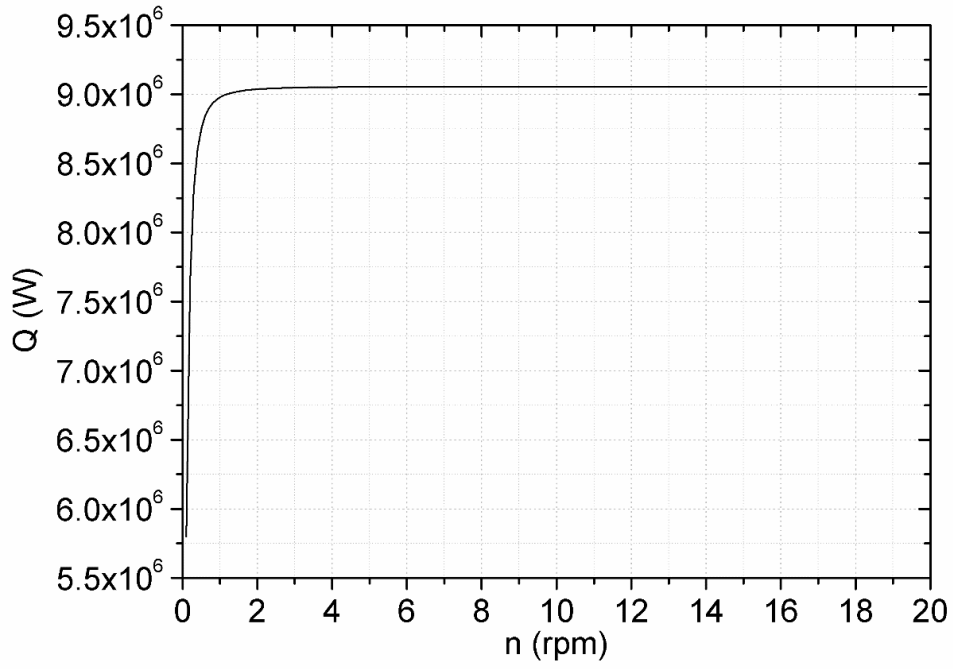

Fig. 7. Heat transfer versus matrix rotation for medium-sized rotary regenerator.

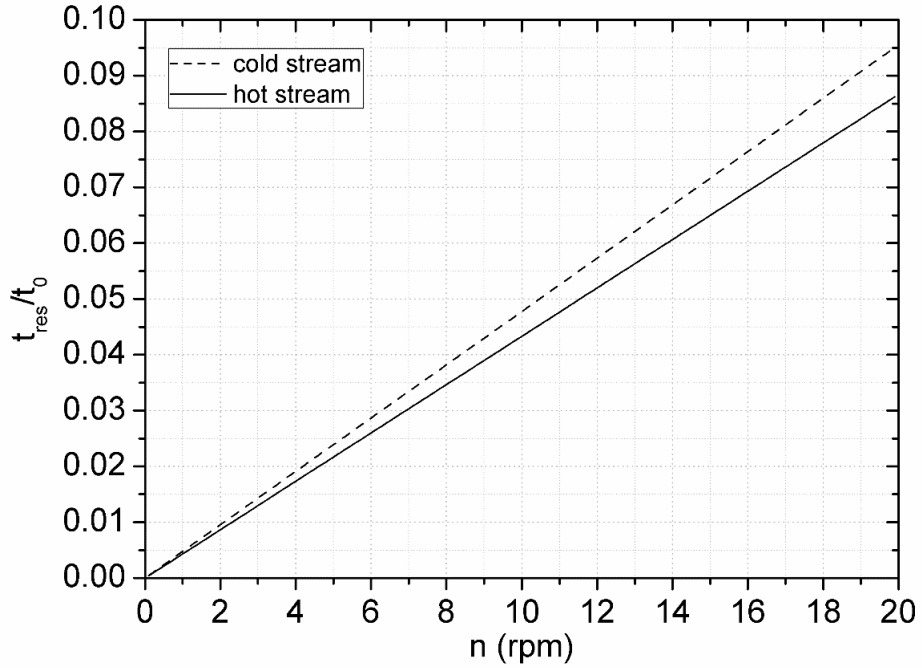

Fig. 8. Contamination from fluid carryover leakage versus matrix rotation for medium-sized rotary regenerator.

Similarly to the analyzed cases for the small and medium-sized rotary regenerators, Fig. 9 shows the total heat transfer as a function of the matrix rotation for the large rotary regenerator. The total heat transfer changes significantly up to matrix rotation values close to $n = 1.4\,rpm$. In this case, the heat transfer rate is $Q \cong 0.07\,GW$ for the matrix rotation $n = 0.1\,rpm$ while $Q \cong 0.084\,GW$ for $n = 1.4\,rpm$, corresponding to an increase in the heat transfer rate close to 20%. The heat transfer rate does not change significantly to matrix rotation values greater than $n = 1.4\,rpm$.Thus, based on Fig. 9, the matrix rotation values $n \geq 1.4\,rpm$ provide high heat transfer rate in the large rotary regenerator. Taking into account the contamination from the fluid carryover leakage in the large rotary regenerator, Fig. 10 shows the ratio (t_{res}/t_0) of both gas streams as a function of the matrix rotation. Considering (2), itis observed that the matrix rotation values must be less than $n = 1.7\,rpm$for negligible

contamination between fluids. The simultaneous analysis of the results observed in the Figs. 9 and 10 shows that the range $1.4 \leq n \leq 1.7\,rpm$ of matrix rotation values can be chosen as suitable for good heat transfer rate and acceptable fluid carryover leakage in the large rotary regenerator.

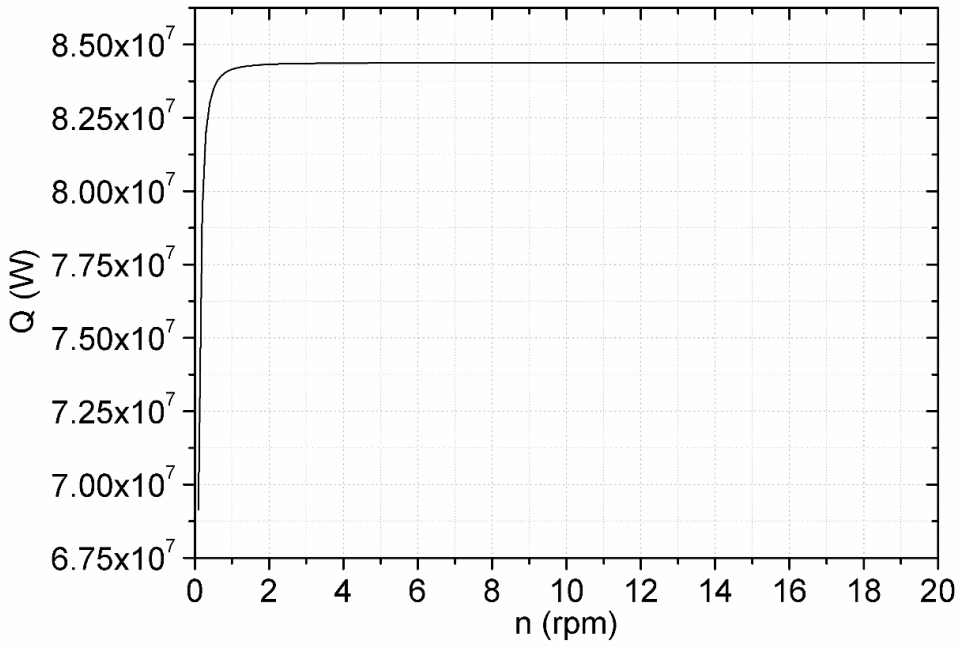

Fig. 9. Heat transfer versus matrix rotation for large rotary regenerator.

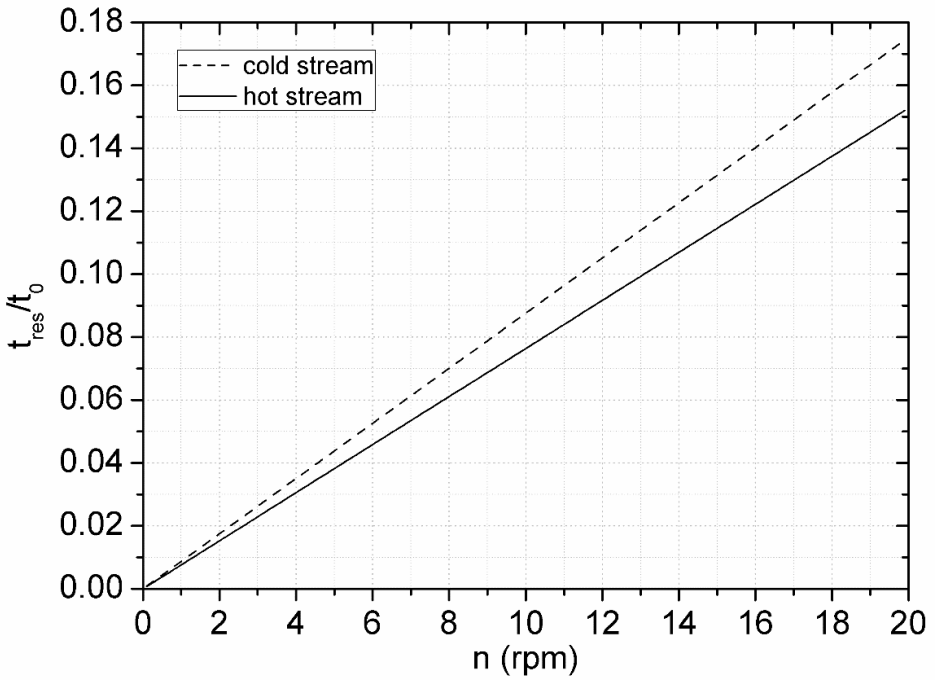

Fig. 10. Contamination from fluid carryover leakage versus matrix rotation for large rotary regenerator.

The analysis of the Figs. 5 to 10 reveals that, when good heat transfer rate and acceptable contamination between fluids are required, the chosen matrix rotation ranges shorten as the size of the rotary regenerator increases. Additionally, these matrix rotation ranges move to the left on the abscissa axis (matrix rotation) as the dimensions and typical operating conditions of the rotary regenerators increase. Another feature is that the chosen matrix rotation range is narrow for the medium-sized and large rotary regenerators whereas it is wide for de small rotary regenerator. The contamination from the fluid carryover leakage in the small equipment is less susceptible as the matrix rotation changes.

The effectiveness of the typical rotary regenerators can be analyzed as a function of the ratio (t_{res}/t_0). The effectiveness of the three rotary regenerators is showed in Fig. 11 as a function of the ratio (t_{res}/t_0) of each gas stream. It is observed that there is a minimum level for this ratio after that the regenerator effectiveness does not change significantly. Since that the $(t_{res}/t_0) \leq 0.015$, (2), for negligible contamination between fluids, a range of (t_{res}/t_0) can be chosen as suitable for good effectiveness and acceptable fluid carryover leakage in the rotary regenerators. Based on Fig. 11, the ranges $0.007 \leq (t_{res}/t_0) \leq 0.015$, $0.008 \leq (t_{res}/t_0) \leq 0.015$ and $0.009 \leq (t_{res}/t_0) \leq 0.015$ for the small, medium-sized and large rotary regenerator, respectively, can be chosen to ensure high effectiveness and acceptable fluid carryover leakage. These ranges are valid for both gas streams of each equipment. Fig. 11 also shows that the maximum effectiveness values of each regenerator are close to $\varepsilon_r = 0.47$, $\varepsilon_r = 0.59$ and $\varepsilon_r = 0.67$ for the small, medium-sized and large rotary regenerator. The maximum effectiveness values for each rotary regenerator are associated with the pre-established operating conditions shown in Table 3.

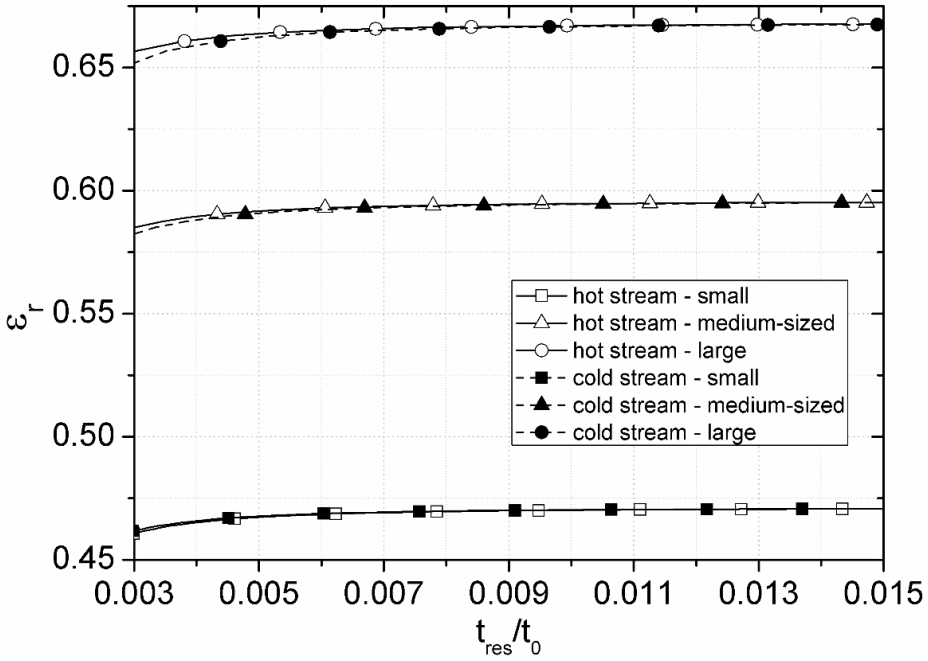

Fig. 11. Regenerator effectiveness versus contamination from fluid carryover leakage.

Fig. 12 shows the effectiveness of the rotary regenerators as a function of the time required for a complete matrix rotation. The effectiveness decreases with increasing time for one matrix revolution in all cases. The decrease in effectiveness has a linear behavior for high t_0 values, which correspond to small matrix rotational speed. The linear behavior can also be seen for small matrix rotation in Figs. 5, 7 and 9. Fig. 12 shows that the decrease in effectiveness is more pronounced for the small regenerator, notably in the interval $10 < t_0 \leq 200\ s$. The effectiveness remains high for a wider range of t_0 in the large regenerator. This range decrease as the size of the regenerator decreases. The effectiveness are high at $t_0 \leq 10\ s$, $t_0 \leq 30\ s$ and $t_0 \leq 45\ s$ for the small, medium-sized and large rotary regenerator, respectively. However, there is a minimum t_0 value, in each simulated case, after that the fluid carryover leakage is acceptable. These values are close to $t_0 \cong 3.4\ s$, $t_0 \cong 19.4\ s$ and $t_0 \cong 35.3\ s$ for the small, medium-sized and large regenerator and theyare associated to the maximum matrix rotation values chosen for acceptable contamination between fluids, as shown in Figs. 6, 8 and 10. Finally, a range of t_0 values can be selected as suitable for good heat transfer rate and acceptable fluid carryover in the simulated typical rotary regenerators. These ranges are $3.4 \leq t_0 \leq 10.0\ s$, $19.4 \leq t_0 \leq 30.0\ s$ and $35.3 \leq t_0 \leq 45.0\ s$ for the small, medium-sized and large rotary regenerator, respectively.

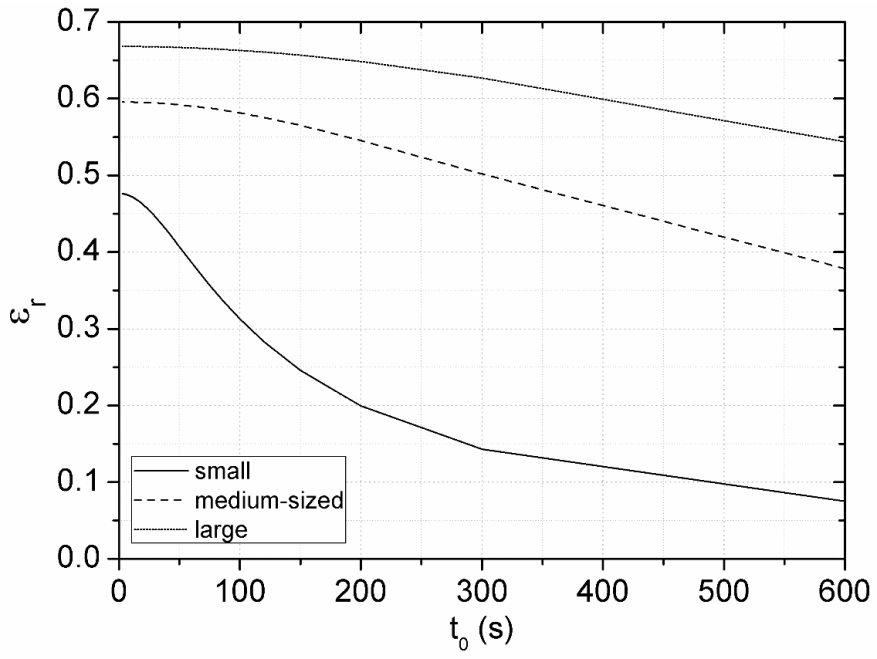

Fig. 12. Regenerator effectiveness versus the time required for a complete matrix rotation.

IV. Conclusion

Typical rotary regenerators were computationally analyzed from the pre-established mass flow rate and inlet temperatures for each gas stream of the equipment and different matrix rotation. The conclusions can be summarized as follows:

- A matrix rotation range that provide good heat transfer rate and acceptable fluid carryoverwas chosen for each simulated typical rotary regenerator.
- The chosen matrix rotation ranges shorten as the size of the rotary regenerator increases. The chosen matrix rotation range is narrow for the large rotary regenerator whereas it is wide for de small rotary regenerator.
- The limit values of the chosen matrix rotation ranges decrease as the dimensions and typical operating conditions of the rotary regenerators increase.
- The propagation of fluid carryover was investigated in the rotary regenerators. A range of the ratio (t_{res}/t_0) for high effectiveness and acceptable fluid carryoverwas also defined for each regenerator.
- Additionally, the range of the time required for a complete matrix rotation that provides high effectiveness and acceptable fluid carryover,was showed for each typical rotary regenerator.
- The decrease in effectiveness is more pronounced in the small regenerator as the time required for a complete matrix rotation increases.
- The results can be used in the prescription of operating conditions of rotary regenerators in search of better performance.

References

[1] R.K. Shah and D.P. Sekulić, *Fundamentals of Heat Exchanger Design* (New Jersey, USA: John Wiley & Sons, 2003).

[2] N. Ghodsipour and M. Sadrameli, Experimental and sensitivity analysis of a rotary air preheater for the flue gas heat recovery, *Appl. Therm. Eng., 23,* 2003, 571–580.

[3] S. Sanaye, S. Jafari and H. Ghaebi, Optimum operational conditions of a rotary regenerator using genetic algorithm, *Energy and Buildings, 40(9),* 2008, 1637-1642.

[4] S. Eljšan, N. Stošić and A. Kovačević, Influence of rotational speed upon heat transfer in a rotary regenerative heat exchanger, *Proc. 12th International Research/Expert Conference "Trends in the Development of Machinery and Associated Technology" TMT*, Istanbul, Turkey, 2008, 26-30.

[5] RV. Rao and V. Patel, Design optimization of rotary regenerator using artificial bee colony algorithm, *Proc. of the Institution of Mechanical Engineers, Part A: Journal of Power and Energy, 225(8),* 2011, 1088-1098.

[6] B.D. Raja, R.L. Jhala and V. Patel, Multi-objective optimization of a rotary regenerator using tutorial training and self-learning inspired teaching-learning based optimization algorithm (TS-TLBO), *Appl. Therm. Eng., 93,* 2016, 456-467.

[7] D. O'Connor, J. Calautit and B.R. Hughes, Effect of rotation speed of a rotary thermal wheel on ventilation supply rates of wind tower, *Energy Procedia, 75,* 2015, 1705–1710.

[8] X. Chen, D. X.N. Duan, L.M. Wang, Y. Yang, D.D. Wang, Y.P. Chen, G.M. Zhu and.F. Che, Influence of rotational speed on thermal performance of tri-sector rotary regenerative air preheater, *American Society of Mechanical Engineers ASME - Power Conference, POWER 2016, collocated with the10th International Conference on Energy Sustainability and the 14th International Conference on Fuel Cell Science, Engineering and Technology*, Charlotte, North Carolina, USA, 2016, Paper No. POWER2016-59551.

[9] W.M. Kays and A.L. London, *Compact Heat Exchangers* (New York, USA: McGraw-Hill, 3rd, 1964).

[10] P. Worsϕe-Schmidt, Effect of Fresh Air Purging on the Efficiency of Energy Recovery from Exhaust Air in Rotary Regenerators, *Rev. Int. Froid., 14,* 1991, 233-239.

[11] O. Buyukalaca and T. Yilmaz, Influence of Rotational Speed on Effectiveness of Rotary-Type Heat Exchanger, *Journal of Heat and Mass Transfer, 38,* 2002, 441-447.

[12] W. Zheng, W.M. Worek and D. Novosel, Control and optimization of rotational speeds for rotary dehumidifiers, *ASHRAE Transactions, n pt 1,* 1993, 825-833.

[13] O. Buyukalaca and E. Dogruyol, Influence of the rotation speed of a rotary regenerator on performance, *Turkish Journal of Engineering & Environmental Sciences, 22(4),* 1998, 315-322. Language: Turkish.

[14] Z. Wu, R.V.N. Melnik and F. Borup, Model-based analysis and simulation of regenerative heat wheel, *Energy and Buildings, 38(5),* 2006, 502–514.

[15] F. Bennhold and D.G. Wilson, Thermal gradients in discontinuously rotated rotary regenerative heat exchangers, *Proc. of the ASME Turbo Expo: Power for Land, Sea and Air, 5,* 2009, 323-330.

[16] A. Grzebielec, A. Rusowicz and A. Rucinski, Analysis of the performance of the rotary heat exchanger in the real ventilation systems, *Proc. of the 9th Conference Environmental Engineering. Selected Papers,*2014, Paper No. enviro.2014.259.

[17] C.R. Ruivo, G. Angrisani and F. Minichiello, Influence of the rotation speed on the effectiveness parameters of a desiccant wheel: an assessment using experimental data and manufacturer software, *Renewable Energy, 76,* 2015, 484–493.

[18] L. Duan, C. Qi, X. Ling and H. Peng, The contact heat transfer between the heating plate and granular materials in rotary heat exchanger under overloaded condition, *Results Phys., 8,* 2018, 600–609.

[19] H. Abroshan and M. Goodarzi, Optimization of a three-layer rotary generator using genetic algorithm to minimize fuel consumption, *Journal of Mech. Eng. and Sci., 14(1),* 2020, 6304–6321.

[20] L.Z. Zhang and J.L. Niu, Performance comparisons of desiccant wheels for air dehumidification and enthalpy recovery, *Appl. Therm. Eng., 22,* 2002, 1347–1367.

[21] C.Q. Zhai, *Performance Modeling of Desiccant Wheel Design and Operation*, PhD thesis, Carnegie Mellon University, Pittsburgh, USA, 2008.

[22] C.R. Ruivo, J.J. Costa, A.R. Figueiredo and A. Kodama, Effectiveness parameters for the prediction of the global performance of desiccant wheels e an assessment based on experimental data, *Renewable Energy, 38,* 2012, 181-187.

[23] R. Tu, X.H. Liu and Y. Jiang, Performance comparison between enthalpy recovery wheels and dehumidification wheels, *Int. Journal of Refrigeration, 36,* 2013, 2308-2322.

[24] A. Kodama, M. Goto, T. Hirose and T. Kuma, Experimental study of optimal operation for a honeycomb adsorber operated with thermal swing, *Journal Chem. Eng. Jpn., 26(5),* 1993, 530-535.

[25] A. Kodama, M. Goto, T. Hirose and T. Kuma, Temperature profile and optimal rotation speed of a honeycomb rotor adsorber operated with thermal swing, *Journal Chem. Eng. Jpn., 27(5),* 1994, 644-649.

[26] A. Kodama, M. Goto, T. Hirose and T. Kuma, Performance evaluation for a thermal swing honeycomb rotor adsorber using a humidity chart, *Journal Chem. Eng. Jpn., 28(1),* 1995, 19-24.

[27] A. Kodama, A. Hirayama, M. Goto, T. Hirose and R.E. Critoph, The Use of Psychrometric Charts for the Optimisation of a Thermal Swing Desiccant Wheel,*Appl. Therm. Eng., 21,* 2001, 1657-1674.

[28] J.L. Niu and L.Z. Zhang, Effects of wall thickness on the heat and moisture transfer in desiccant wheels for air dehumidification and enthalpy recovery, *International Communications in Heat and Mass Transfer, 29(2),* 2002, 255-268.

[29] C.E.L. Nóbrega and N.C.L. Brum, Modeling and simulation of heat and enthalpy recovery wheels, *Energy, 34,* 2009, 2063–2068.

[30] A. Jedlikowski, S. Anisimov, P. Kanaś and M. Skrzycki, The influence of rotor speed on the formation of frost accumulation zone inside the rotary heat exchangers,*Proc. of the 17th international scientific conference "indoor air quality and environment",* Volgograd, Russia, 2019, 87-89.

[31] A. Jedlikowski, S. Anisimov, P. Kanaś and S. Anisimov, Heat and mass transfer inside the rotary heat exchanger operating under high speed rotor conditions, *International Journal of Heat and Mass Transfer, 152,* 2020, 119558.

[32] K.M. Smith and S. Svendsen, Development of a plastic rotary heat exchanger for room-based ventilation in existing apartments, *Energy and Buildings, 107,* 2015, 1-10.

[33] G.H. Kopfler, *The design of periodic-flow heat exchangers for gas turbine engines*, Technical Report HE-1, Dept. of Mechanical Engineering, Stanford University, Stanford, CA, 1969.

[34] P.J. Banks, Effect of fluid carryover on regenerator performance, *Journal of Heat Transfer, 104(1),* 1982, 215-217.

[35] D.B. Harper, Seal leakage in the rotary regenerators and its effect on rotary regenerator design for gas turbines, *Trans. ASME, 79,* 1957, 233-245.

[36] P.J. Banks and W.M.J. Ellul, Predict effects of by-pass flows on regenerator performance, *The Institution of Engineers, Australia, Mechanical and Chemical Engineering Transactions, M09,* 1973, 10-14.

[37] R.K. Shah, Thermal design theory for regenerators, in S. Kakaç, A.E. Bergles and F. Mayinger (Ed.), *Heat Exchangers: Thermal Hydraulic Fundamentals and Design,* (Washington, DC: Hemisphere, 1981) 721-763.

[38] R.K. Shah, Counterflow rotary regenerator thermal design procedures, in R.K. Shah, E.C. Subbarao and R.A. Mashelkar (Ed.), *Heat Transfer Equipment Design,* (Washington, DC: Hemisphere, 1983) 267-296.

[39] P.J. Banks, The representation of regenerator fluid carryover by bypass Flows, *Trans. ASME, 106,* 1984, 216-220.

[40] K.C. Leong, K.C. Toh and S.H. Wong, Microcomputer-based design of rotary regenerators, *Heat Recovery Systems & CHP, 11(6),* 1991, 461-470.

[41] R.K. Shah and T. Skiepko, Influence of leakage distribution on the thermal performance of a rotary regenerator, *Appl. Therm. Eng., 19(7),* 1999, 685-705.

[42] X. Wu, H. Ye, J. Wang, J. He and J. Yang, Effectiveness analysis and optimum design of the rotary regenerator for thermophotovoltaic (TPV) system, *Frontiers in Energy, 6(2),* 2012, 193-199.

[43] S. De Antonellis, M. Intini, C.M. Joppolo and C. Leone, Design optimization of heat wheels for energy recovery in HVAC systems, *Energies, 7,* 2014, 7348–7367.

[44] P.C. Mioralli, *Heat transfer in a rotary regenerator with fixed pressure drop*, doctoral thesis, Faculty of Mechanical Engineering, State University of Campinas, Brazil, 2009. Language: Portuguese.

[45] A. Alhusseny and A. Turan, An effective engineering computational procedure to analyse and design rotary regenerators using a porous media approach, *International Journal of Heat and Mass Transfer, 95,* 2016, 593–605.

[46] H.J. Chung, J.S. Lee, C. Baek, H. Kang and Y. Kim, Numerical analysis of the performance characteristics and optimal design of a plastic rotary regenerator considering leakage and adsorption, *Appl. Therm. Eng., 109,* 2016, 227–237.

[47] F.M. White, *Viscous Fluid Flow* (New York, USA: McGraw-Hill, 1974).

[48] K. Wark, *Thermodynamics* (New York, USA: McGraw-Hill, 4th, 1983). Based in NASA SP-273. U. S. Government Printing Office: Washington, 1971.

[49] P.C. Mioralli, *Thermal analysis of a rotary regenerator*, master diss., Faculty of Mechanical Engineering, State University of Campinas, Brazil, 2005. Language: Portuguese.

International Journal of Innovation Engineering and Science Research
(ISSN: 2581-4591)

www.ijiesr.com

Modeling of Soil Erosion from Rains and Wind Using Remote Sensing andGeographic Information Systems

Ayhan CAMUROGLU
Lüleburgaz MunicipalityParksandGardensDirectorate,
Kırklareli Turkey

Selcuk ALBUT
TekirdagNamik Kemal University, AgriculturalFaculty
Department of BiosystemsEngineering
Tekirdag -Turkey

ABSTRACT

Soil erosion is a growing problem especially in areas of agricultural activity where soil erosion not only leads to decreased agricultural productivity but also reduces water availability. Revised Universal Soil Loss Equation (RUSLE) is the most popular empirically based model used globally for erosion prediction and control. Remote sensing and GIS techniques have become valuable tools,especially when assessing erosion at larger scales due to the amount of data needed and the greater area coverage. The present study area is a part of the Thracian region with undulating topography, with a risk of soil erosion. In the present study, an attempt has been made to assess the annual soil loss caused by water and wind in the province of Krklareli using RUSLE in GIS framework. Such information can be of immense help in identifying priority areas for the implementation of erosion control measures. The soil erosion rate was determined as a function of land topography, soil texture, land use/land cover, rainfall erosivity, and crop management, and practice in the province using the Revised Universal Soil Loss Equation (for Kırklareli), remote sensing and GIS techniques. The rainfall erosivity R-factor of RUSLE was found from 40,48-375,00 and the soil erodibility K-factor varied from 0,00 -0,40. Elevations in the province varied between 10 and 1031 m having LS factor values ranging from 0 –17,34. The C factor was found using the CORINE 2018 data. The P-value was computed from existing cropping patterns in the province. The annual soil loss estimated in the province using RUSLE is 10,0 ton/ha/yr.

Keywords*Soil erosion, RUSLE, Kırklareli, CORINE, QGIS*

I. INTRODUCTION

Today, soil degradation with erosion due to rainfall and wind is a serious problem especially in developing tropical and subtropical countries. Erosion is a natural geomorphic process that occurs continuously on the earth's surface. However, the acceleration of this process by anthropogenic degradation can have serious effects on soil and environmental quality.

56% of our country consists of mountainous lands [1]. Turkey's topography and climatic dynamics of this aspect, it is quite susceptible to erosion formation. In order to take control measures, which have an important place in combating erosion, areas where erosion is effective should be determined quickly. Erosion studies carried out on large lands with methods based on traditional land surveys are labor-intensive and costly and take a long time [2].

In the light of the developments in technology, mostly Remote Sensing (RS) and Geographic Information System (GIS) techniques have been used in agriculture. Determining the amount and distribution of available agricultural land in agricultural activities plays an important role in better planning of the country's agriculture [3].

Soil erosion has negative economic and environmental effects [4]. The economic impacts are due to the loss of farm income due to the decrease in on-site and off-site incomes and other damages affecting the plant / animal production negatively. Soil erosion has both on-site and off-site effects on productivity. In situ efficiency loss of soil erosion is due to three reasons. The first of these is short-term productivity losses and these are factors such as loss of crop yield, loss of seeding, loss of input (seed, fertilizer), loss of water, additional tillage, time loss due to delayed planting. The second is long-term productivity losses and these are losses such as top soil loss, decrease in soil structure, decrease in soil organic matter content, soil cultivation erosion. The third factor is the reduction in land / soil quality, and these are factors such as temporary decrease in land / soil quality, temporary pollution of surface water by chemicals from sediment. The non-situational economic impact of soil erosion also depends on three reasons. The first of these is seedling deaths due to short-term effects, flooding of the low floor area, chemical effects on seedlings, delayed planting. Its long-term effects are the burying of top soil by infertile soils, change in drainage conditions and changing the slope with tillage erosion. The third and last effect is the reduction in land / soil quality, including temporary decrease in land / soil quality due to floodplains, changes in the soil-water regime and water layer, and additional water management (irrigation, drainage, etc.).

Obtaining agricultural land, excessive and irregular grazing, destruction of forests, etc. anthropogenic impact and erosion is accelerated by the increasing violence in Turkey Besides the natural factors [5].

Erosion is one of the important environmental problems that our country has to tackle. While erosion is observed in an area of approximately 25 million hectares per country in the European Union countries, 57 million hectares are seen in our country. Although erosion is considered as an ecological problem alone, it occasionally causes hunger and migration. Approximately 500 million tons of fertile soil is lost every year. It reveals how great a threat erosion is for our country, that 99% of our soils are affected by water erosion and 1% by wind erosion [6].

In this study, databases of erosion caused by precipitation and wind in Kırklareli province will be created. All data will be processed using Remote Sensing and Geographical Information System software (QGIS) and the results obtained will be accessed on the internet. The first part of the study, which consists of three main parts, includes source research and definitions. In the second part, the material and method used in the study are explained. In the third part, the results obtained in the study were summarized, suggestions were made and presented for discussion.

II. Material and Method

Research area is Kırklareli province, and human-induced land degradation, such as industrialization and urbanization, continues to grow day by day due to multifaceted socio-economic and environmental factors. For these reasons, the research area was chosen in the province of Kırklareli on the grounds that it will serve as a model for evaluating the current soil erosion risk and soil erosion situation due to possible water and wind use of remote sensing and geographical information systems. Place, northwest of Turkey, is on the European continent in the Marmara region of Turkey and is situated in cut Thrace. Because of its position in the country, it is situated between 41°13'34"and 42°05'03" northern latitudes and 26°54'14"and 28°06'15" east longitudes. The elevation is 203 metres. The province has 6,466.85 km2 of land area. Bulgaria is 58 km from the East with a frontier range of 159 km from the north. It is surrounded by the coastlength of the Black Sea, Edirne from the west, Istanbul from the southeast and Tekirdağ from the South (Fig.1). In these municipalities there are 8 districts, 21 counties, 108 districts and 179 villages, according to TURKSAT data of 01 February 2019.

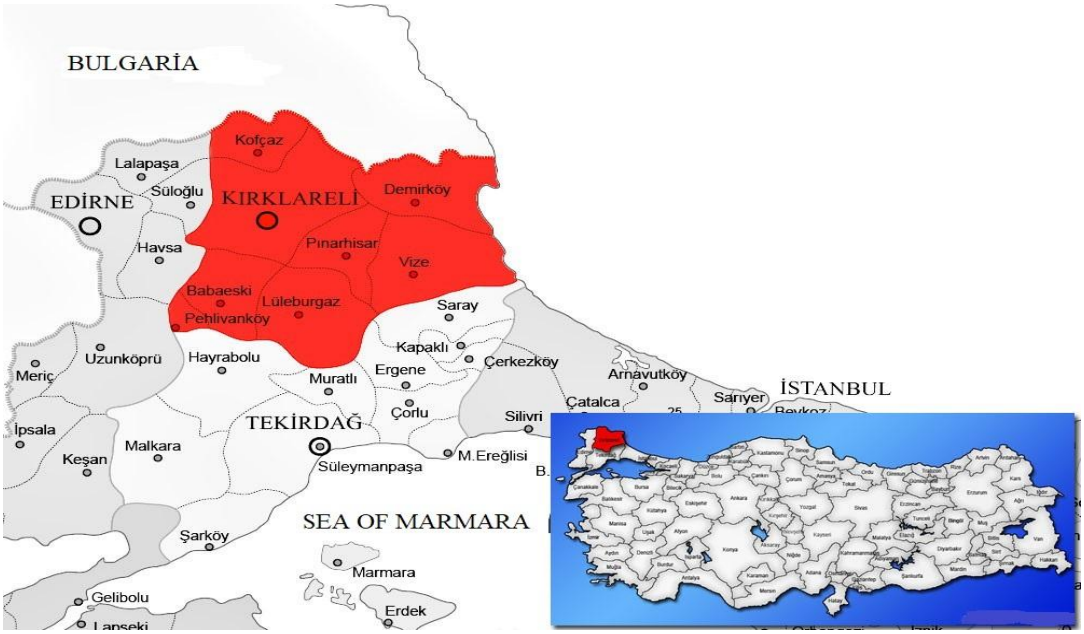

Fig.1. Kırklareli province location map

A. *What is QGIS & Why QGIS?*

From the QGIS website, "QGIS is a user friendly Open Source Geographic Information System (GIS) licensed under the GNU General Public License. QGIS is an official project of the Open Source Geospatial Foundation (OSGeo). It runs on Linux, Unix, Mac OSX, Windows and Android and supporting various vector, raster, and database formats and functionalities.". That means the code is available for you to read or modify, should you choose to, but you don't have to. QGIS is an open source, community-driven desktop GIS software that allows users to visualize and analyze spatial data in a variety of ways. There are many reasons to use QGIS, but here are a few:

- It's a robust, powerful desktop GIS
- Runs on all major platorms: Mac, Linux, & Windows
- Free of charge, all access (no paid add-ons or extensions)
- Frequent updates & bug fixes
- Responsive, enthusiastic community
- Integration with other geospatial tools & programming languages like R, Python, & PostGIS
- Access to analysis tools from other established software like GRASS and SAGA
- Native access to open data formats like geo JSON & Geo Package

Comes in a more than 40 languages, making it easier to work with a larger variety of colaborators [7], [8].

B. *CORINE Land Cover Data*

The pan-European component is coordinated by the European Environment Agency (EEA) and produces land cover / land use (LC/LU) information in the CORINE Land Cover data, High Resolution Layers, Biophysical parameters and European Ground Motion Service [9]. The CORINE Land Cover is provided for 1990, 2000, 2006, 2012, and 2018. This vector-based dataset includes 44 land cover and land use classes. The time-series also includes a land-change layer, highlighting changes in land cover and land-use. The high-resolution layers (HRL) are raster-based datasets which provides information about different land cover characteristics and is complementary to land-cover mapping (e.g. CORINE) dataset (Table-1) [9].

C. Preparation of Data Elevation Model (DEM) Map

The Kırklareli DEM maps were created using NASA-ALOS satellite images. The plugin "SRTM Downloader" in QGIS was used to prepare DEM maps for Kırklareli province. The resolution of the ALOS satellite images, consisting of 5 sections that cover the entire Kırklareli province, is 16.5x16.5 m. With the aid of the "Raster / Miscellaneus / Merge" command, DEM images, each consisting of 5 pieces, were combined as one object. In the next step, with the aid of the vector-based layer map showing the provincial borders of Kırklareli, the DEM map was determined with the command "Raster / Extraction / Clip Raster By Mask Leyer" according to the provincial borders (Fig.2).

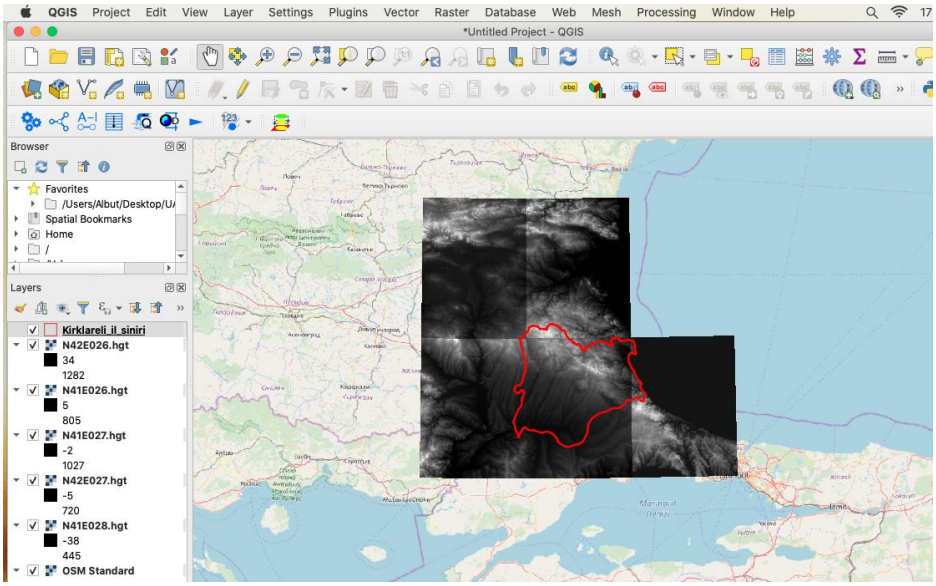

Fig.2. Preparation of Kırklareli DEM map

D. *Potential Estimation of Soil Loss Distribution (A)*

According to the RUSLE model, the potential soil loss of the area was multiplied by placing it in the GIS method and thus the potential soil loss of the Kırklareli province was estimated as (ton / ha / yr) (1).

$$A = R * K * LS * P * C \quad (1)$$

In GIS environment, the factor of slope and slope length (LS), precipitation erosion factor (R), soil erosion sensitivity factor (K), plant management factor (C), and soil protection measure factor (P) was obtained as one sheet. Soil loss suitable for agricultural production is 10 tons/ha/yr according to Morgan (1995). This tolerable amount has been taken into account when determining soil loss rates for the classes.

The primary method of this research is the modeling of the soil erosion process based on the integrated RUSLE equation using the Open Source GIS technique (using QGIS software and its add-ons). The QGIS software is used in particular to prepare and standardize certain input data; the GRASSGIS plugin also fulfills the key tasks of analysis, estimation, creation, transformation, incorporation of map coefficients into the model, statistics, current situation, potential erosion. The flow diagram for the following research method is shown in Fig. 3 [10], [11], [12], [13].

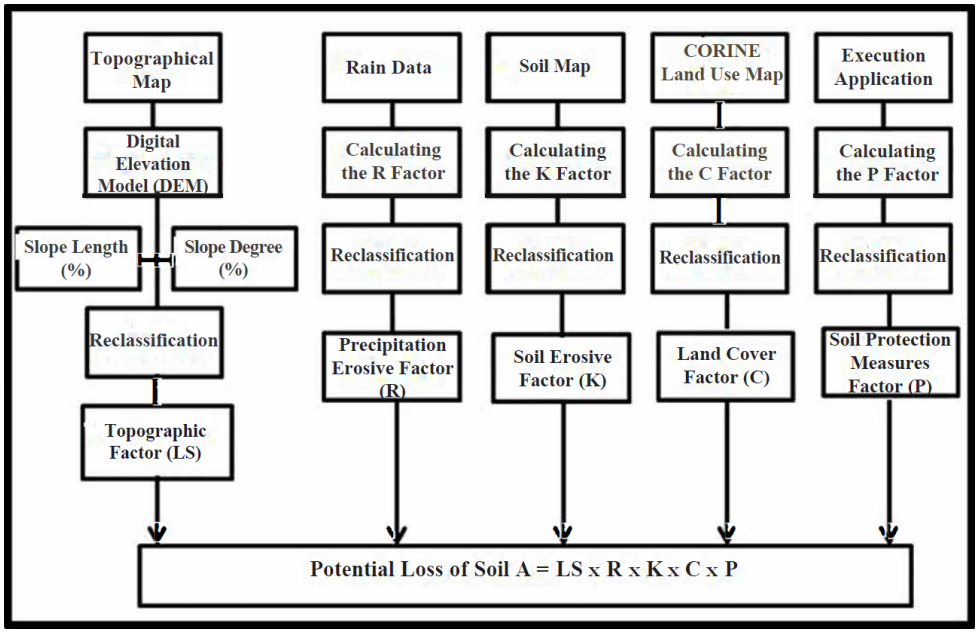

Fig.3. Modelling flowchart fort he soil erosion.

E. Calculating Precipitation Erosion Factor (R)

Meteorological data of several years were used in the calculation of the R coefficient in the RUSLE model, taken from 9 meteorological stations in the province of Kırklareli and its surroundings, which is a research field of the General Directorate of Meteorology. The Arnoldous (1980) Modified Fournier Index (MFI) formula, one of the formulas developed to find the value of the "Erosion Index," was used to measure the R value (2) [14], [15], [16], [17].

$$\text{MFI} = 1 = 112\text{pi}2\text{p} \qquad (2)$$

Equality; Pi monthly precipitation (mm) is expressed as annual precipitation (mm) average of P. Equation used in the Erosive Factor (R) calculation for precipitation (3);

$$\text{R} = (4{,}17\ \text{MFI}) - 152 \qquad (3)$$

F. Calculating soil erosion sensitivity (K)

The erodibility of soils is largely due to the physical and chemical properties of the soil that form its internal structure. In other words, the hydraulic permeability of the soil depends on the organic material properties, texture and structure. Although some soils are resistant against the same erosive forces, some other soils are easily dissolved and eroded [18]. K Factor is the expression of soil lost from hectare in tons with unit erosion index on a land with a slope of 9% and a slope length of 22.1 m.

A method has been developed for determining the K value using silt and very fine sand (%), sand (%), organic matter (%), soil parameters for structure and permeability [13], [19].

The soil map obtained from the Kırklareli Atatürk Research Institute for Soil, Water, and Agricultural Meteorology was used in the K factor calculation. The map is opened numerically in the QGIS software and simplified from the options in the "Attributes Table" according to the Major Soil Groups function. This was changed to the Kırklareli soil database, in other words. This process is achieved by combining the values of the same class category with the aid of the QGIS software plugin "Vector/Geoprocessing Tools/Dissolve". Classification process for Kırklareli province is conducted according to soil erodibility values (K factor). Finally, the values of the K factor were calculated for the province of Kırklareli, the areas covered by them and the proportional distributions.

G. Calculating Land Cover Factor (C)

An approach from CORINE 2018 data using remote sensing technology and GIS is recommended when calculating the C coefficient in the RUSLE model. Via these data the calculation of the C coefficient in the RUSLE model becomes easier.

In general, the data needed for the analysis are data on soil, land use, topography, vegetation, and climate. It reviewed the literature on the subject, providing information on remotely sensed data and geographic information systems in Turkey and in the world of modeling erosion, soil loss assessment models and modeling. Our land was chosen using GIS techniques, and research was conducted on it [18], [20].

H. Calculating soil erosion sensitivity (LS)

With the aid of NASA-ALOS satellite images, the Kırklareli DEM model was created to produce Kırklareli Slope Length and Slope Degree Factor (LS). The sub-modul operation in the QGIS application's GRASS extension raster sub-module was added to the Kırklareli DEM model improved DEM map [15].

I. Potential Soil Loss Distribution (A) Calculation

According to the RUSLE model, the potential basin soil loss (A = R * K * LS * P * C) has been multiplied by replacing it in the GIS setting and thus the potential soil loss of the province of Kırklareli is estimated as (tons/ha/yr). According to Morgan (1995) the appropriate soil loss is 10 tons/ha/yr for agricultural production. This tolerable limit was taken into consideration when defining classes of soil loss rates.

The resolution values of all images in raster format to be used to measure possible soil loss are corrected as 30 m * 30 m.

The values of K, R, C, LS factors and images in the RUSLE formula and measured in the QGIS application are used in the Geotiff raster format, the "Raster / Raster calculator" command in the QGIS application Raster command.

The Geotiff formatted maps were written in the process window that opens, instead of the values in the equation "A = R * K * LS * P * C" that we use to measure the A value, and the R factor was measured visually in the format of raster data (Fig.4).

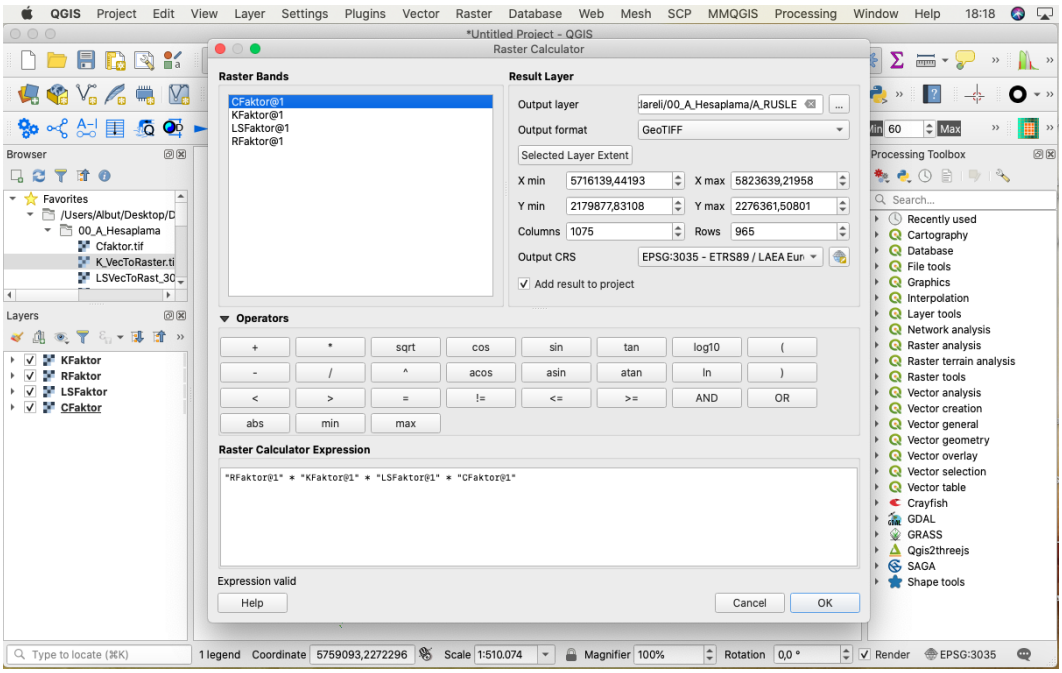

Fig.4. Calculate with the "Raster Calculation" command from the QGIS application Raster Info.

III. RESULTS AND DISCCUSSION

Results of factors LS, R, K, C and P in the RUSLE equation obtained from the research are given in this section.

J. LS Factor

The results and ratios of the LS values obtained by using the DEM map for Kırklareli province are given below (Table 1 and Fig.5).

TABLE I. LS VALUES

LS CLASS	COVERED AREA (km²)	THEIR RATIO COVERED (%)
0-2	5.703,80	88,20
2-5	612,30	9,47
5-10	137,76	2,13
10-17,34	12,92	0,20
Total	**6.466,78**	**100,00**

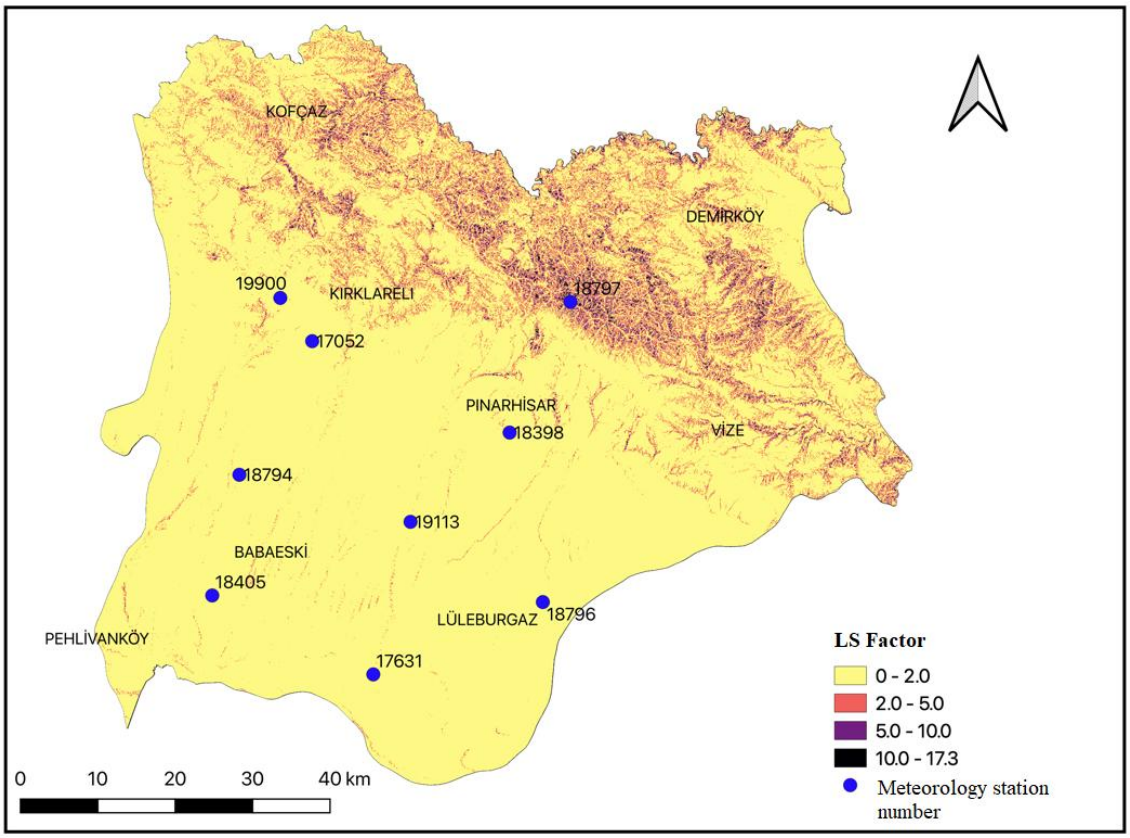

Fig.5. LS factormap of province Kırklareli.

In Kırklareli Province, LS values are in 4 classes and vary from 0 to 17.34. As the table shows, areas with LS values between 0-2 cover most research area (5.703.80 km² and 88.20 per cent). Areas with LS values between 2-5 are 9.47 percent (612.30 km²), areas with LS values between 5-10 percent are 2.13 (137.76 km²), and areas with LS values between 10 and 17.34 are 0 percent, 20 (12.92 km²) are spread. When examining the LS Factor distribution map (Figure 5), generally low LS values are observed from the middle to the south in the SW part of the region, and high LS values are observed in the mountainous areas close to the sea, i.e. in the north and north-east parts of the region. The results are displayed on the research area's LS factor map in Figure 5.

K. R Factor

The locations of the meteorological stations in the province of Kırklareli, station altitude in metres, latitude and longitude, and annual average rainfall in mm type, Arnoldous formula (1980), CFC values and R factor values are all given in Table 2and Fig.6.

TABLE II. KIRKLARELİ MFI AND R-FACTOR VALUES

ID	Station Name	Altitude (m)	Latitude	Longitude	AnnualAveragePrecipitation	MFI	R FACTOR
18405	Babaeski	89,00	41,443300	27,062200	662,56	61,1153	102,8508
1879	Yenimahall	107,00	41,5833	27,10440	561,20	57,477	87,679

4	e-Babaeski		00	0		1	5
17052	Kırklareli	233,00	41,738200	27,217800	615,14	54,9849	77,2870
17631	Lüleburgaz-TİGEM	44,00	41,351300	27,310800	562,45	52,0971	65,2449
18796	Ahmetbey	108,00	41,434200	27,573300	466,72	56,7402	84,6066
18398	Pınarhisar	265,00	41,631100	27,523600	534,37	46,1316	40,3688
19113	Celaliye-Lüleburgaz	127,00	41,528140	27,369300	636,70	84,6377	200,9392
18797	Mahyadağı-Pınarhisar	1020,00	41,782200	27,619200	1125,95	126,8002	376,7568
19900	Kırklareli Uni.	270,00	41,788442	27,168334	512,30	75,6473	163,4492

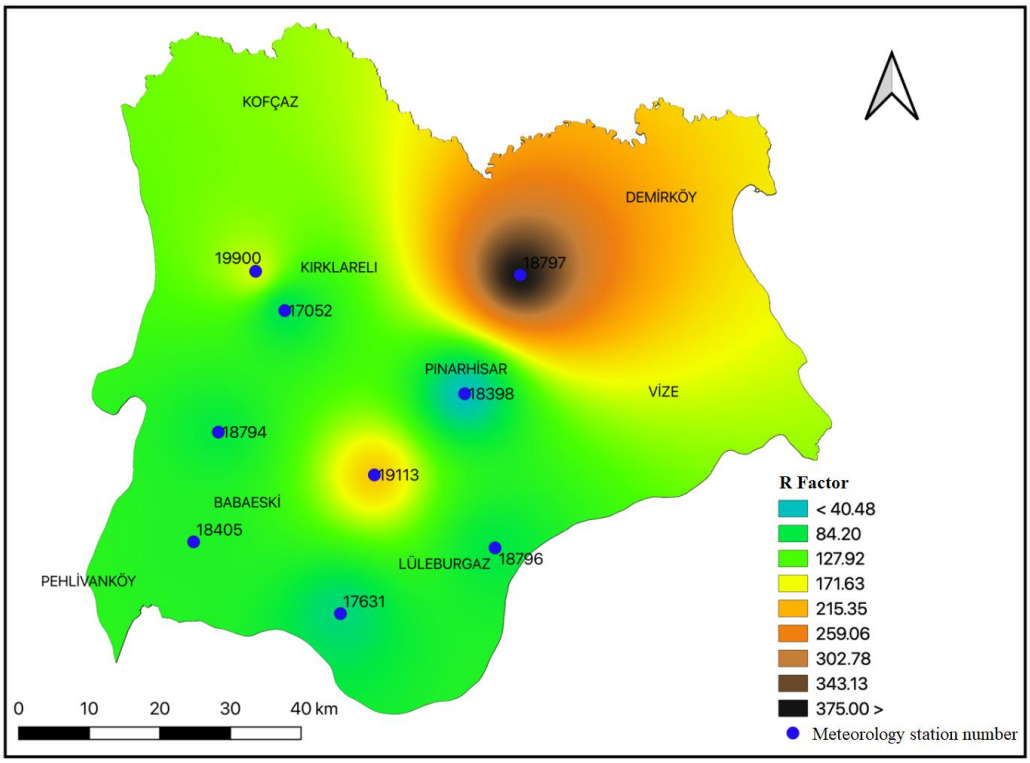

Fig.6. Rfactormap of province Kırklareli.

As can be seen from the map of factor R (Figure 6), elevation plays an enormous role on R values. When we compare the region's map of elevation and the map of factor R, we see that the sections with high R values correspond to the province's high places, that is, they decrease when one goes from north to south. In the higher parts of the province's Mahya Mountains the areas with the highest R value appear. Furthermore, if the rainfall is expected to increase due to the rise in altitude, this relationship would be seen as natural. Again, R values display a small increase around the village of Celaliye, in the central part of the province. The fall in district values at Pınarhisar is alarming. The values drops on the foothills of the mountains.

L. K Factor

The interpolation method was used as a geostatistical method to spread the point-specific K values obtained in Kıklareli province over the surface of the study area and the K factor map (layer) of the site was obtained (Figure 7). This layer was formed according to the degree of erosion of the soils, and the areal and proportional distributions of the K factor classes were calculated by classifying them according to the K factor classes for the province of Kırklareli. The results are given in the table below (Table 3).

TABLE III. SOIL CLASSIFICATION AND K FACTOR VALUES OF KIRKLARELI PROVINCE

Soiltype	Description	K factor	Ares (km^2)	Ratio (%)
S	Alluvial BeachSwamp Soil	0,15	12,97	0,20
V	Vertisols	0,10	1.001,22	15,48
U	Non-calcareousBrown Soil	0,21	1.396,49	21,59
R	Rendzinas	0,12	11,21	0,17
X (another)	Settlements and veWater Surfaces	-	92,17	1,43
K	Colivial Soils	0,17	17,11	0,26
N	Non-calcareous BrownForest Soil	0,29	3.227,15	49,90
M	Brown Forest Soil	0,20	350,62	5,42
A	AlluvialSoil	0,15	357,92	5,53
	TOTAL		6.466,85	100,00

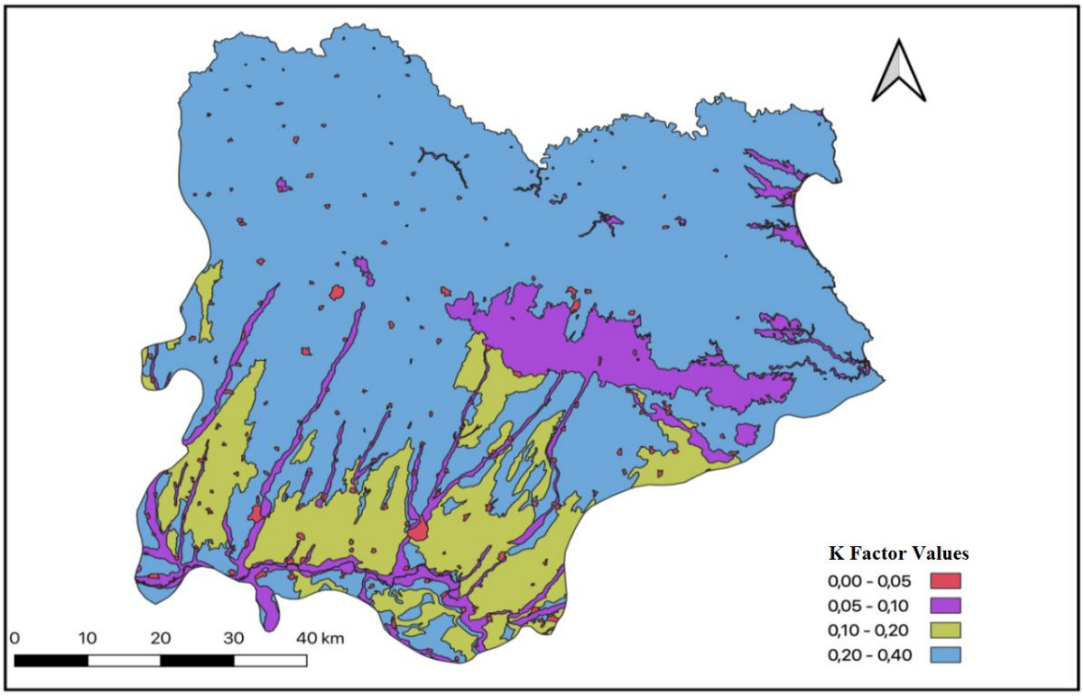

Fig. 7. Kfactormap of province Kırklareli.

M. C Factor

According to the Land Cover / Use Classification developed by the CORINE European Environment Agency, Kırklareli Land Cover Factor (C) provides agricultural land classes and land use maps generated at Kırklareli province level by means of satellite images and the area data obtained on those maps in the QGIS programme. (Tab. 4 and Fig. 8).

TABLE IV. THE AREA AND RATES DETERMİNED FOR KIRKLARELİ PROTECTED BY THE RUSLE C FACTOR VALUES

Soiltype	Description	K factor	Ares (km^2)	Ratio (%)
311	BroadleafForest	0,001	1.869,28	28,91
312	ConiferousForest	0,010	80,24	1,24
313	MixedForests	0,050	106,95	1,65
322-324	Shrubbery, PlantChange Areas	0,038	556,43	8,60
231-321	Meadow Pasture	0,090	370,52	5,73
221-222	Vineyards and Orchards	0,180	6,51	0,10
211-212-213	CultivatedAgriculturalLands	0,280	2.566,86	39,69
242-243	EmptyAgriculturalLands	0,500	670,10	10,36
511-512	Water Surfaces	0,001	42,91	0,66
331-333	Bare Lands	1,000	47,25	0,73
112-411	Other areas of use	-	149,80	2,33
	TOTAL		6.466,85	100,00

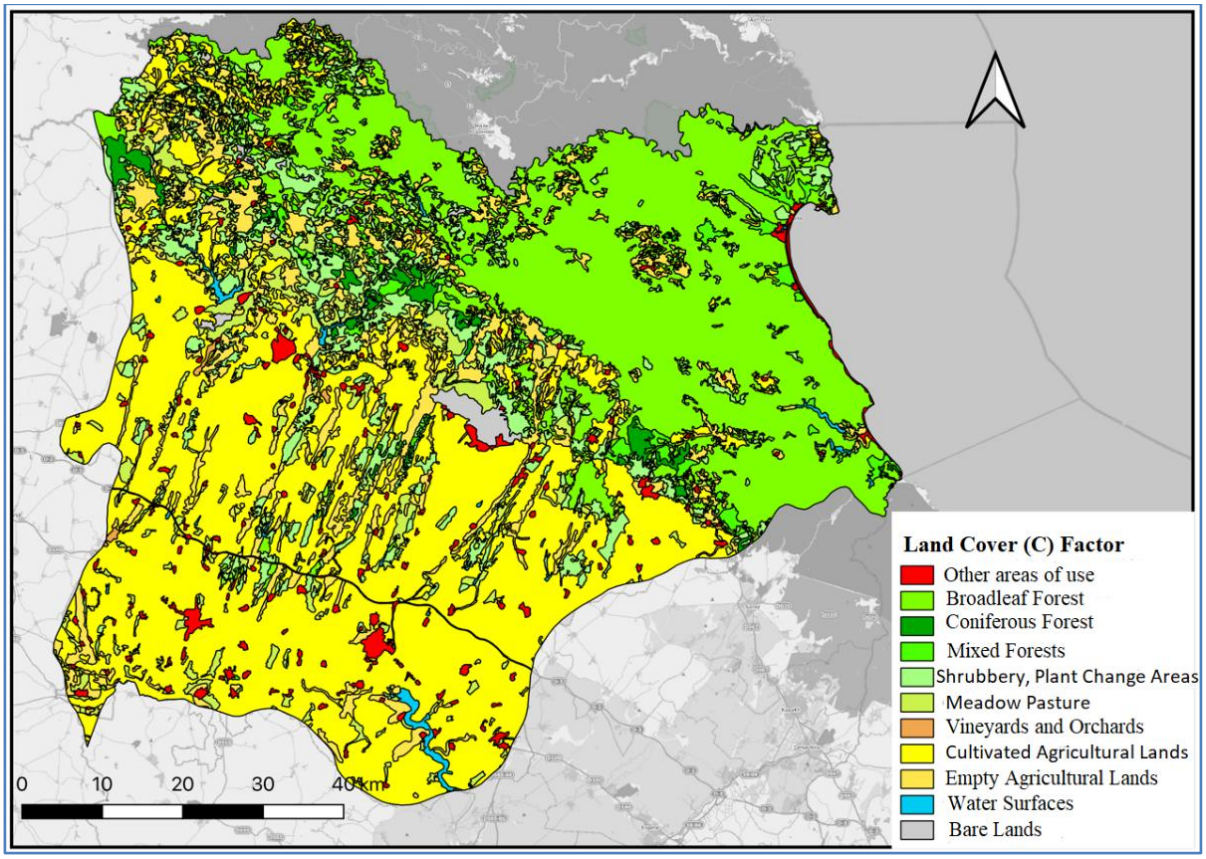

Fig. 8. C factormap of Kırklareli provincecalculatedfrom CORINE 2018.

It is understood that, as it includes more up-to - date data, the base data map prepared with CORINE provides more reliable results. The rate of areas exposed to erosion was, moreover, quite low. It should not be forgotten that the amount of erosion from sloping lands is higher than that of other fields. Areas of higher breakup and degradation in the northern portion of the study region are at higher risk of erosion. How major land use and land cover have on erosion should not be ignored. It was found that the map with a low amount of erosion has higher areas of oak and forest which reduced the amount of soil loss. The hazard of erosion seen in agricultural areas has been observed to be closer.

Study region where the slope is low has found cultivated agricultural areas. It is noteworthy that broad-leaved trees, shrubbery, meadows, and pasture areas are located in high places in the Yıldız Mountains, where the altitude in the north of the region is rising. These areas are places that, for different purposes, can not be opened up to agriculture and are mainly used as pasture for livestock activities.

N. P Factor

The Element (P) of Kırklareli Soil Conservation Measures represents soil management activities. Depending on whether the soil is cultivated in the slope direction or perpendicular to the slope or by rotation, erosion processes may be accelerated or slowed down. Within the framework of this analysis no soil conservation measure was identified in the agricultural areas within the Kırklareli boundaries. For this reason the value of 1.0 was accepted as constant for soil protection measures in the relevant erosion model. This means that Elements P will not influence the erosion calculation process. This value of 1.0 is the P factor value to be taken in the RUSLE model when there is no application in the studied field for soil security calculation (Wischmeier and Smith, 1978).

O. Potential Estimation of Soil Loss Distribution (A)

According to the RUSLE model, this was compounded by putting it in the GIS setting to determine the province's potential soil loss and as a result estimated the Kırklareli province's potential soil loss.

The spatial and proportional risk classes for the distribution of land loss in the province of Kırklareli are given in Table 5. Low soil loss occurs in the province of Kırklareli at a rate of 92.31 per cent with

1-5 erosion distribution values in a region of 5969.23 km². Light level soil loss is 3.68 per cent at second level.

TABLE V. POTENTİAL RATE OF EROSİON İN KIRKLARELİ PROVİNCE

Erosion class	Erosion dispersion value	ClassofVulnerablet oerosion	Area (km^2)	Rate they cover (%)
1	0 – 1	Very low	59,79	0,92
2	1 – 5	Low	5969,23	92,31
3	5 – 10	Light	238,18	3,68
4	10 – 20	Middle	102,05	1,58
5	20 - 50	Strong	62,87	0,97
6	50 -100	Severe	27,69	0,43
7	100>	Extremely Severe	7,03	0,11
	TOTAL		**6.466,85**	**100,00**

The Kırklareli Province Soil Loss Map obtained through the multiplication of variables Rusle-R-K-LS and C is given in Figure 9. Soil loss in the province of Kırklareli was found to be 10.0 ton/ha/yr.

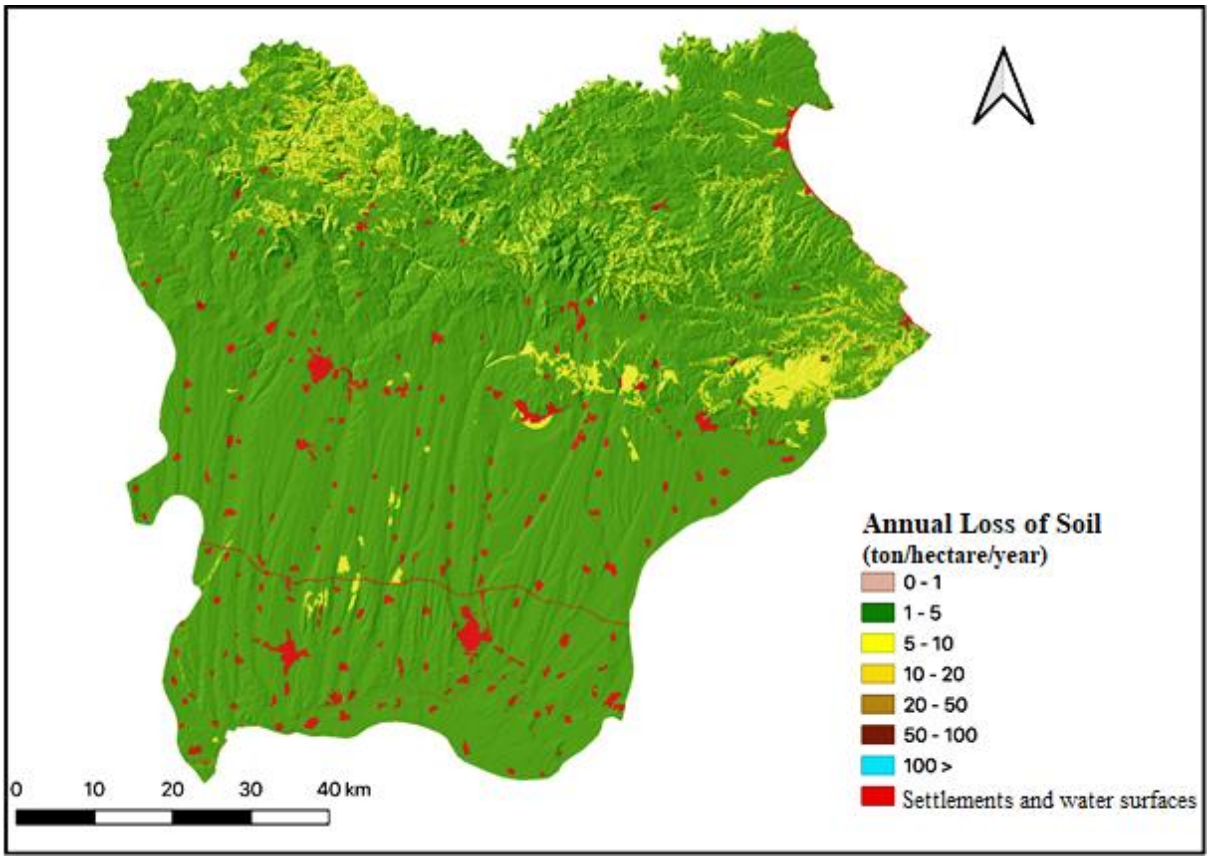

Fig. 9. Potentialerosionmap of Kırklareli province

Possible risk of erosion is shown to be minimal when analyzing the distribution chart of potential groups of risk of erosion. If a generalization is made, the possible risk of erosion in the plain and near-flat plain parts and in the areas around them is seen to be minimal. On the other hand, the possible risk of erosion is seen to be high in the high parts of Yıldız Mountains in the north where the elevation and slope values are high.

IV. CONCLUSIONS

Potential erosion is a phase where the erosion process is not viewed as an effect of human causes, technologies and cultural traditions. Method models and physically based models give advantages over

simple statistical empirical models when describing simply and efficiently individual processes and components causing erosion. The drawbacks of these models, however, are that the mathematical representation of a natural operation can only be approximate, and parameter estimation difficulties remain. RS and GIS techniques are very effective modelling methods for soil erosion and risk assessment for erosion. In Kırklareli Province, remote sensing and open source GIS software (QGIS) is an approach to soil erosion research methods. RUSLE, which is the most commonly used model, was used in this study to calculate the volume and spatial distribution of erosion and sediment load generated as a result of it. This research also added methods for modeling soil erosion using the RUSLE equation using the data from CORINE 2018 for C-factor interpolation. With this study , potential soil erosion status map for the Kırklareli area was generated with RS and GIS, which was clearly analyzed using RUSLE and QGIS technology in terms of spatial distribution.

ACKNOWLEDGMENT

This article was produced from the samemaster's thesis conducted by TNKU Institute of Natural and Applied Sciences.

REFERENCES

[1] E.Görcelioğlu. Effects of Forests on Erosion and Sedimentation. Journal of IU Faculty of Forestry, Series B, Volume: 47, Number: 1-2-3-4, p.1-12,1997.

[2] J.H. Pan, and Y. Wen. Estimation of soil erosion using RUSLE in Caijiamiao watershed China. Natural Hazards, 71 (3), 2187-2205, 2014.

[3] S. Albut, andM. Sağlam. Determination of Land Distribution and Spectral Characteristics of The Wineyard Crop Grown in Tekirdağ Region by Using Digital Satellite Data. AGRO-ENVIRON 2004, Role of Multi-purpose Agriculture in Sustaining Global Environment, p.63-70, Udine, Italy, 2004.

[4] R. Lal. Soil erosion impact on agronomic productivity and environment quality: Critical Review. Plant Science, 17, p.319-464,1998.

[5] M. Zengin, S. Özer and M. Özgül, (2009). Determination of Coruh Basin (İspir-Pazaryolu) Erosion Status with GIS and Solution Proposals, Journal of Atatürk University Faculty of Agriculture, 40 (1), 9-19.

[6] DPT, (2001). Eighth Five-Year Development Plan, Agricultural Policies and Structural Regulations Special Expertise Commission Report, Ankara

[7] QGIS User Guide. 2020. https://github.com/MicheleTobias/Intro-to-Desktop-GIS-with-QGIS

[8] QGIS Manual. 2020. https://docs.qgis.org/3.10/en/docs/user_manual/

[9] CORINE Land Cover - Copernicus Land Monitoring Services https://land.copernicus.eu/pan-european/corine-land-cover

[10] Renard, K.G., Foster, G.R., Weesies, G.A., Mc Cool, D.K. and Yoder, D.C. (1997). Predicting soil erosion by water: A guide to conservation planning with the revised USLE. USDA Hand Book No. 703, USDA, Washington, D.C.

[11] Şeker, B. T. (2005). The Internet and the Information Gap. Comic Bookstore Publishing, Konya.

[12] H.M.J. Arnoldous. An Approximation of the Rainfall Factor in the USLE. In Assessment of Erosion. Chichester: Wiley, p. 127-132, 1980.

[13] W.H. Wischmeier, and D.D: Smith. Predicting rainfall erosion losses. A Guide to conservation planning. United States Department of Agriculture, Agricultural Research Service (USDA-ARS) Handbook, No. 537. United States Government Printing Office, Washington, DC.1978.

[14] I. Ege. Determination of the erosion effect on the geomorphological features and formations of the Kula-Manisa Fairy Chimneys by RUSLE method. The Journal of Academic Social Science Studies, Number: 74, p. 455-479.2019.

[15] Y.E. Mutlu, andA. Soykan. Soil erosion prediction using the Rusle (3D) model. Journal of geomorphological research, p. 50-66.2018.

[16] S. Albut. Determination of R Factor in Revised Universal Soil Loss Equation (RUSLE) With Open Sources Geographical Information System (GIS) Software. Journal of Multidisciplinary Engineering Science and Technology (JMEST) ISSN: 2458-9403 Vol. 7 Issue 8, August – 2020

[17] M.A.Nearing, S.G. Yin, P. Borelli and O.V. Polyakov. Rainfall Erosivity: An Historical Rewiew. Catena, Issue 157, p. 357-362, 2017.

[18] M. Erdem. Erozyon tahmin modelleri ile toprak kaybının hesaplanması, (Yüksek Lisans Tezi), Ordu Üniversitesi Fen Bilimler Enstitüsü. 2017.

[19] E. Kanar, ve O. Dengiz. Madendere havzasında potansiyel erozyon risk durumunun iki farklı parametrik model kullanarak belirlenmesi ve risk haritalarının oluşturulması. Türkiye Tarımsal Araştırmalar Dergisi, Türkiye Journal Agricultural Research 2: 123-134. 2015.

[20] P. Panagos, P. Borrelli, K. Meusburger, C. Alewell, E. Lugato and L. Montanarella. "Estimating the Soil Erosion Cover Management Factor at the European Scale" Land Use Policy Vol. 48, 38-50. 2015.

International Journal of Innovation Engineering and Science Research
(ISSN: 2581-4591)

www.ijiesr.com

Expandable covers of skew modules for emergency buildings

J. Pérez-Valcárcel, M. Muñoz-Vidal, M. J. Freire-Tellado, Isaac R. López-César, F. Suárez-Riestra

Group of Architectural Structures (GEA). Singular structures (GES)
Universidade da Coruña, Corunna. Spain

ABSTRACT

Deployable structures can be a good response to disaster situations, where it is necessary to provide services to a displaced population. They can be compacted into a lightweight and easily transportable package and deployed where needed providing an enclosure for use, quickly and efficiently. In this article, the possibilities of deployable structures of oblique modules are investigated, a subject little studied, but of great interest due to its many possibilities. The geometric conditions of the different modules and the typologies that can be considered are analyzed. The possibility of using the reciprocal links system developed by the authors is also estudied in these meshes. Finally, the performance of a pyramidal dome that uses reciprocal linkages at the ends of its bar, is analyzed in an analytical and experimental way. Both the theoretical calculations and the experimental tests allow demonstrating the viability and effectiveness of this structural type.

Keywords— *Expandable structures; deployable structures; reciprocal linkages; lightweight structures; temporary buildings; emergency buildings*

I. INTRODUCTION

Emergency situations produced both by natural disasters and by human action, are an obvious social concern. A catastrophic situation can occur anywhere at any time and in any country. It is necessary to provide mechanisms that can alleviate the consequences of the disaster, among them one of the most pressing is the housing needs of affected people.

The authors are conducting research on possible solutions to these housing needs during an emergency. It is necessary to solve both the housing needs and the various services demanded after the disaster. This article proposes and analyzes solutions for common areas such as canteens, schools, nurseries, restrooms, meeting places, places of worship, etc., uses for which solutions based on deployable structures represent a quick and effective response.

Deployable structures are articulated bar structures that can radically alter their shape from a folded position in which they are collected in a compact bundle of bars to an open or unfolded position in which they cover a wide space: an umbrella is a classic example of deployable structures.

Most of the deployable structures are formed by elements composed of a pair of bars with a central through joint, similar to that of scissors, which are usually called scissor-like elements, hereinafter SLE. Joining these SLEs at the ends of the bars by means of articulated joints, triangular, squared, pentagonal, hexagonal can be formed. Combining these modules generates a deployable structure.

The structure in the closed position can be stored awaiting its use. In an emergency situation that requires it, it is loaded onto a lorry and moved to the point where it is needed. Therefore, a correct design of deployable structures must take into account that they are light, compact, easy to transport and easy to deploy with simple means. With these characteristics, the structure can be deployed in a very short time and be quickly operational.

According to their geometry, the SLEs are classified between straight, polar (curved), translational (oblique) or angulated units, which combined form straight, curved or oblique modules, according to the SLEs employed. These basic modules are shown in Figure 1.

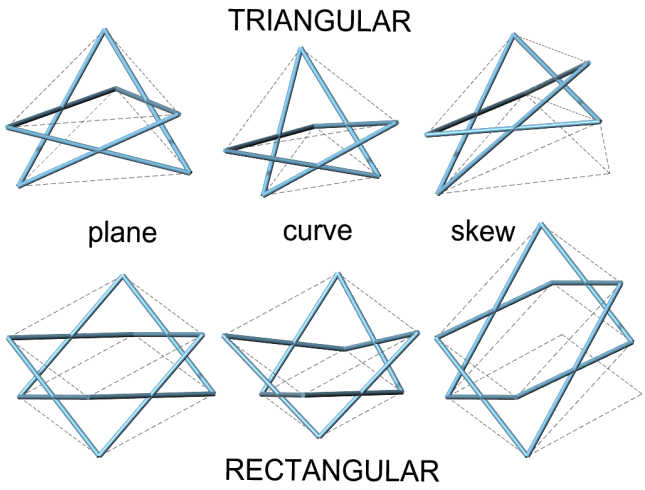

Figure 1. SLE modulus used for explandable structures.

In this article, various proposals based on the use of oblique module structures will be analyzed, but implementing a radical advance proposed by the authors: the nodes used are limkages on reciprocal supports (Perez-Valcárcel et al. 2021) that multiply the load bearing capacity and rigidity of the deployed structure under gravitational loads.

Deployable structures have a long history, despite being fairly recent. In the 1960s, the Spanish architect Emilio Pérez Piñero (1961a, 1961b, 1968) designed and built the first deployable structures of bundles of bars with a central joint.

In Spain, starting in 1984, the group formed around Escrig resumed research on deployable structures, which included Pérez-Valcárcel in 1986 and also Sánchez Sánchez since 1992 on the occasion of the construction of the San Pablo pool cover in Seville (Escrig et al. 1988, 1996, 1999) (Pérez-Valcárcel et al. 1992, 1995).

On the other side of the Atlantic, a research group was organized around Professor Zalevsky in which ideas such as bistable deployable structures were developed, with the decisive contributions of Zeigler (1976) and Krishnapillai (1985) and which would be the subject of a successful study continued by Professor Gantes since 1989. (1989, 1991, 1993, 2001). Outside the bistable sphere but also related to this group, the works of Hernández and Zalewsky (1991, 2005) should be mentioned. The contributions of Hoberman and Pellegrino are equally remarkable.

In this century the work of De Temmerman (2007) and Akgün (2011) have been decisive for the formation of research groups about the matter.

Regarding the use of translational elements,: Escrig et al (1986) proposed their use in large deployable umbrellas in the 1980s but without characterizing them; Sánchez-Cuenca (1996) identifies the type and developed a good number of geometric proposals for roofs, Raskin (1998) applies it to columns with flat and spatial blades; Lagnbecker (1999, 2001) conceived 'stress-free' fold-out covers of translational units with positive and negative curvature; Krishnapillai (1985) and then Gantes (1991) propose diagonalized translational modules to form bistable structures. In 2017 Roovers and De Temmerman carried out a complete analysis of the conditions of the type. Later, Freire et al (2020) added a new group of solutions called Bias Deployable Grids, BDG.

The contributions of this text are framed in the following four aspects.

- Study of the constructive constraints of the meshes formed by oblique modules and the conditions for their geometric and kinematic compatibility.

- Proposal of various designs with oblique modules. The different types of possible modules are analyzed. Proposals are developed for triangular and square modules and other structures that combine both types of modules. These structures apply specifically to emergency buildings.
- Development of reciprocal nodes to the specific case of these structures.
- Theoretical and experimental analysis of this type of structure.

From the initial definition, the characteristics of oblique module meshes and their construction conditions are described (Section II). Section III describes the different solutions proposed for emergency buildings. The materials and methods used in the experimental analysis are described, as well as the models tested (Section IV). The results obtained are analyzed and the results of the theoretical calculation and those obtained in the tests are compared (Section V). The conclusions and perspectives are presented in Section VI.

II. DESCRIPTION OF SKEW MODULE MESHES

The meshes to be analyzed are designed to be employed as common use enclosures in emergency situations. For this reason, it is necessary their design and, especially, their linkages -that are the most expensive elements of the set- be as simple as possible. It is also necessary that they be lightweight, both for their transport and above all to facilitate the unfolding and fixing tasks, without resorting to powerful mechanical aids. For this type of use, the most suitable are solutions with medium spans, between 8 and 12 m.

In other works of the research project that is being developed, various typologies have been studied. In this article, the structures formed by triangular or square skew (translational) modules will be analyzed. They are very regular modules that normally only need two types of bars and whose nodes can have all the same size, which allows a simple and economical manufacture and assembly. In addition, the resulting structures allow defining sloping roofs with easy water evacuation.

A. Oblique module typologies

In the case of triangular modulus, the oblique modulus condition is achieved by raising one of the vertices, so the affected vertex is indifferent (Figure 2a). On the other hand, in square modules, three different situations are possible:

- Displacement of two contiguous vertices in the same direction (Figure 2b). This module is generally used to generate gable roofs.
- Displacement of two opposite vertices in opposite directions (Figure 2c). This module is generally used to generate pyramidal domes.
- Displacement of two opposite vertices in the same direction (Figure 2d). This module is generally used to generate meshes whose coverage is formed by hyperbolic paraboloids.

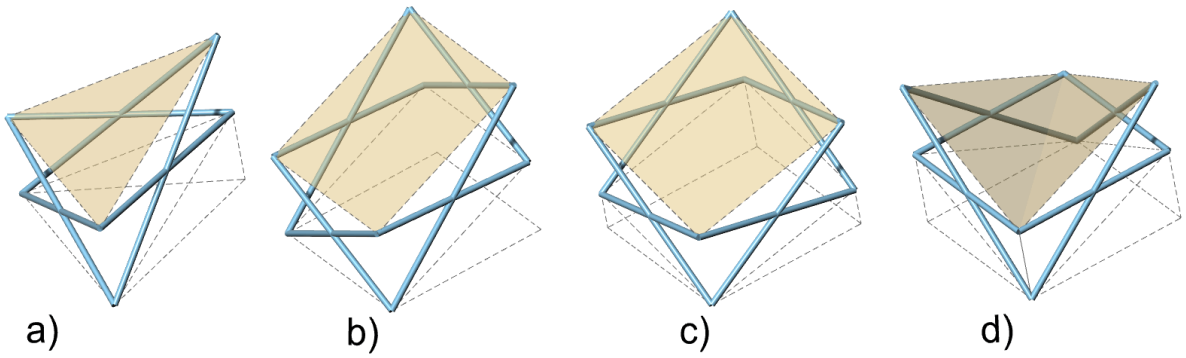

Figure 2. Oblique modulus

B. Used linkages

The essential element in the design of the deployable structures is a linkage that allows the necessary turns for the deployment of the structure. In most cases, the linkages at the ends of the SLEs are hinges which allow an unlimited rotation of the bars. However, reciprocal linkages that limit the rotation and also allow reducing the stresses on the bars and the deformations of the structure are also possible.

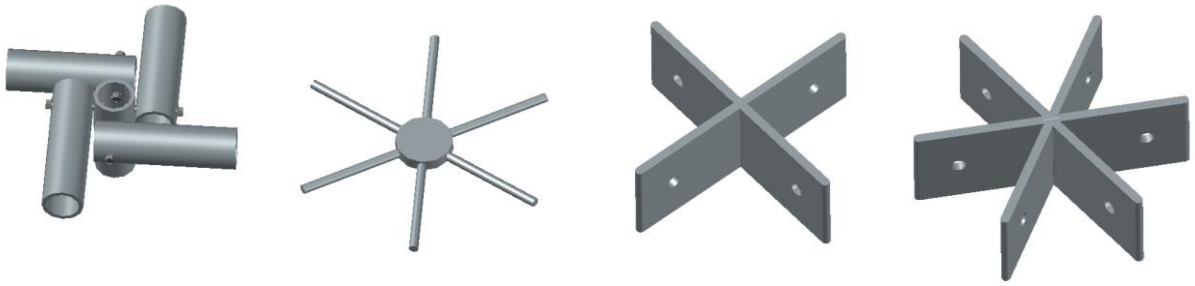

Figure 3. Articulated linkages

Articulated linkages have been widely studied since the first works (Figure 3). In general, the only condition is that they have a sufficient size to allow the packing of the bars in the folded position. The two most common types are the cylindrical and the fin linkages. They are the best solutions for meshes with triangular modules, since six bars concur in the interior nodes and a reciprocal linkage would require such a large size that it would be very ineffective.

Reciprocal linkages must have a specific width that depends on the diameter of the bars that meet in it and the angles they form. These nodes have been studied in detail in reference in a recent article (Pérez-Valcárcel et al., 2021).

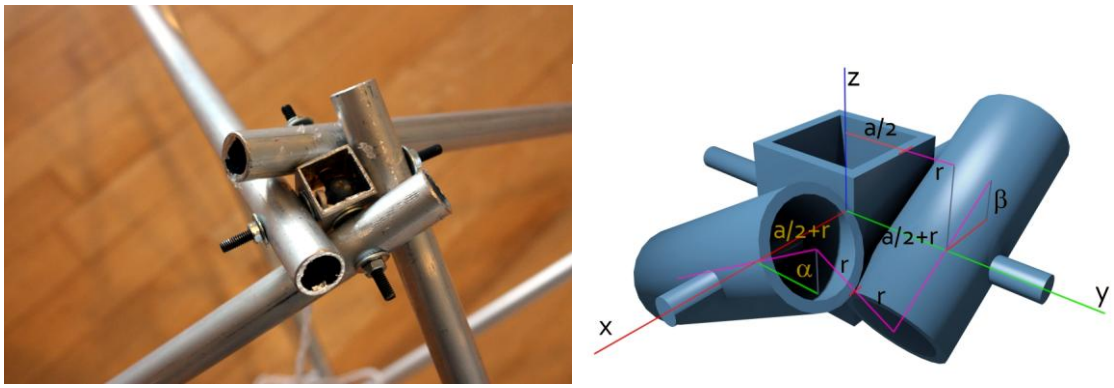

Figure 4. Reciprocal linkages

The use of the reciprocal joints means that the linkage has to be of minimum size which depends on the diameter of the bars and the desired angle of opening. To analyse the most general case, the bar opening angles are hypothesised to be different, **α, β**, where **a** is the width of the linkage and **d** is the diameter of the bars which meet it, respectively.

The separation between the axes of the bars may be determined by applying the condition that the distance between the two straight lines that cross is **d** = **2r**, considering that the bars touch at the point of contact. The relationship between the width of the linkage **a** and that of the bar **d** is

$$\frac{a}{d} = \frac{2 \cdot \sqrt{\sin^2\alpha \cdot \cos^2\beta + \cos^2\alpha \cdot \sin^2\beta + \cos^2\alpha \cdot \cos^2\beta}}{\sin(\alpha+\beta)} - 1 \qquad [1]$$

This equation makes it possible to determine the diameter or width that the linkage must have so that the bars form a reciprocal joint with specific angles of opening α and β.

For this reason, in the generation of reciprocal linkages meshes, it is especially important to determine the angles formed by the bars that concur in the linkage in the deployed position to ensure that the bars rest each one on the adjacent one, making this link effective. This condition implies a certain complication in the case of oblique modules, as they have different angles. The width of the linkage would be different in both directions, but the construction of irregular linkages is complicated and expensive. The best solution is to use a link with the minimum size necessary and supplement with a nut or washer the end where it is necessary.

C. Geometrical condictions of depployement

In the case of skew modules, the way of packing the bars is somewhat different from that of other types of meshes. In flat or curved structures the height of the closed package is practically that of the length of the longest bar. On the other hand, in skew modules, each module folds somewhat lower (or above) than the previous one, so the height of the package is somewhat higher (Figure 3). It can be estimated approximately as.

$$H = 2 \cdot L_1 + 2 \cdot (n-1) \cdot (L_1 - L_2) \qquad [2]$$

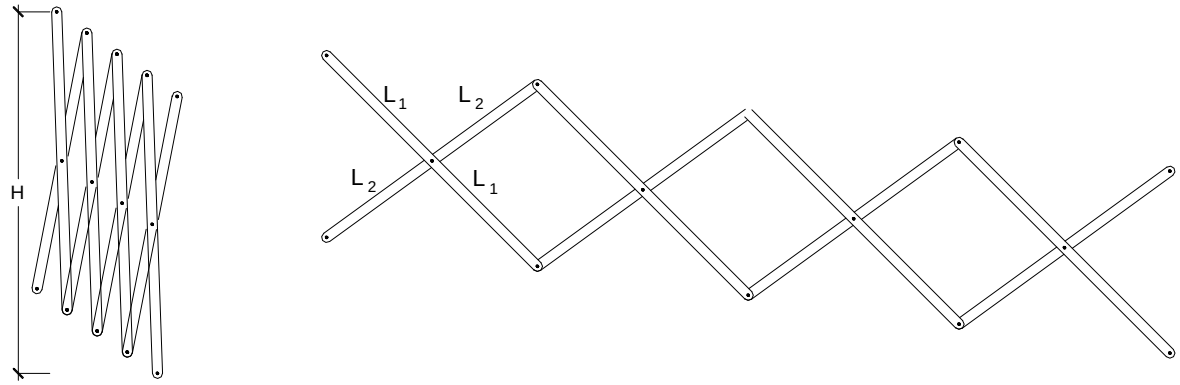

Figure 5.- Scheme of folding of an oblique module.

This means that as the number of modules and the inclination of the planes increases, the package can acquire somewhat larger dimensions, which can make it difficult to transport. With everything for, average spans like the ones that are proposed does not pose a problem.

It is interesting to define the geometric conditions to determine the lengths of the bars, as seen in figure 4.

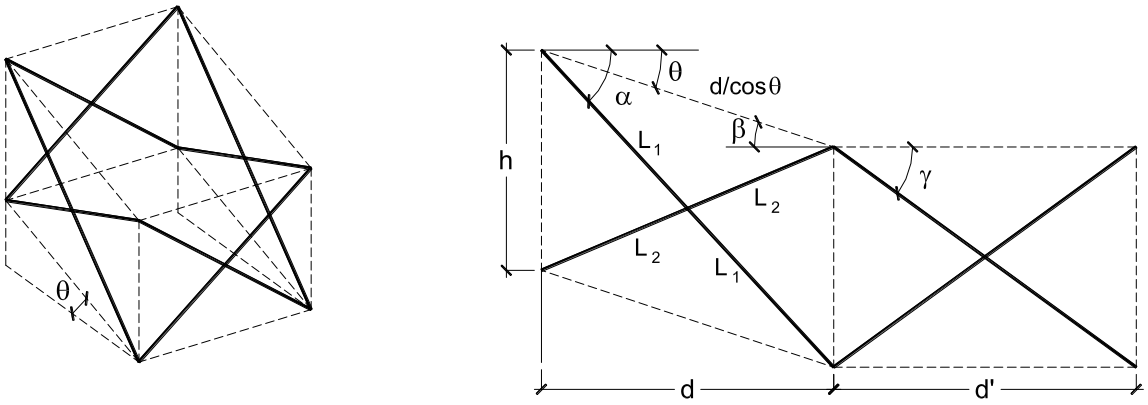

Figure 6.- Definition of the lengths of the bars and the angles with the horizontal plane.

For oblique deployment, it is important to define as parameters the height of the mesh **h** and the opening of the SLE **d**, but also the slope of the roof **θ**. Applying the cosine theorem

$$L_1 = \frac{1}{2}\sqrt{h^2 + \frac{d^2}{\cos^2\theta} + \frac{2d\cdot h}{\cos\theta}\cdot\sin^2\theta}$$
$$L_2 = \frac{1}{2}\sqrt{h^2 + \frac{d^2}{\cos^2\theta} - \frac{2d\cdot h}{\cos\theta}\cdot\sin^2\theta} \qquad [3]$$

It is also important to determine the angles that the bars make with the horizontal plane, because the direction of the axis of the link is vertical.

$$\cos\alpha = \frac{d}{2L_1} \quad ; \quad \cos\beta = \frac{d}{2L_2} \quad ; \quad d' = \sqrt{(L_1+L_2)^2 - h^2} \quad ; \quad \cos\gamma = \frac{d'}{L_1+L_2} \qquad [4]$$

D. Support conditions

The skew module structures have a structural behavior similar to that of other typologies studied in previous works. In order for them to be folded and unfolded, it is necessary for them to be mechanisms, which are subsequently applied external constraints that turn them into authentic structures, that is, they are capable of resisting the external loads to which they will be subjected. Therefore, the correct definition of these constraints is essential to achieve a lightweight and efficient structure.

In some cases of structures such as vaults or curved domes, their profile may allow the roof structure to rest directly on the ground. The linkages are fixed on it providing sufficient constraint. However, skew module structures do not normally have enough inclination to allow this type of support without losing excessive interior space. The most common solution in this case is to support them on masts.

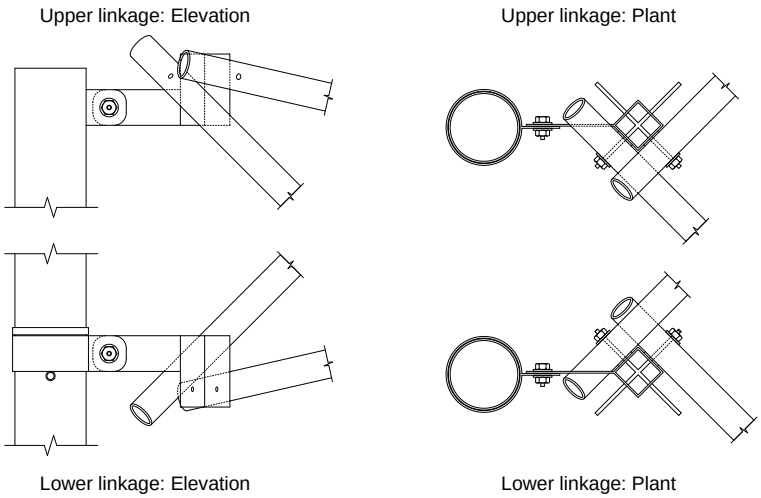

Figure 7. Support of the folding structure on the mast

The structural behavior of this type of roof improves considerably if the two nodes that concur in it are fixed to the mast. For this it is necessary to design specific elements so that the upper knot allows articulation and the lower knot slides on the mast until it is locked in its final position. Simple systems similar to the umbrella top or a simple bolt are effective enough.

E. Textile cover

In expandable structures, the definition of the roof is especially important. In most cases, textile covers have been used (Escrig et al. 1994; Pérez-Valcárcel et al. 2019). Rigid sheet metal systems that are placed on the structure after deployment have also been used Pérez Piñero 1968. Finally there are some interesting proposals with rigid sheets that are folded with the bar structure (Pérez-

Valcárcel et al. 1995). They are very attractive solutions, but they are not applicable for emergency buildings as they are excessively complicated and expensive.

For emergency buildings, the most suitable solution is a textile cover that can be folded together with the bundle of bars and that when unfolded is placed in its final position. Various systems have been proposed and it was even used on the San Pablo pool cover with success (Escrig et al. 1996).

The design of a controlled folding system of the textile is very necessary, since otherwise the SLEs when closed could work like a scissors, cutting the textile. A simple and efficient system is the one indicated in the figure. It consists of a ribbon attached at its ends to the linkages of the opposite layer. When closing the structure the opposing linkages of the scissors move away and the ribbon pulls the textile, that folds into the gap between the SLEs. When the textile is placed on the upper face, the ribbon is fixed at the linkages on the lower face and vice versa. It is advisable to leave enough slack in the ribbon and adjust it in the workshop before assembly. For this to occur, the sum of lengths between the ribbon section and the textile must be equal to that of the two sections of the SLE.

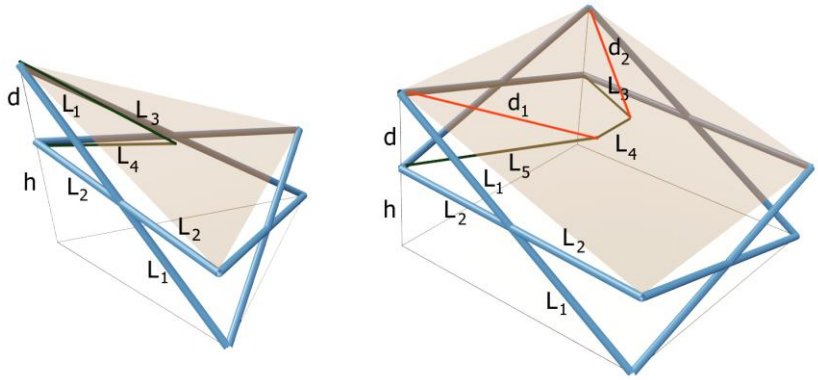

Figure 8. Geometric conditions for the self-folding of the textile cover

Triangular modules $L_1 + L_2 = L_3 + L_4$

Square modules $L_1 + L_2 = L_3 + d_1 = L_5 + d_2$ [5]

When the modules are regular, the length of the tape can be calculated immediately. With irregular modules the geometric conditions can be more complex, so it is advisable to calculate it by trial and error.

III. APPLICATION TO EMERGENCY BUILDINGS

The aforementioned modules allow you to define a large number of deployable structures, but not all of them are useful for use in emergency situations. Those of greatest interest are the umbrellas that allow the construction of stands for small businesses and the vaults and domes for community areas.

A. Umbrelas

Umbrellas are some of the easiest deployable structures to build. They are also especially suitable for temporary use, since they can be easily folded and unfolded depending on the weather conditions. In the case of emergency constructions, they are especially useful for markets, an essential element for exchange or small business functions. This activity is essential after a catastrophe, since it allows the resumption of part of the social uses, seriously affected after a disaster.

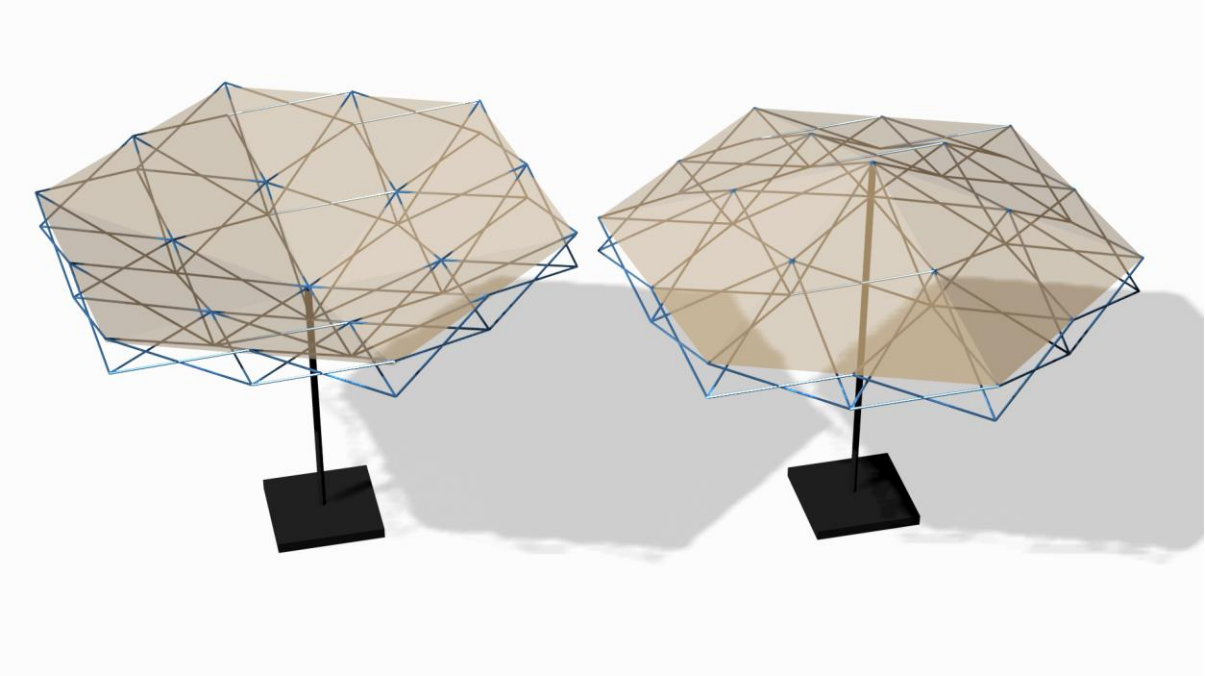

Figure 9. Expandable umbrella with triangular modulus

These structures were one of the first proposals by Escrig and Pérez-Valcárcel, as in the case of those designed to cover the Plaza de San Francisco in Seville, which was never realized (Escrig et al. 1986). Curved beam umbrellas were also proposed for the roof of the Asturias Pavilion at EXPO'92 in Seville, which was also not executed (Pérez-Valcárcel et al. 1991b).

With oblique triangular modules, triangular or hexagonal, concave or convex umbrellas can be executed. Concave roofs have better structural behavior, but convex roofs provide a better solution for the evacuation of rainwater.

The most interesting solutions for oblique square modules consist of the generation of four-sided structures, both towards the outside and inside. Even if we use modules of the hyperbolic paraboloid type, textile surfaces with continuous valleys can be generated, which allow an excellent evacuation of rainwater.

Figure 10. Expandable umbrella with square modulus

.

B. Gable roofs

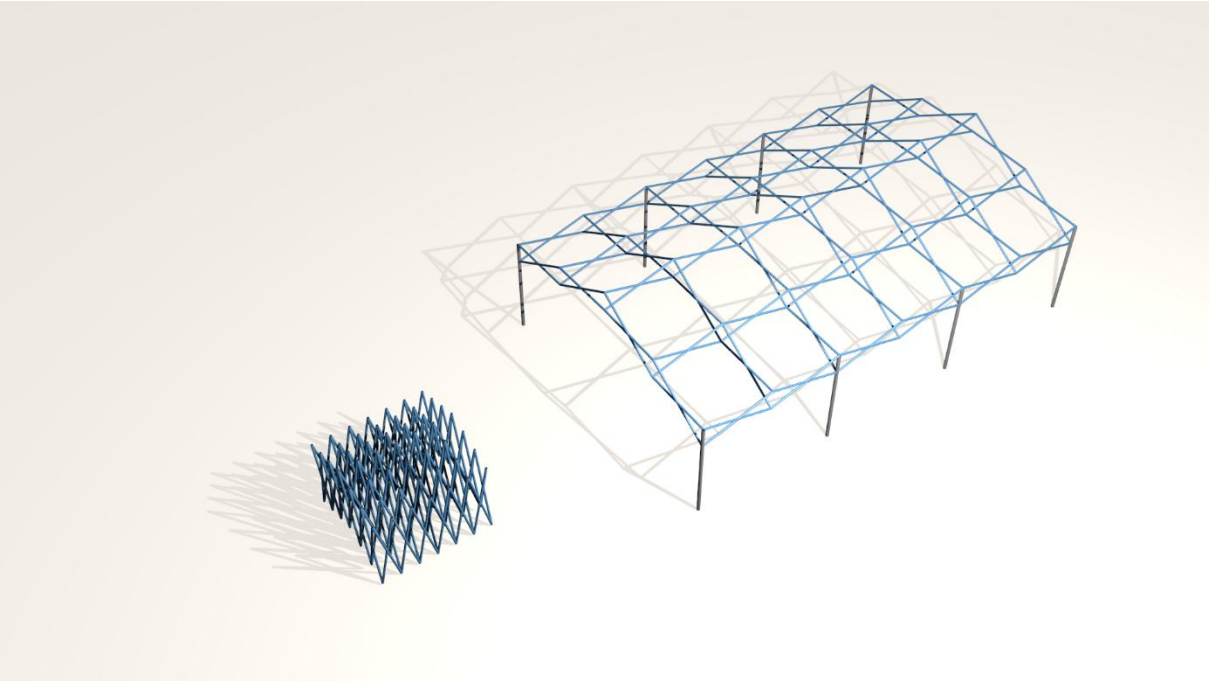

Figure 11. Gable roof folded and deployed

Gable roofs are one of the simplest and most useful structures that can be executed with oblique square modules. They have two drawbacks that need to be taken into account. On the one hand they have a low stiffness to angular distortion. On the other hand, if solid support is not sought, they have a tendency to strong horizontal movements. In emergency buildings with medium spans, effective solutions can be designed at low cost.

The problem of angular bracing is usually solved with additional bars in large structures. For small span roofs, the bracing provided by the textile roof is sufficient. Regarding horizontal displacements, the structure improves its performance when supported by properly designed masts, as indicated in II.D.

C. Pyramidal domes

Deployable domes have also been widely studied and several have even been built, using triangular or square modules. Spherical domes have generally been proposed, such as those of the Pérez Piñero Theater or the sail domes of the San Pablo roof, already mentioned. The proposal for the competition for the roof of the Bergisel Stadion in Innsbruck can also be mentioned as example of big expandable structures (Pérez-Valcárcel et al. 1992). By contrast, pyramidal domes have received little attention, despite their good performance.

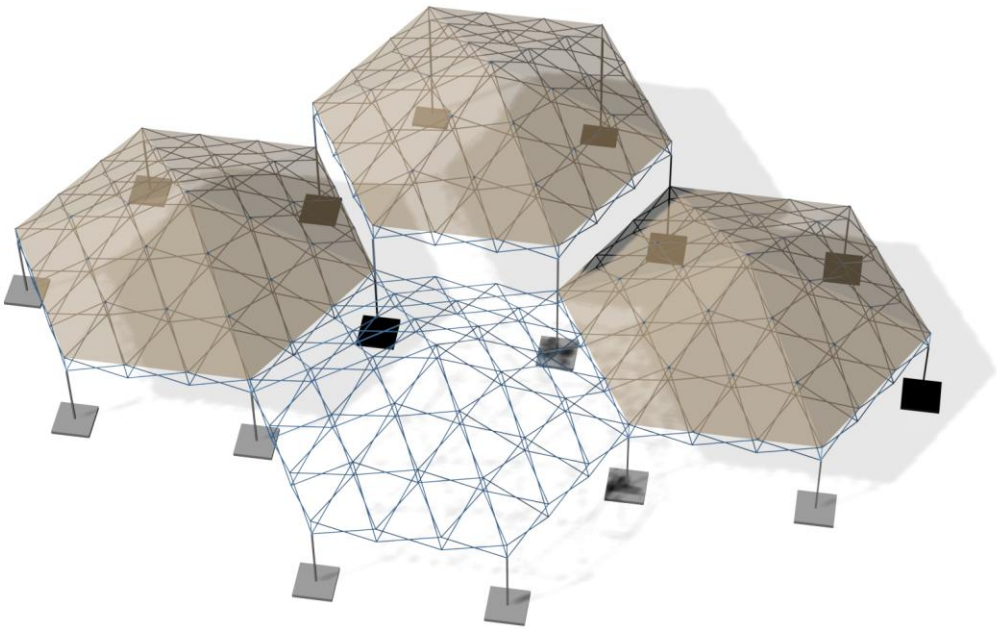

Figure 12. Pyramidal domes of triangular modules

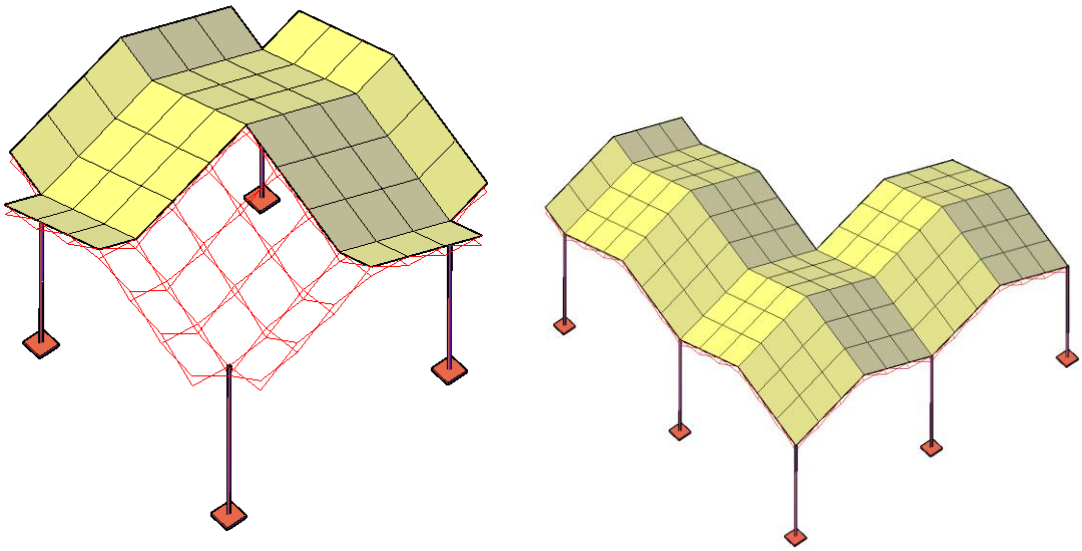

Figure 13. Pyramidal domes of square modules

These domes require a perimeter strapping with cables in case of large spans. In spans of medium or short width, as is usual in the proposed use, the supports on the masts described may be sufficient (Figures 12, 13). However, the most effective system is also the strapping with cables that can be combined with the support on masts. In the tests carried out it has been possible to verify the effectiveness of these systems.

D. Other typologies

The modules analyzed allow the execution of various typologies, even mixing modules of different types, as shown in the figure 14.

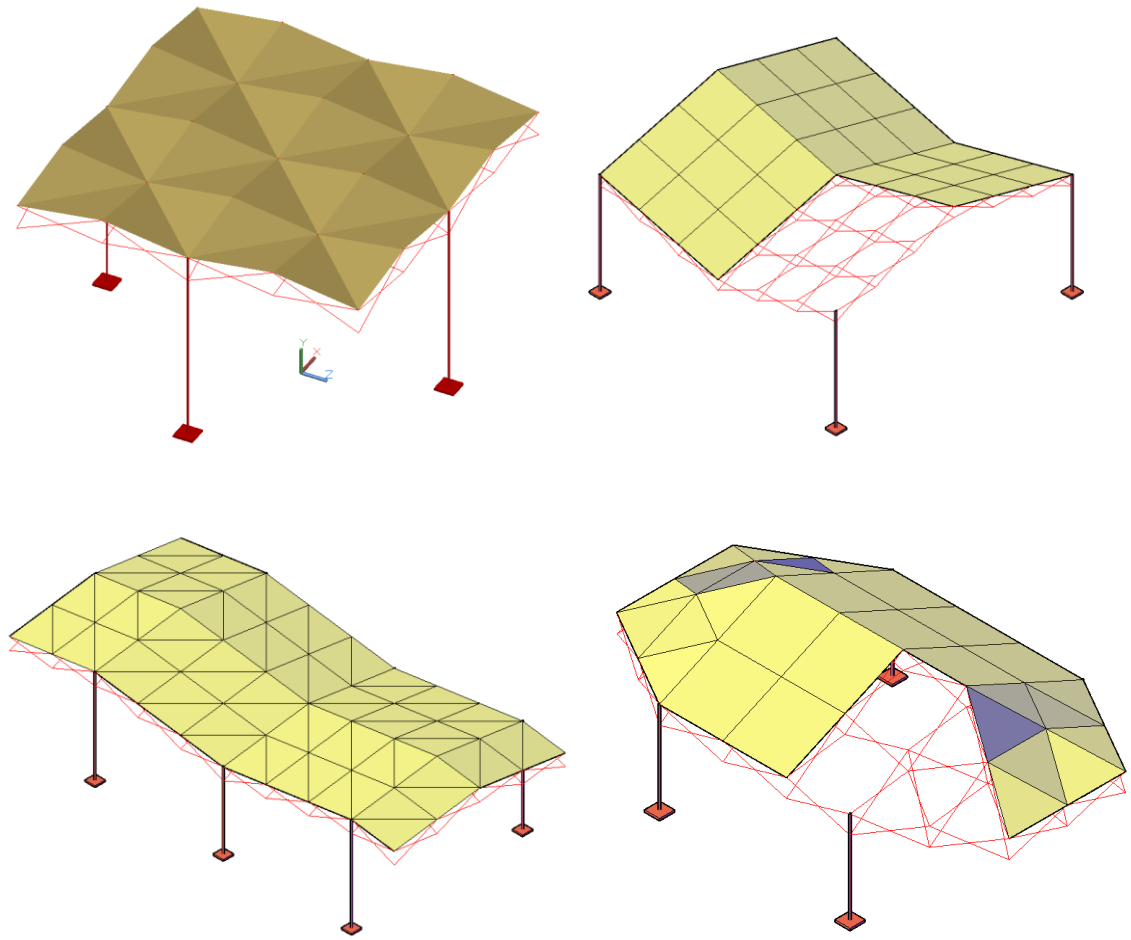

Figure 14. Other types of expandable structures with oblique modules

IV. MATERIALS AND METHODS

To verify the effectiveness of this type of mesh, a series of tests have been carried out with a pyramidal cover model. It has been built with reciprocal linkages and has been tested in four different situations, with and without cross bars in the corner, and in both cases with a perimeter tie with and without a cable. The aim is to verify the effectiveness of both systems to propose the most suitable solutions in reality.

A. Materials

The test model bars are T5 6060-type Ø16 mm and 1.9 mm thick aluminium tubes (aluminium – magnesium - silicon) (figure 20). They have a specific weight of 2700 kN/m^3, a modulus of elasticity of 69500 N/mm^2, an elastic limit of 185 N/mm^2 and a failure load of 220 N/mm^2. Ø13 mm and 1.5 mm thick aluminium tubes made of the same material were used for the bracing bars that were placed at the corners of the mesh in some tests.

The linkages are composed of sections of hollow aluminium tube (SHS) of the same quality. They are 20 mm across, 1 mm thick and 20 mm tall. The pivots are composed of 4 mm threaded steel bars that are welded to the central part. The bolts and threaded bars are in 5.6 quality steel according to ISO 898-1. They have a modulus of elasticity of 200000 N/mm^2, an elastic limit of 300 N/mm^2 and a failure load of 500 N/mm^2 with a 20% elongation.

The bracing cables are 1x19, 1.5 mm, according to the European EN 1906: 2012 standard. They have an ultimate strength of 1960 N/mm^2 and yield strength of 1570 N/mm^2.

B. Used models

The test model has been built at 1: 4 scale with the bars and nodes described. It is a simple structure, since they can be made with two types of bars that have the same lengths. In addition, the ratio between the diameter of the node and that of the bar D / d is always the same, so all the nodes are equal, although it is necessary to increase the distance in some of them by means of washers. For all this, its manufacture and assembly are especially simple according to the intended use.

C. Test organization

The mesh was tested in four different cases. First, the mesh was tested without bracing bars in the corners and without cables. The deformations were very large, in accordance with the provisions of the theoretical calculation, which is why it was found that a structure under these conditions is excessively deformable and lacks practical utility. Subsequently, three tests were carried out with different bracing systems that were effective. In the first case, bracing bars were placed in the corners, joining the upper and lower linkages. In the second, cables were placed connecting the support points of the base. Finally, the tests were carried out with the bracing bars and the tying cables. In all the tests, a previous loading step was performed first so that the linkages were adjusted. This is an aspect of the utmost importance in deployable structures. Being mobile structures, it is necessary that the joints and linkages have a certain tolerance. Upon entering into load, the structure readjusts and has a certain initial displacement. After the discharge of this previous step, the structure retains that adjustment position, although there is a slight recovery. When carrying out the next load step, the structure deforms according to the applied load. This is essential if you want to validate the calculation methods with the experimental results. Adjustment shifts would distort the measured results and prevent effective contrast.

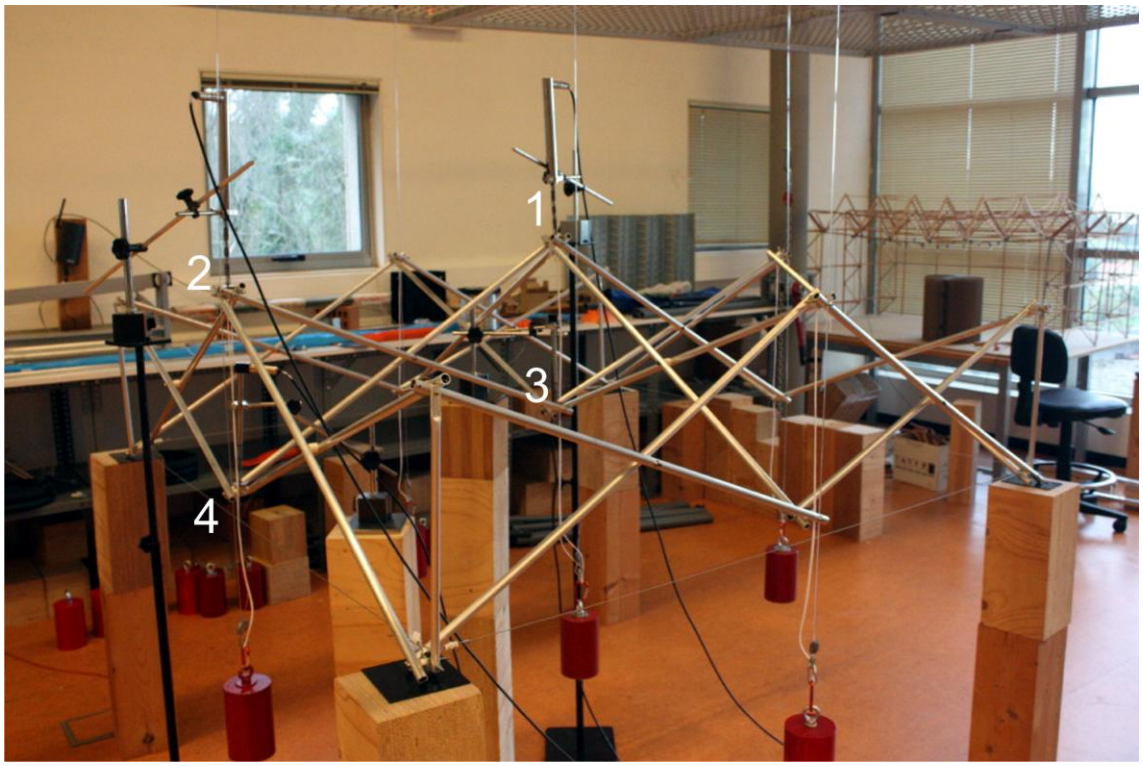

Figure 15. Model test

V. RESULTS AND DISCUSSION

A. Theoretical model

Verifications of the tested models have been carried out through the Despleg19.1 program that uses matrix structural analysis. In this case, the mesh uses reciprocal linkages and the program assigns to the end linkages of the bars a degree of embedment that is calculated by the program and entered as data (Pérez-Valcárcel et al., 2019). In the internal points of the bars, the program assumes a bolt connection. Consider that the displacements of both points attached to the linkage are equal, but the bars can rotate freely around the pivot.

Table 1 Displacements calculated by Deepleg

	With additional bars No cables				Without additional bars Braced cables				With additional bars Braced cables			
	Displacements mm				Displacements mm				Displacements mm			
Points	1	2	3	4	1	2	3	4	1	2	3	4
Theoretical	-27.79	-18.22	-23.18	-8.59	-14.38	-4.97	-10.59	-4.86	-9.47	-3.04	-6.89	-3.09

B. Experimental results

The tests were carried out with the loads placed on the nodes of the upper layer and with the displacement sensors at the points indicated in figure 14. A progressive load was entered for about 5 seconds. The charge was held for a period sufficient to fully stabilize the displacements for approximately 10 seconds and then progressively discharged for 5 seconds. For each of the cases, three tests were performed. The results are very similar, so no further tests were considered necessary. Table 2 indicates the measured results and their average value.

Table 2 Displacements measured in test

	With additional bars No cables				Without additional bars Braced cables				With additional bars Braced cables			
	Displacements mm				Displacements mm				Displacements mm			
Points	1	2	3	4	1	2	3	4	1	2	3	4
Test 1	-28.42	-18.75	-23.47	-9.67	-15.38	-6.67	-11.57	-4.76	-11.72	-3.00	-9.90	-4.85
Test 2	-28.71	-19.19	-23.70	-9.77	-15.09	-6.30	-11.37	-4.69	-11.21	-2.86	-9.23	-4.37
Test 3	-27.98	-18.75	-23.20	-9.22	-15.01	-6.37	-11.34	-4.56	-11.43	-3.00	-10.11	-4.82
Averaged	-28.37	-18.90	-23.46	-9.55	-15.16	-6.45	-11.43	-4.67	-11.45	-2.95	-9.75	-4.68

C. Discussion

As indicated, the first test of the mesh without additional bars and without bracing cables was unsuccessful. The only resistant mechanism that the mesh had to not be a mechanism, were reciprocal linkages. These linkages prevented the collapse of the structure, which with articulated ones would undoubtedly have occurred, but instead the displacements were so strong that their use was not suitable. Therefore, the tests focused on analyzing the effects of the different possible bracing systems.

The results obtained have been compared to test the effectiveness of these bracing systems. It is observed that in the case of meshes without tying cables, the coincidence is very high, especially in the central nodes, which are the ones with the greatest deformations. In this case, the fit of the model is

very high, so the experimental results are very close to the theoretical ones, which supports the effectiveness of the calculation model. The results of the meshes with bracing cables show little differences in absolute value, but greater in relative terms. In the realization of the model there have been difficulties to tension the cable effectively, which justifies these differences.

Table 3 Displacements comparison

	With additional bars No cables				Without additional bars Braced cables				With additional bars Braced cables			
	Displacements mm				Displacements mm				Displacements mm			
Points	1	2	3	4	1	2	3	4	1	2	3	4
Theoretical	-27.79	-18.22	-23.18	-8.59	-14.38	-4.97	-10.59	-4.86	-9.47	-3.04	-6.89	-3.09
Averaged	-28.37	-18.90	-23.46	-9.55	-15.16	-6.45	-11.43	-4.67	-11.45	-2.95	-9.75	-4.68
Increase mm	-0.58	-0.68	-0.28	-0.96	-0.78	-1.48	-0.84	0.19	-1.98	0.09	-2.86	-1.59
Increase %	2.1%	3.7%	1.2%	11.2%	5.4%	29.7%	7.9%	-3.9%	20.9%	-2.8%	41.5%	51.4%

For the meshes braced by cables, the experimental results are more representative, which even with the errors in the assembly of the cables, show that the efficiency of the bracing systems is very high. The inclusion of bracing cables only causes the displacements of the central node to be 53.43% of those of the mesh with only the bracing bars. If additional bars are placed in addition to the cables, the displacement decreases to 40.36%.

VI. CONCLUSIONS

The use of oblique modules in the design of deployable structures allows a wide set of meshes of great interest and utility for emergency enclosures. These modules can incorporate the textile cover so that the deployment and putting into use is faster. They also allow the use of reciprocal links, which improves their resistance capacity and limits displacements. Likewise, the effectiveness of the proposed bracing systems has been demonstrated.

ACKNOWLEDGMENT

This study is part of the research project "Deployable and modular constructions for situations of humanitarian catastrophe", funded by the Ministry of Economy and Competitiveness of the Kingdom of Spain with reference BIA2016-79459-R.

REFERENCES

[1] Escrig F.; and Pérez-Valcárcel, J. (1986) "Great Size Umbrellas solved with Expandable Bar Structures," First International Conference on Ligthweight Structures in Architecture, LSA 86, eds. M. Burgess & M. De Bono. University of New South Wales, Sydney, 676-683.

[2] Escrig, F.; and Pérez-Valcárcel, J. (1988). "Estructuras espaciales desplegables curvas" Informes de la Construcción, 39(393), 53-71.

[3] Escrig, F.; Pérez-Valcárcel, J. (1996). "Deployable Cover on a Swimming Pool in Seville," Bulletin of the International Association for Shell and Spatial Structures". 120(37), 39-70.

[4] Escrig, F.; Sánchez, J.; P. Valcárcel, J. (1994). "Foldable structures with textil cover". 6th International Techtextil Symposium fot Technical Textiles and Textile-Reinforced Materials. Frankfurt am Main.

[5] Escrig, F.; and Sánchez Sánchez, J. (1999). " Estructura plegable de malla para la cubrición de recintos". Patente 2 158 787 A1.

[6] Freire-Tellado, M. J. Muñoz-Vidal, M. and Pérez-Valcárcel, J. (2020), "Scissor-Hinged Deployable Structures Supported Perimetrally on Rectangular Bases" Journal of the International Association for Shell and Spatial Structures 61(2) 204. (DOI: https://doi.org/10.20898/j.iass.2020.204.009).

[7] Gantes, C. J. J. Connor, J. Logcher R. D. and Rosenfeld Y. (1989), "Structural Analysis and Design of Deployable Structures," Computers and Structures, 32(3/4), 661-669, (DOI: 10.1016/0045-7949(89)90354-4).

[8] Gantes C.J. (1991), "A design methodology for deployable structures,". PhD Thesis. Massachusetts Institute of Technology, MIT, USA.

[9] Gantes C.J. (1993), Geometric constraints in assembling polygonal deployable units to form multi-unit structural systems. Space Structure 4, 793–803.

[10] Gantes C.J. (2001), "Deployable structures: analysis and design." Boston: WIT Press.

[11] Hernández, C.H. (1996), "New Ideas on Deployable Structures," Mobile and Rapidly Assembling Structures II. Proceeding of the 2nd MARAS 1996, Seville, Spain, June 17-20, 1996, Escrig & Brebbia, Ed. Computational Mechanics Publications, Southampton, 63-72

[12] Hernández, C.H. and Zalewski, W. (2005), "Pabellón Itinerante de Exposiciones TaraTara, Estado de Falcón, Venezuela (based on the ESTRAN 1 Protoype developped by Hernández and Zalewski, 1987-2000 IDEC - FAU – UCV).

[13] Krishnapillai A., Zalewski W. P., (1985), "The design of deployable structures - Kinematic design," Unpublished Research Report, Department of Architecture, MIT, Cambridge, Massachussets, USA, October (ref. from Gantes 2001)

[14] Langbecker, T. (1999), "Kinematic Analysis of Deployable Scissor Structures, " International Journal of Space Structures, 14 (1), 1-16.

[15] Langbecker, T., Albermani, F. (2001), "Kinematic and Non-Linear Analysis of Foldable Barrel Vaults," Engineering Structures 23, 158-171.

[16] Pérez Piñero, E. (1961). "Estructura reticular estérea plegable". Spanish Patent 266801. (1965) US Patent 3,185,164.

[17] Pérez Piñero, E, (1961) "Project for a mobile theatre," Architectural Design, 12, 154-155.

[18] Pérez Piñero, E. (1968)." Estructures reticulées". "L'Architecture d'Aujourd'hui", 141, 76-81

[19] Pérez-Valcárcel, J.; Escrig, F. (1991)" Expandable Structures with Self-folding Textile Cover". International Conference on Mobile and Rapidly Assembled Structures. WIT. Southampton.

[20] Pérez-Valcárcel, J.; Estévez Cimadevila, J.; Martín Gutiérrez, E.; Freire Tellado, M. 1991. "Asturias. Expo'92. Ideas para un pabellón". Chapter "Nao". Consejería de la Presidencia del Principado de Asturias. Oviedo.

[21] Pérez-Valcárcel, J.; Escrig, F.; Estévez, J.; Martín, E. (1992), "Large Span Expandable Domes". Int. Conference on Large Span Structures. Toronto, (2), 619-630.

[22] Pérez-Valcárcel, J.; Escrig, F.; Martín, E.; Vázquez, J.A. 1995. "Analysis of expandable domes of squared modulus with self-folding roofing plates". International Conference on Spatial Structures: Heritage, present and future IASS. Milano. (2), 551-558.

[23] Pérez Valcarcel, J., Freire Tellado, M., & Muñoz Vidal, M. (2019). "Estructuras desplegables para actividades lúdicas". BAc Boletín Académico. Revista de investigación y Arquitectura contemporánea, 9, 129-146

[24] Pérez-Valcárcel, J. Muñoz-Vidal, M. Suárez-Riestra, F. R.López-César, I.R. Freire-Tellado. M.J. (2021) "A new system of deployable structures with reciprocal linkages for emergency buildings," Journal of Building Engineering, 33, 101609. (DOI https://doi.org/10.1016/j.jobe.2020.101609)

[25] Raskin, I. and Roorda, J. (1996), "Buckling force for deployable pantographic columns," Proceedings of MARAS '96, the 2nd International Conference on Mobile and Rapidly Assembled Structures, Seville, Spain.

[26] Raskin, I. (1998), Stiffness and stability of deployable pantographic columns, Ph.D. Thesis, Civil Engineering Department, University of Waterloo, Waterloo, Ontario, Canada.

[27] Roovers, K. and De Temmerman, N. (2017), "Deployable scissor grids consisting of translational units", International Journal of Solids and Structures, 121, 45–61. (DOI 10.1016/j.ijsolstr.2017.05.015)

[28] Sánchez Cuenca, L. (1996). "Geometric models for expandable structures," Mobile and Rapidly Assembling Structures II Escrig & Brebbia. Computational Mechanics Publications, Southampton, 93-102

[29] Zeigler, T. R. (1976). "Collapsible self-supporting structure." U.S. Patent nº 3,968,808. United States. (Filed Nov. 6.1976).

International Journal of Innovation Engineering and Science Research
(ISSN: 2581-4591)
www.ijiesr.com

Evaluation the Impacts of Dams

Zeyneb KILIÇ

Adıyaman University, Engineering Faculty, Department of Civil Engineering, Adıyaman, Turkey.
Corresponding author e-mail: zeynebboybay@gmail.com

ABSTRACT

Dams; are used for various purposes as drinking water supply, energy production, recreation, strategical purposes, fisheries, socio-economic purposes, irrigation, flood control, river transport and others. Food, water, and energy, three of the most critical issues for human development, are all connected with dams. Dams are one of the most important structures in the water resources transmission and storage systems. Dams are the most natural and cheapest way of energy production in the country; due to the significant positive or negative effects to the natural environment and human life have always became focal point of the national and international society past and today. However dams have some positive and negative effects on the environment; very large dams increase the humidity of the air and change the climate and ecological balance of the region. Hence, given the importance of the positive impacts of dams, it is essential that negative environmental impacts of the dam to be minimized for sustainable development. The current paper evaluates the positive and negative environmental effects of dams.

Keywords: Dam, ecosystem, environment, positive effects, negative effects.

I. INTRODUCTION

Dam; the set built on rivers with human labor and technique to collect water is defined as lakes or artificial lakes. In other words, dam lakes; are artificial lakes built on rivers for electricity generation, drinking water supply, irrigation, fishing, flood control, river transportation and recreation, where water accumulates in the basin formed by a blocking structure. Dams are structures that prevent the flow of water and allow it to accumulate in a certain area. Dams can be established in large or small areas where geographical conditions are suitable. Established dams are used in many ways, from inland water supply to electricity generation. However, dams can cause some problems in the regions where they are established. At the present time, dams are considered as important water structures constructed in all parts of the world, especially in arid and semi-arid areas for surface water management. Dams have close relationship with geological conditions in which they were constructed. Hence, all risks and all negative effects of dam and reservoir need to be reduced, as much as possible [1]. The dam construction has been known for long time as being a suitable solution to supply water for agricultural, industrial consumptions, stopping the river flow and water storage, drinking, flood control, production of hydroelectric energy, quality control, and so on. In addition, construction of dam can result in development of urbanization, agriculture, industry and it finally leads into a suitable environment for biological activities of microorganisms and reduced water quality [2].
Although dams have benefits, it should be claimed that there is almost no dam without environmental negative affects in various forms [3]. “The environmental effects of construction of dams and reservoirs after the end of the World War II were well recognized and knowledge on the risks of dam construction on the environment reached its peak in the twentieth century” [4]. “Paying increased

attention to environment has caused conflicts among engineers, planners, and some eco-friendly groups against structural activities. Moreover, preventing the construction projects will not possible for development of technology and enhancing the quality of life. Thus, in addition to technical and economic standards, environmental standards should be considered" [5]. The construction of dam and reservoir projects plays important roles in the development of hydropower and the regulation of water resources of a country. But it also makes a profound effect on regionecological environment. It has become the key issue of dam and reservoir projects how to coordinate the relationship between construction and environmental protection, and to realize their harmony development. Impacts of dams can be positive or negative. Before the dam is built, some important considerations should be taken into account to mitigate adverse effects of dams, such as; reservoir project mainly focuses on water temperature, aquatic livings, environmental geology, terrestrial livings, hydrological regime, landscape and heritage, and the resettlement of migrants from reservoir. Dams substantially affect their places and close vicinity from sociocultural, economic, ecological and ecosystem aspects. Nowadays studies about positive and negative affects of dams on the environment and on the ecosystem often deal with impacts of dams on both local and regional climate; it was found out that dams often affect the climate at local level. In addition, all the effects of dams on the ecosystem should be taken into account and the dam construction should be decided accordingly.

According to the studies of the World Dams Commission, while the economic output of dams is generally increased, their social and environmental costs are not taken into consideration or shown low. The socio-economic and cultural effects of dams are felt positively or negatively from the construction phase. Today, due to dams, many settlements are inundated, nature and cultural riches are damaged, fertile agricultural areas disappear, transportation systems routes change.

When the positive and negative effects of dams are examined, we see that they have more positive effects. Therefore, hydroelectric energy generated from dams is considered as renewable energy. In addition, the use of the current stream potentials is an important issue for countries and our country. In this article, we give information about the positive and negative effects of dams, and the precautions and suggestions that should be taken in order to minimize the damage of the said structures to the environment.

II. EFFECTS OF DAMS ON THE ECOSYSTEM

Dams, besides all these positive effects; they also have negative environmental impacts on seismic events, ecological balance of the basin, architectural and cultural values, water quality, parasitic diseases caused by water, hydrological regime, the forest and agricultural areas in the reservoir, and the effects on the local people who are forced to migrate. Therefore, when planning dam projects, technical and economic considering many environmental and social factors as well as feasibility, environmental and social feasibility criteria are also important. In these projects, the importance of national and universal values that are likely to be lost or affected should be evaluated in terms of the future of the society.

Rivers are one of the most important factors that shape the earth. Dam construction is seen as the most intensive use of rivers all over the world.The intensive use of dams brings environmental problems with it. The increase in the number and size of dams on a river is directly proportional to the magnitude of natural destruction. These negativities caused by the construction of the dam generally arise due to the land potential not being evaluated correctly. It is also known that the dam lakes change the climate characteristics of the region in which they are located and give a different climate structure to the region. The changes that occur with the start of dam construction are two fold. The first of these emerges in space as a human living space. It causes the change of settlements and the destruction of cultural areas. Secondly, it shows itself in physical conditions. These are destruction of

flora and fauna or forced migration, shrinkage of agricultural areas and all kinds of environmental pollution.
The impact of the environment on lake of dam might emerge in two forms; negative or harmful environmental impacts and positive or beneficial environmental impacts. "Generally, environmental studies of dams should be conducted in the form of sections, which include physical and chemical impacts, biological impacts, health impacts, and social and economic impacts. However, in most of the cases, the environmental impacts are examined and evaluated separately for the two periods of construction and exploitation" [5]. Some social and economic effects of Dams; the majority of people settle around the reservoir of the dam's lake, and this phenomenon leads to increased population of cities; dam construction also has a negative impact on facilities and structures; loss of agricultural lands to provide materials cause unemployment for great number of people and the employment gets some problems such as security of city and village, attracting tourists, and they can change the traditional and cultural structure of settlement unit; historical places with special and beautiful topography, found rarely by going under water [6]; by development of region because of dams, traffic state will change and the traffic of vehicles increases, leading to increased air pollution [7]. Some physical and chemical effects of Dams; dam construction acts as a barrier for movement of floating objects along rivers; sediment materials in the lake of dam causes reduction of the solid materials, blocking the floodgates and dischargers; occurrence of many floods causes some physical, chemical, and biological changes in downstream of dams; it can causes salinization and salinization of lands reduces yield of salinity-sensitive products, which it make land unproductive [8].

Dams have negative effects on natural systems, from deterioration of water quality to the change in the balance of the water flow of rivers, from the decrease in groundwater level to the drying of reeds, the destruction of many species due to the endangerment of living habitats and coastal erosion. The rivers with dams on them hold the nutrients transported due to the sediments of the dams. For this reason, efficiency in the deltas decreases as it cannot carry sediment to the deltas on the coasts. Such impacts have serious consequences as they are not fully taken into account during project phases.

Some health effects of Dams; lake of dams can be source of malaria and blood diseases; insects and pathogenic bacteria is seen more [9]. Some negative effects of aquatic organisms of dams; in the construction phase of the dam erosion and sedimentation occurs at the dam downstream, which causes aquatic animals die and interference of ecological balance of these environments [7]; dams are considered barriers for movement of fish from the upstream of river to downstream of river; "Drainage of swamps and cases like this and drilling operations alongside of river will have destructive impacts on aquatic animals and even lead to their death" [10]. Temperature, salinity, and oxygen amount can be changed vertically, resulting in non-oxygen conditions in the dams lake; flow regime of river might change, and the sudden flood of water behind the dam threatens the vegetation and animal life around the coasts [5]. Some biological impacts of dams; decrease amount of the nutrients at dam downstream and these situtiation affects on the plant and animal community of cited area; water storage impact in shallow reservoirs on the growth of planktons and may causes eutrophication; water temperature, water quality, distribution of salt, and oxygen might be changed due to formation of the reservoirs; some species might change or die out due to erosion or water turbidity; one of the most affected areas are coastal waters, when the reservoirs are filled, as lands are pulled toward under water, dry lands are reduced and water boundaries are expanded, therefore, habitat of humans, animals, and plants is changed, and the forests and agricultural lands may be pulled toward under water; the concentration of surface water pollutants is increased in downstream parts pending the water shortage time [7].

The evaporation of some of the water in dams causes an increase in the ratio of salt and other minerals in the water. In addition, as the oxygen intake capacity of the stagnant water in the dams

decreases, the natural cleaning capacity decreases and the eutrophication process begins in the lake. Changes in lake water quality also change aquatic life.

Some effects of dams lake on atmospheric system; dams cause change in the content of air humidity, air flows, air temperature and climate in the region and the surrounding areas and these changes affect the human health and other living organisms; some of these changes are increased absorption of solar energy at the region level, the exchange of temperature between the lake water of dam and surrounding atmosphere and changes in the rate of evaporation and fog; dams is release of greenhouse gas from reservoirs due corrosive vegetation and carbon flow from the basin and these causes global warming [8]. Some effects of dams lake on noise pollution; machinery, devices and explosions used for construction of the dam during the construction phase, the noise level in the region is increasing sharply and these operations disrupts the relaxation of the region and leaves undesirable impacts on wildlife and human life.

Some impact of dams construction on seismicity and hydraulic system; some earthquakes and erosions are attributed to dam construction; these earthquakes occur due to the heavy weight of lake water and disturbed balance of pressure in various layers of the earth; the main important hydraulic effect is the drainage of the basin flows into a fixed water resource rather than discharge into river bed; thus,the stability change will occur in the downstream, since downstream would dry partially or completely due to closure of floodgate it leads to disturbed balance in the downstream ecosystem,

III. RESULT AND RECOMMEDATIONS

As the size and number of dam projects increase, their environmental impacts and the magnitude of destruction increase in parallel. Large dam projects that cause rapid changes in the geographical environment, in general, due to incomplete and erroneous planning, due to the fact that the land potential is not evaluated correctly, it causes serious problems in catastrophic scale and causes the hydro-electricity projects to be viewed with suspicion. The dam and reservoir construction play the important role in Turkey's hydropower development and water resources regulation. Dam construction projects are considered as national basic items, fort his reason it is necessary to carry out environmental impact post assessment to assess the actual impacts of the dam construction on ecology and environment, which can provide scientific basis for better development of dam projects and propose some reasonable measures to reduce the adverse impacts.As discussed in the present paper, despite many benefits of construction of dams and ignoring their negative impacts on the environment, and finally human life in the long term, it might be better to think on using alternative methods to control water and flood.

Some of the measures can be taken in order to decrease the negative impacts of dam construction: plant and animal species especially endemic ones in the region must identified by experts; ecological boundaries of the project should be determined; training and enhancing the knowledge of residents of the affected region to reduce environmental damage especially when dam's lake is used as a tourism region. Dams are also one of the most important sources of energy production in countries like our country, whose economic policies are largely industry-centered and are rapidly industrializing. With the construction of the dam, spatial and socio-economic changes have occurred in our country as in the world. In addition to contributing to the national economy, the projects developed in particular accelerate the social and economic development of the region, thus creating different employment areas in the region and increasing the income level and living standards. On the other hand, dam construction causes many physical and human problems in the region and indirectly throughout the country.

Today, various problems have arisen with rapid industrialization. The most important of these problems is the deterioration of the balance in the ecosystem. Ecosystem disorders affect humanity

directly or indirectly. For this reason, planning dams considering their pressures on the ecosystem is of great importance both for the protection of our country's natural resources and for the future of humanity. In addition, a regular layout plan should be constructed in addition to the functions that existed in the previous settlement and suitable for the settlements that were evacuated with the dam construction. Otherwise, the people in these evacuated settlements are forced to migrate because they cannot continue their activities and social lives in the area they were previously and these migrations cause unresolvable problems in big cities.

Due to the increased needs of people to hydroelectric power, dam projects has become a highly essential issue in human life. As the positive side in the cannot be neglected. On the other hand construction of dams has a great negative impact to the environment. Therefore hiding behind the construction of dams must involve the introduction of latest techniques which would further minimize the negative effects of dams on environmental, ecosystem, climate, health, biological, chemical, physical, social impacts that are which should focus on the sustainability of the environment and the nature.

References

[1] M. R. Parhizgar, Investigation the geological hazards in the Tang-e-Sorkh dam area of Shiraz (with a view to solubility of gypsum) (Unpublished master's thesis). Tarbiat Modarres University, Iran, 2007.

[2] O. Alizadeh, A.M. Pourazari, Cross-sectional study of water quality changes in the lake behind the Aras dam. Scientific and Research Journal of Wetland Eco-biology, 6, 2015.

[3] M. Shabankari, AH. Halabian, Investigating the environmental impact of Zayandehrud dam lake. Journal of Human and Environment, 8, 2010.

[4] K. Baba, T. Hirose. Water Storage, Transport and Dıstrıbutıon. Environmental Impact Assessment of Dams and Reservoirs. 2009. E book.

[5] M.S. Tahmiscioğlu, N. Anul, F. Ekmekçi, N. Durmuş, Positive and Negative Impacts of Dams on the Environment, International Congress on River Basin Management, 22-24 March, Turkey, 2007.

[6] K. Jashni, M. Chamanchi, M, Comparing the destructive environmental impacts of dams with using Veten-Verau matrix. The First Specialized Dam and Environment Workshop. 2007.

[7] M. Kamali, M. Kukhekzadeh, M, The impact of environmental factors on water resources development Planning: A Case Study of Kalghan Dam. The First Specialized Dam and Environment Workshop. 2007.

[8] MS. Cadiver, Dams and Development (1st ed.), 2007.

[9] Naderi, M, Investigating the environmental impact of dams. 11th National Civil Students Conference, Iran. 2004.

[10] M.R. Pirestani, M. Shafghti, M, Investigating the environmental impact of dam construction. Quarterly journal of human geography, 1, 2009.